UNIVERSIDADE DA BEIRA INTERIOR
Covilhã | Portugal

FCT
Fundação para a Ciência e a Tecnologia
MINISTÉRIO DA CIÊNCIA, TECNOLOGIA E ENSINO SUPERIOR

UNIVERSITY OF BEIRA INTERIOR
Aerospace Science

Numerical Study of the Spray Impingement onto a Solid Wall

Christian Michel Gomes Rodrigues

Dissertation for the Degree of Master of Science in

Aeronautical Engineering

(2nd Cycle of Studies)

Supervisor: Dr. André Resende Rodrigues da Silva

Co-Supervisor: Dr. Jorge Manuel Martins Barata

Covilhã, June 2011

This page has been intentionally left blank for double-sided copying.

Acknowledgments

I would like to take this opportunity to express my appreciation to my supervisor, Professor André Resende Rodrigues da Silva, for its support and encouragement during the course of my study at the University of Beira Interior and for giving me the opportunity to belong and collaborated in the activities of AeroG – Aeronautics and Astronautics Research Center. My thanks go also to my Scientific Coordinator, Professor Jorge Manuel Martins Barata, for providing research grants in this Department and for its guidance during the fellowship.

I want also to express my acknowledgments to the Foundation for Science and Technology for their financial assistance under the project PDTC/EME-MFE/102190/2008 in the form of a research grant with the reference "BI/AeroG/01/2010".

This page has been intentionally left blank for double-sided copying.

Abstract

The modelling of turbulent multiphase flows has been gathering high interest in the last decades in the scientific community due to its relevance in several applications, such as in industrial and environmental processes or for chemical and biomedical purposes. In fact, regarding the industrial applications, the impingement of liquid fuel sprays onto engine surfaces has become a subject of interest due to its influence on the mixture preparation prior to combustion and, consequently, engine performance and pollutants emission (Barata and Silva, 2005). However, there is still a lack of knowledge concerning the spray-wall interaction but also concerning the exact phenomenon occurring during the process. These gaps do not allow defining the most favourable conditions for the optimal engine performance. Hence, the main challenge for the investigators lies in attaining a much deeper understanding of the phenomena involved in the spray impingement process, through either theoretical analysis or experimental investigation.

Meanwhile, the splash phenomenon has been the focus of many researchers due to its relevance in the combustion process of small-bore, direct-injected gasoline and diesel engines, as well as in a variety of other industrial devices in which sprays impinge on solid surfaces. Bai and Gosman (1995) developed a model to predict the outcomes of spray droplets impacting on a wall with temperatures below the fuel boiling point. This model, which has been formulated using a combination of simple theoretical analysis and experimental data from a wide variety of sources, was later improved (Bai *et al.,* 2002) by refining the dissipation energy term and by enhancing the post-splashing characteristics. In fact, recently, significant attention has been given to this regime either through the definition of transition criteria that better fit specific conditions of the experimental configuration under study or by characterizing the behaviour of the drop during all stages of the regime (expansion of the lamella, crown formation and propagation, etc.) through both theoretical analyses and experimental data. Beyond the transition criteria, another aspect that controls the characteristics of the secondary droplets after the impacts is the energy dissipation term and thus, it is essential its proper definition for adequately modelling these multi-phase flows. However, contrary to spreading, there is little literature available related to this particular parameter and, more important than that is the fact that there is a certain ambiguity even for what it represents exactly. In addition, the majority of the dissipative energy loss relationships have been deduced for the spread regime, i.e., from the beginning of the expansion of the lamella until the drops reaches its maximum extent (without splashing). This situation can be overcome through some simplifying assumptions, which obviously carries inaccuracy.

The present work is dedicated to the study of the sprays impingement onto a solid wall through a crossflow. The major purpose of the thesis is to improve the accuracy of the base model, which is the model of Bai *et al.* (2002), through the employment of both new

correlations for the deposition/splash transition criteria and energy dissipation loss relationships available in the literature. The numerical predictions are then compared with the experimental data of Arcoumanis *et al.* (1997) for two crossflow rates (5 and $15\ m/s$).

From the results, it can be concluded that the employment of different transition criteria can bring better results (see also Silva *et al.*, 2011). On the other hand, no improvements were seen by the employment of the new energy dissipative loss relationships in the base models, which calls for further research in this particular matter.

Keywords

Spray, Wall Impingement, Droplet Impact, Splash, Transition criteria, Energy Dissipation

Resumo

A modelação de escoamentos turbulentos multifásicos tem vindo a gerar grande interesse nas últimas décadas na comunidade científica devido à sua importância em diversas aplicações, como por exemplo em sistemas industriais e ambientais, ou em processos químicos e biomédicos. De facto, no que diz respeito às aplicações industriais, o impacto do spray de combustível nas superfícies dos motores tornou-se um assunto de elevado interesse devido à sua influência na preparação da mistura antes da combustão e, consequentemente, no desempenho do motor e emissão de poluentes (Barata e Silva, 2005). Contudo, continua a ser necessária bastante investigação no que toca à interacção spray-parede mas também relativamente aos fenómenos específicos que ocorrem durante todo o processo. Estas lacunas não permitem ainda definir quais as condições óptimas no cilindro para o melhor desempenho do motor. Assim, o principal desafio para os investigadores prende-se com o estudo aprofundado dos fenómenos envolvidos no processo de impacto de sprays tanto através de análises teóricas como de investigações experimentais.

Entretanto, o fenómeno de *splash* tem vindo a ser objecto de estudo de muitos investigadores devido à sua relevância no processo de combustão em motores de injecção directa a gasolina e gasóleo, mas também numa grande variedade de outros dispositivos industriais nos quais ocorre impacto de sprays em superfícies sólidas. Bai and Gosman (1995) desenvolveu um modelo para prever os resultados do impacto de gotas de sprays em paredes com temperatura abaixo do ponto de ebulição do combustível. Este modelo – formulado usando uma combinação de análises teóricas e dados experimentais de uma grande variedade de fontes – foi mais tarde melhorado (Bai *et al.,* 2002) refinando o termo da energia de dissipação e melhorando as características de pós-impacto. De facto, recentemente tem sido dada uma grande atenção a este regime quer através da definição de critérios de transição que melhor se adequam às condições da configuração experimental em estudo, quer através da caracterização do comportamento das gotas durante todos os estágios do regime (expansão da "lamela", formação da coroa e sua propagação, etc.) através de análises teóricas e de dados experimentais. Para além dos critérios de transição, outro dos aspectos que controlam as características das gotas secundárias após impacto é a energia de dissipação viscosa, sendo assim essencial a sua correcta definição para a modelação destes escoamentos. Contudo, ao contrário do *spreading*, existe pouco literatura disponível relacionada com este parâmetro em específico e, mais importante ainda, existe alguma ambiguidade sobre aquilo que este parâmetro representa exactamente. Além disso, a maioria das relações da energia de dissipação foram deduzidas para o regime de *spread*, i.e., desde o início da expansão da lamela até que a gota atinja a sua extensão máxima, ou seja, sem ocorrer *splash*. Esta situação pode ser superada através de algumas hipóteses assumidas mas que, obviamente acarretam erros.

O presente trabalho é dedicado ao estudo de impacto de sprays em paredes sólidas com a presença de um escoamento cruzado. O principal objectivo da tese é melhorar a qualidade do modelo de atomização de base utilizado (modelo do Bai *et al.*, 2002) através da utilização de novas correlações – para os critérios de transição entre *deposition* e *splash* –, e novas relações – para a energia de dissipação – disponíveis na literatura. Os resultados numéricos são então comparados com os dados experimentais do estudo do Arcoumanis *et al*. (1997) para escoamentos cruzado com duas velocidades diferentes (5 e 15 m/s).

Dos resultados apresentados, conclui-se que a utilização de diferentes critérios de transição pode trazer melhores resultados mas apenas em alguns parâmetros estudados (ver também Silva *et al., 2011)*. Por outro lado, não foram encontradas melhorias quando se introduziram no modelo de base as novas equações para a energia de dissipação, deixando claro a necessidade premente de maior investigação nesta área em particular.

Palavras-chave

Spray, Impacto de parede, Impacto de gotas, Splash, Critérios de transição, Dissipação de energia

Resumo Alargado

A modelação de escoamentos turbulentos multifásicos tem vindo a gerar grande interesse nas últimas décadas na comunidade científica devido à sua importância em diversas aplicações, como por exemplo industriais e ambientais, ou em processos químicos e biomédicos. De facto, no que diz respeito às aplicações industriais, o impacto do spray de combustível nas superfícies dos motores tornou-se um assunto de elevado interesse devido à sua influência na preparação da mistura antes da combustão e, consequentemente, no desempenho do motor e emissão de poluentes (Barata e Silva, 2005). Contudo, continua a ser necessária bastante investigação no que toca à interacção spray-parede mas também relativamente aos fenómenos específicos que ocorrem durante todo o processo. Estas lacunas não permitem ainda definir quais as condições óptimas no cilindro para o melhor desempenho do motor. Assim, o principal desafio para os investigadores prende-se com o estudo aprofundado dos fenómenos envolvidos no processo de impacto de sprays tanto através de análises teóricas como de investigações experimentais.

Entretanto, o fenómeno de *splash* tem vindo a ser objecto de estudo de muitos investigadores devido à sua relevância no processo de combustão em motores de injecção directa a gasolina e gasóleo, mas também numa grande variedade de outros dispositivos industriais nos quais ocorre impacto de sprays em superfícies sólidas. Bai and Gosman (1995) desenvolveu um modelo para prever os resultados do impacto de gotas de sprays em paredes com temperatura abaixo do ponto de ebulição do combustível. Este modelo – formulado usando uma combinação de análises teóricas e dados experimentais de uma grande variedade de fontes – foi mais tarde melhorado (Bai *et al.,* 2002) refinando o termo da energia de dissipação e melhorando as características de pós-splash. De facto, recentemente tem sido dada uma grande atenção a este regime quer através da definição de critérios de transição que melhor se adequam às condições da configuração experimental em estudo, quer através da caracterização do comportamento das gotas durante todos os estágios do regime (expansão da "lamela", formação da coroa e sua propagação, etc.) através de análises teóricas e investigações experimentais.

Para além dos critérios de transição, outro dos aspectos que controlam as características das gotas secundárias após impacto é a energia de dissipação viscosa, sendo assim essencial a sua correcta definição para a modelação destes escoamentos. Contudo, ao contrário do *spreading*, existe pouco literatura disponível relacionada com este parâmetro em específico, mas, mais importante ainda, existe alguma ambiguidade sobre aquilo que este parâmetro representa exactamente. Além disso, a maioria das relações da energia de dissipação foram deduzidas para o regime de *spread*, i.e., desde o início da expansão da lamela até que a gota atinja a sua extensão máxima, ou seja, sem ocorrer *splash*. Esta situação pode ser superada através de algumas hipóteses assumidas mas que, obviamente acarretam erros.

O presente trabalho é dedicado ao estudo de impacto de sprays em paredes sólidas com a presença de um escoamento cruzado. O principal objectivo da tese é melhorar a qualidade do modelo de base (modelo do Bai *et al.,* 2002) através da utilização de novas correlações – para os critérios de transição entre *deposition* e *splash* –, e novas relações – para a energia de dissipação – disponíveis na literatura.

O modelo de Bai *et al.* (2002) considera quatro regimes de impacto: *stick, rebound*, *spread* e *splash*. A existência de cada um destes regimes depende das características das gotas incidentes e das condições da superfície sólida, incluindo se esta se encontra seca ou molhada (Bai and Gosman, 1995). Para ambos os casos, o critério de transição que define a separação entre os regimes de *spread* e *splash* foi derivada do dados de Stow e Hadfield (1981), resultando num número de Weber crítico dependente do número de Laplace. Os limites entre os regimes de *stick* e *rebound*, e *rebound* e *spread* – que foram derivados dos dados de Lee e Hanratty (1988) – para paredes molhadas foram estabelecidos com números de Weber de 2 e 20, respectivamente. Além disso, Bai and Gosman (1995), na primeira versão do modelo, deduziram as suas próprias equações para a energia de dissipação (função do número de Weber crítico) e, posteriormente refinadas no modelo seguinte (Bai et al, 2002).

Este modelo foi incorporado num método computacional 3D baseado nas soluções das equações de *Reynolds-averaged Navier-Stokes* para a fase do gás, e um modelo SSF (*stochastic separated flow*) baseado no *Eddy lifetime* para a fase dispersa. O modelo resolve as equações de energia para cada gota secundária – podendo esta resultar em (até) seis parcelas – e os tamanhos das gotas secundárias resultantes do *splash* seguem uma distribuição característica. O modelo produziu resultados satisfatórios para o caso particular testado pelos autores, mas não obtiveram evidências claras da aplicabilidade do modelo a outras condições.

Assim, numa primeira fase deste trabalho, para além do critério de transição original do modelo de atomização usado (Bai *et al.,* 2002), foram testadas no modelo global as correlações estabelecidas por Mundo *et al.* (1995), Cossali *et al.* (1997), Senda *et al.* (1999) e, Huang e Zhang (2008). Na segunda fase do trabalho, testaram-se várias equações para a energia de dissipação encontradas na literatura e deduzidas pelos seguintes autores: Chandra *et al.* (1991) e Pasandideh-Fard *et al.* (1996), para além da equação original do modelo. Os termos não-identificados da equação deduzida por Chandra *et al.* (1991) foram quer deduzidos de outras hipóteses assumidas, quer obtidos de dados de outras fontes. Os termos da energia de dissipação foram inseridos no modelo de base original. Numa segunda instância, trocou-se o critério de transição do modelo original (Bai *et al.,* 2002) pelo do Cossali *et al.* (1997) que tinha apresentado bons resultados no estudo anterior para um caso específico. Todos os resultados numéricos são comparados com os dados experimentais do estudo do Arcoumanis *et al.* (1997) para escoamentos cruzado com duas velocidades diferentes (5 e $15\ m/s$). São apresentados gráficos referentes à distribuição da frequência dos diâmetros das gotas mas também gráficos apresentando a velocidade normal de cada classe de gotas em função do diâmetro das gotas. Todos os resultados são apresentados em quatro posições diferentes ao longo da extensão do domínio da solução tanto para gotas com movimento

ascendente como descendente. Além disso, todas as simulações foram efectuadas para um escoamento cruzado de $5\ m/s$ e $15\ m/s$.

Dos resultados apresentados, conclui-se que a utilização de diferentes critérios de transição pode trazer melhores resultados (ver também Silva *et al., 2011)*. A utilização de critérios de transição do Cossali *et al.* (1997) apresentou significativas melhorias nos resultados das distribuições dos diâmetros das gotas com movimento ascendente para ambas as velocidades de escoamento cruzado utilizado. Contudo, o mesmo critério apresentou resultados menos coerentes nos gráficos das velocidades das gotas com sentido ascendente. Por outro lado, não foram encontradas melhorias quando se introduziram no modelo de base as novas equações para a energia de dissipação, o que alerta para a necessidade de mais estudos sobre este parâmetro em particular.

This page has been intentionally left blank for double-sided copying.

Index

This page has been intentionally left blank for double-sided copying.

Figure Index

This page has been intentionally left blank for double-sided copying.

Table Index

This page has been intentionally left blank for double-sided copying.

Nomenclature

C_k , $C_{\varepsilon 3}$	Empirical constant
C_μ, C_1, C_2	Dimensionless model constant
c_f	Friction coefficient
c_p	Specific heat
C_T	The turbulence coefficient
C_D	Drag coefficient
d	General diameter of a droplet
$\bar{d}$	Scale parameter; mean diameter
d_{max}	Maximum spread of the droplet upon impact
d_{32}	Sauter mean diameter
d_{sp}	Diameter of film disc
dt	The time step
d_v	Volumetric mean diameter
e	Restitution coefficient
E_K	Droplet kinetic energy
E_σ	Droplet surface energy
E_D	Dissipated energy
F	Force
f	Frequency
G	Turbulence energy production term
g	Gravitational acceleration
g_i	External forces
h	Thickness of the film disc
K	Splashing/deposition dimensionless parameter
k	Correction factor; turbulent kinetic energy
K_1	Modified Bessel function of third kind and first order.
l_e	Eddy length scale
m	Mass
N_S	Total number of secondary droplets
N	Number of droplets
N_{IB}	Number of impacts causing break-up
N_{IT}	Total number of impacts

q	Scale parameter
p	Number of secondary parcels; random number [0;1]; pressure
Q_i	Source terms
R_{uv}	Correlation coefficient
r_{32}	Sauter mean radius (SMR)
R_a	Surface roughness
r	General droplet radius
S_U, S_H, S_m S_k, S_ε	Inter-phase source terms
$S_{\Phi, g}$	Source term of the gas
$S_{\Phi, d}$	Source term of the droplet.
$S_{\Phi i}$	Source term due to interphase transport
$S_{\Phi m}$	Source term due to transfer caused by evaporation
T_B	Liquid boiling point temperature
T_{Leid}	Leidenfrost temperature
T_N	Nukiyama temperature
T_{PA}	Pure adhesion temperature
T_{PR}	Pure rebound temperature
T_s	Surface temperature
T_W	Wall temperature
t	Time
t_c	Time scale; eddy transit time
V	Velocity; volume
v_{drift}	Relative velocity between the particle and the fluid

Greek symbols

α	The form of the density function; random number [0;1]
β	The shape of the density function
Δt	Time steps
ε	Turbulent kinetic energy dissipation rate
δ	Wall film thickness; scale parameter
δ_{bl}	Boundary layer thickness
ρ	Density
β_{max}	Maximum diameter ratio of film disc
σ	Surface tension; variance of a Gaussian distribution
σ_k	Turbulent Prandtl numbers for kinetic energy

σ_ε	Turbulent Prandtl numbers for dissipation
τ_{air}	Shearing force between the film and the gas by unit surface area
τ_p	Droplet relaxation time
τ_{FL}	Eddy lifetime
τ_w	The shearing stress
μ	Viscosity; location parameter
ν	Dynamic viscosity
ν_T	Turbulent kinematic viscosity
Γ	Effective diffusion coefficient
Φ	Dependent variable
Φ_p	Scalar value
ϕ	Dissipation function
ϕ_{az}	Azimuthal angle
θ_a	Advancing contact angle
θ_I	Incident angle
θ_S	Reflection angle; ejection angle of secondary droplets
ψ	Break-up probability

Subscripts

a	After impact
b	Before impact
c	Critical value
d	Droplet
f	Liquid film
I	Incoming droplet or incident droplets
N	Normal components
p	Refer to the particle
S	Splash or secondary droplets; refer to surface conditions
R	Rebound
T	Tangential components

Superscripts

u'	Fluctuation (rms) velocity
$\dot{m}$	Evaporation rate
$\vec{V}$	Velocity vector

Non-dimensional numbers

La	Droplet Laplace number	$La = \frac{\rho_d \sigma d_I}{\mu^2}$
Oh	Droplet Ohnesorge number	$Oh = \frac{\sqrt{We}}{Re} = \frac{\mu}{\sqrt{\rho_d \sigma d_I}}$
Re	Droplet Reynolds number	$Re = \frac{\rho_d d_I \lvert u_{rel} \rvert}{\mu}$
r_m	Mass ratio	$r_m = \frac{m_S}{m_I}$
We	Droplet Weber number	$We = \frac{\rho_d V_{IN}^2 d_I}{\sigma}$
R_{ND}	Dimensionless roughness	$R_{ND} = \frac{R_a}{d_I}$
δ_{non}	Non-dimensional wall film thickness	$\delta_{non} = \frac{\delta}{d_I}$

I. Introduction

1. Background

The modelling of multiphase flows has been gathering high interest in the last decades due to its relevance in several applications, such as in industrial processes (e.g. spray drying, transport systems, and manufacturing and material processing), energy conversion and propulsion (e.g. pulverized-coal-fired furnaces and solid propellant rocket) and fire suppression (e.g. Sprinkler system). Multiphase flows can be subdivided into four categories: gas-liquid, gas-solid, liquid-solid and three-phase flows (Crowe *et al.,* 1998). The spray impingement onto solid walls is a very specific example of gas-liquid flows, which can be found in each one of the application specified above. Fuel injection systems in internal combustion (IC) engines, gas turbines, ink jet printing, cooling systems, spray painting and coating are some examples of this particular multiphase flow.

The impact of fuel droplets onto a solid wall became a subject of great importance in the scientific community because it is a frequent event in injection systems (both in direct and indirect), which affects the mixture preparation before the combustion and, consequently, the engine performance and pollutant emissions (Cartellieri and Wachter, 1987). In small bore direct injection (DI) engines, the effects of droplet/wall interactions can be quite evident due to the reduced distance between the injector and the piston and the higher rates of injection, which results in increased emissions of gases such as nitric oxides and unburned hydrocarbons (Matsui and Sughiara, 1988).

However, there is still a lack of knowledge concerning the spray-wall interaction but also regarding the exact phenomenon occurring during the process, which does not allow clarifying the most favorable conditions for the optimal engine performance. Hence, the main challenge for the investigators lies in attaining a much deeper understanding of the phenomena involved in the spray impingement process, through either theoretical analysis or experimental investigations.

Despite spray impact phenomena are difficult to analyze in operating engines – because of the problems of access –, useful information can be obtained, for example, through photographic techniques in specially adapted engines (e.g. Winterbone *et al.,* 1994). The details of the information that can be obtained from this approach are very limited, and it is difficult to alter the test conditions. For these reasons, most of the recent experimental investigations of impacting sprays have been conducted in specially constructed test rigs or bombs (e.g. Arcoumanis *et al.,* 1997; Kalantari and Tropea, 2010). Under these circumstances, many experimental investigations have already been carried out to study the complex interactions between individual design parameters and working conditions: Katsura *et al.,* (1989), and Chandra and Avedisian (1991) studied the region of impingement of single droplets on rigid surfaces; Fujimoto *et al.,* (1990) and Hardalupas *et al.* (1991) investigated

the influence of different angles of impact in the size range of the droplets; Andreassi *et al.* (2007) studied the influence of high injection pressure on the spray impingement phenomenon; and Su and Yao (1999) found that the spray-wall impactions depends on the distance from the nozzle to the impacted surface. In addition, numerous parameters were found to influence the outcomes during the impingement process. The frequency of injection alters the boundary conditions at the spray nozzle and greater injection pressures extend the area of impact (Park and Lee, 2004) and increase the droplet impact velocity. The latter parameter improve the number flux of small size droplets which are prone to interact with the surrounding air and therefore with vaporization and mixing (Meingast *et al.,* 2000). Arcoumanis and Chang (1993) showed that the heat transfer rate increase with the impact velocity and with the frequency of injection and later (Arcoumanis and Cutter, 1995) added crossflow to simulate the swirl movement used in practical engines to enhance the mixture preparation inside the cylinder. Also, the effect of a fluid film on the spray impingement experiment has been studied (Ozdemir and Whitelaw, 1992). It was found that that the impact on the wall generated a new fraction of larger droplets which were spattered out of the liquid film.

In order to clarify the characteristics of the spray/wall interaction and taking part of the detailed information that was difficult to measure by mean of the experimental work, the computational modelling also grew up in the lasts decades. The first attempt to clarify the spray wall interaction process through numerical simulation of spray impingement was performed by Nabber and Reitz (1988), who considered three alternative ways of tracking the droplets after the impact: the stick model, in which impinging droplets are stick on the wall; the rebound model, in which the droplets are reflected elastically; and, finally, jet model which assumes that after impingement the droplets are moving along the wall surface with the same velocity magnitude as before the impact. The authors employed the KIVA code (Amsden *et al.* 1989) and of the three ways of post-impingement droplet tracking, the Jet model was found to produce the best results.

Later, Senda *et al.* (1994) developed an impingement model to predict the secondary atomization and liquid film formation resulting from the impact of the incident droplet on the wall but also the heat transfer between the wall film and the heated wall. The model was mainly based on the previous work of Wachters and Westerling (1966) but obtained good results only for the particular initial injection and impingement conditions considered.

In 1993, Yoshikawa *et al.* (1993) performed a 3-D modelling of the spray-valve interaction and observed extensive drop interaction between the induction port and intake valve. This interaction is an important source of liquid atomization and vaporization. A better understanding of these interactions between the liquid and induction surfaces was thinking to help in designing injection systems and control strategies to improve engine performance and to control emissions. Nagaoka *et al.* (1994) used a particle film model in 3D calculations of SI engines. However, their model could not predict the transient behaviour of the wall film effectively because of the assumption that the wall film did not move. As an effort to resolve

this problem, Lee (1999) proposed the static model for predicting transient behavior of films by modifying the lens model of Nagaoka *et al*. (1994).

Meanwhile, it turned out that splash was an important physical phenomenon in small-bore, direct-injected gasoline and diesel engines, as well as in a variety of other industrial devices in which sprays impinge on solid surfaces. Bai and Gosman (1995) developed a model to predict the outcomes of spray droplets impacting on a wall with temperatures below the fuel boiling point. This model, which has been formulated using a combination of simple theoretical analysis and experimental data from a wide variety of sources, was later improved (Bai *et al.*, 2002) by refining the energy dissipation loss and by enhancing the post-splashing characteristics. Similarly, Stanton and Rutland (1996) proposed a sub-model involving the splash effect and liquid film model. However, while in the Bai and Gosman model, the ejection angle was randomly chosen in the range from 5° and 50°, in the Stanton and Rutland model, it was uniformly determined from linear interpolation of the experimental data obtained by Mundo *et al*. (1995).

In fact, recently, significant attention has been given to this regime either through defining transition criteria and post-impingement characteristics that better fit specific experimental configuration with certain conditions or by characterizing the behavior of the drop during all the stages of the regime (expansion of the lamella, crown formation and propagation, etc.) through both theoretical analysis and experimental investigation.

2. Literature Review

The review of the relevant background and central concepts required for the comprehension of the work is introduced in this chapter and the various phenomena are presented in the following sections.

2.1. Wall Impingement

The characterization of the various phenomena resulting from the impact of droplets onto solid and liquid surfaces is a complex and interdisciplinary task which cover a wide variety of technical applications, such as ink-jet printing, rapid spray cooling of hot surfaces (turbine blades, rolls in rolling mills for steel production, lasers, semiconductor chips, and electronic devices), annealing, quenching of aluminium alloys and steel, fire suppression by sprinklers, internal combustion engines (intake ducts of gasoline engines or piston bowls in direct-injection diesel engines), incinerators, spray painting and coating, plasma spraying, and crop spraying. Understanding the associated physical phenomena is of utmost importance in order to formulate reliable boundary conditions in numerical codes for spray simulation. This explains the large number of studies, reported in the literature, on the dynamics of impinging droplets, within quite dissimilar scientific areas.

Pioneering studies on certain aspects of droplet impact were conducted by Tomlinson (1861; 1864), Worthington (1876; 1877; 1908), Thompson and Newall (1885) in the second half

of the nineteenth century. In fact, Worthington (1908) was the first to investigate these impacts systematically and to photograph water droplets as they impinged on a solid surface. Despite the limited technology of that time, the author could distinguish between spread and disintegration, which he related to the different impact velocity. Subsequently, many experimental studies have been carried out with the aim of describing the impact of droplets and determining impact regimes (Rein, 1993; Prosperetti and Oguz, 1993; and Tropea, 1999).

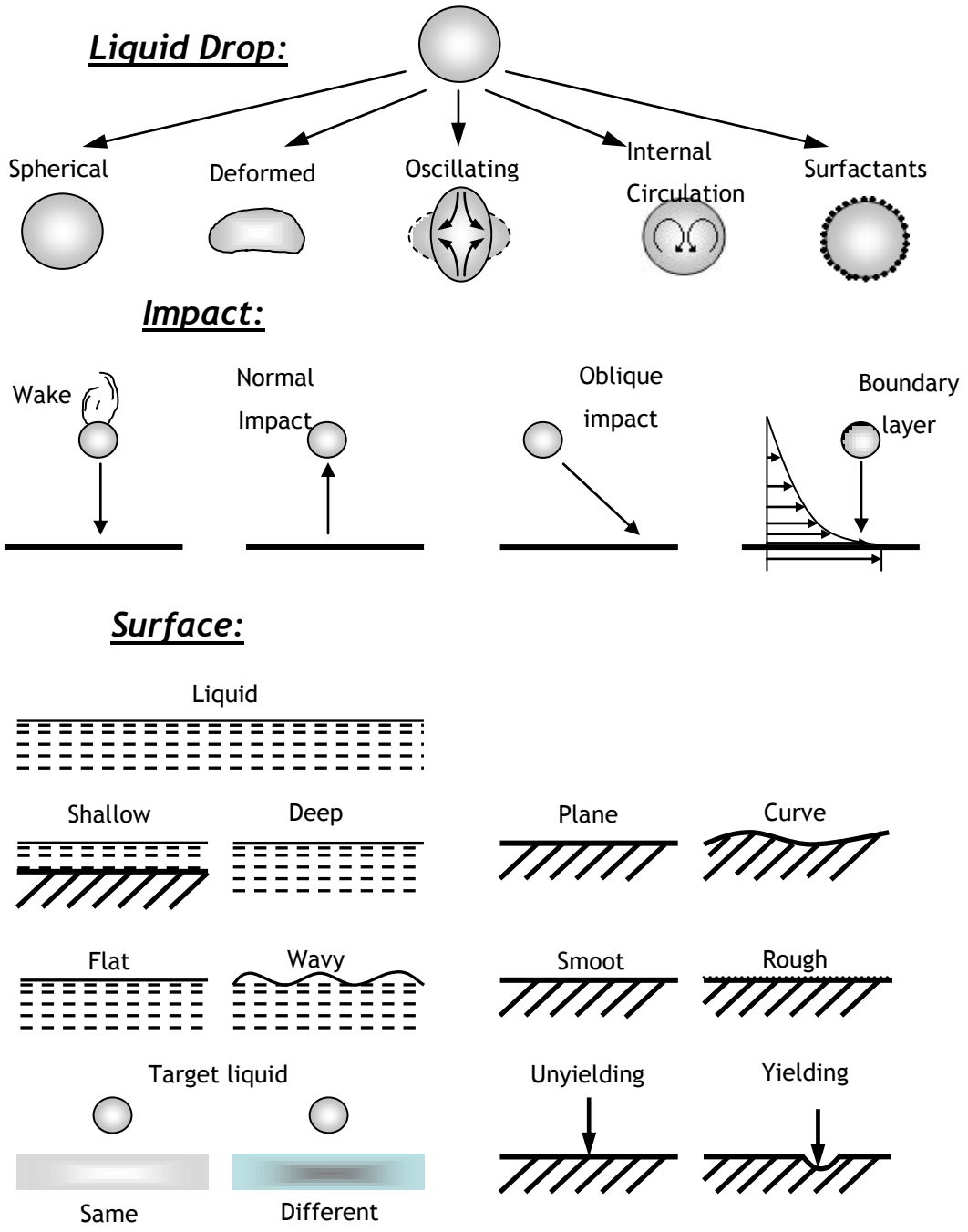

Figure I-1: Survey of parameters governing the impact of a liquid drop (Rein, 1993).

However, there are numerous parameters that influence the droplet and the collision regime (Figure I-1) which result on different outcomes: a drop may be spherical or elliptic (due to oscillations) at the moment of impact; it may impact on the free surface of a liquid in a deep pool, on a thin liquid film on a wall, or on a dry solid surface; the impact may be normal (perpendicular) or oblique, in air or in vacuum; the liquid may be Newtonian or non-Newtonian (e.g., a viscoelastic polymer or a surfactant solution); the liquids of the drop and pool/film may be miscible or immiscible; the solid surface may be hard or soft, rough or smooth, chemically homogeneous or heterogeneous, it may also be porous, flat or curved, at a temperature different from that of the drop or the same. On liquid surfaces, pre-existing or generated waves may affect the flow pattern. The impact may result in the drop spreading over the solid surface, receding, rebounding, or even levitating if the evaporation near a hot wall is sufficiently strong for the Leidenfrost effect; a crater may form in the liquid bulk in a pool and later on collapse, leading to the formation of the so-called Worthington jet, which flows out from its centre and is subjected to capillary breakup. The impact on a liquid film may result in crown formation, propagation, and breakup, as well as in tiny bubble trapping, or, under certain conditions, non-coalescence and even rolling over the surface. In addition, the outcome of drop impact depends on the impact velocity, its direction relative to the surface, drop size, the properties of the liquid (its density, viscosity, viscoelasticity, and some other non-Newtonian effects for rheological complex fluids), the surface or interfacial tension, the roughness and wettability of the solid surface, the non-isothermal effects (e.g., solidification and evaporation), and air entrapment. In very strong impacts, liquid compressibility is also a factor (Yarin, 2006).

Prediction of the exact mechanism involves accounting for the relative magnitude of the forces involved at the impact of the droplet, which are usually grouped in dimensionless numbers. The main dimensionless groups governing drop impact and employed in the present work are presented as follow:

Table I-1: Main dimensionless groups governing drop impact.

Dimensionless Number	Description	Definition	Relation
Weber Number	Represents a measure of relative importance of droplet kinetic energy and surface energy.	$We = \frac{\rho_d V^2 d_I}{\sigma}$	
Reynolds Number	Shows the relation between inertial and viscous forces.	$Re = \frac{\rho_d d_I \lvert u_{rel} \rvert}{\mu}$	
Laplace Number	Measures the relative importance of surface tension and viscous forces acting on the liquid.	$La = \frac{\rho_d \sigma d_I}{\mu^2}$	$La = \frac{Re^2}{We} = Oh^{-2}$
Ohnesorge Number	Describes the relation between capillarity and viscous forces and is important in the characterization of disintegration processes.	$Oh = \frac{\mu}{\sqrt{\rho_d \sigma d_I}}$	$Oh = \frac{We^{\frac{1}{2}}}{Re}$

The essential influencing parameters affecting drop impact are reviewed in the following sections in order to provide an essential state of the art related with droplet and spray impingement.

2.1.1. Impingement Regimes

Fuel sprays impinging on surfaces involve a collection of droplets that interact between them. However, given the complexity of the spray flow, an accurate description of single droplet impacts provides an essential understanding of the fundamental mechanism which constructs a spray. From experimental data of single droplet impinging on surfaces, Bai and Gosman (1995) identified four main impingement regimes (ordered according to the impact energy, in ascendant order): stick, rebound, spread and splash. These regimes describe how a droplet behaves in the impingement process and the existence of each one depends on the properties of the impinging droplets and the impingement surface.

The *stick regime* occurs at low Weber numbers and when the wall temperature, T_w, is below a characteristic temperature, T_{PA}. Here, the droplet adheres to the wall in a nearly spherical form. Increasing the impact energy and under specific conditions, the droplet may bounces off the surface after the impact (see Figure I-2 a)):

- If the wall is dry and $T_w \geq T_{PR}$, it occurs where the contact between the liquid in the droplet and the wall is prevented by a layer of vapour.
- If the wall is wet and the impact energy is low, it happens when an air film is trapped between the droplet and the liquid film, which makes energy losses low and results in bouncing.

a) Rebound and Partial Rebound

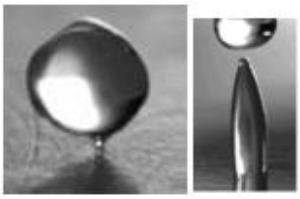

b) Spread (Deposition)

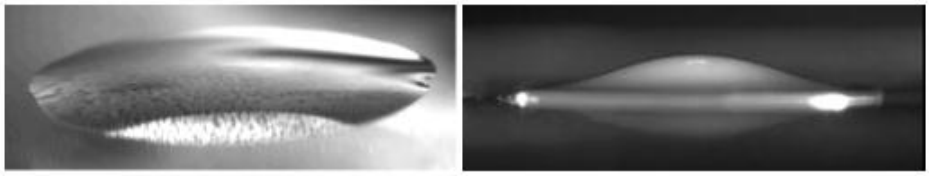

c) Prompt and Corona Splash.

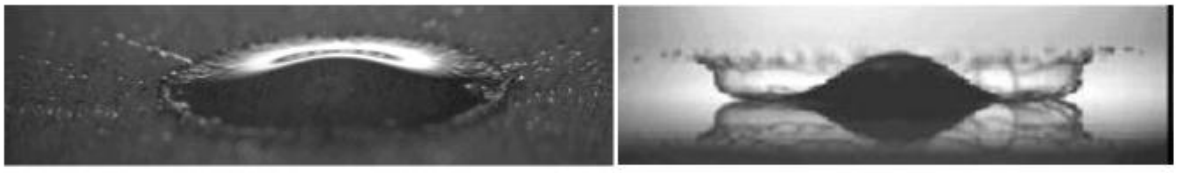

Figure I-2: Morphology of drop impact. (Rioboo et al., 2001)

The *spread regime* happens when the droplet impact on the wall with moderate energy and spread out to form a wall film taking the shape of a lamella with visible outer rim, as shown in Figure I-2 b). If there is a wall film on the surface, the droplet will merge with it. For last, at very high impact velocities, the lamella take the shape of crowns consisting on a

thin liquid sheet with an unstable free rim – the *splash regime* – as shown in Figure I-2 c). Splashing may be manifested in a variety of forms ranging from ejection of a single, central droplet via jetting to numerous droplets evolved from a crown.

In 2001, Rioboo *et al.* (2001) added the occurrence of fingering, replaced the ambiguous splash with "disintegration" and differentiated four disintegration mechanisms: prompt splash, corona splash, receding splash and partial rebound. The authors categorized the impact regimes according to their characteristics time scale as presented in Figure I-3. Later, Moita and Moreira (2007) added the finger breakup regime.

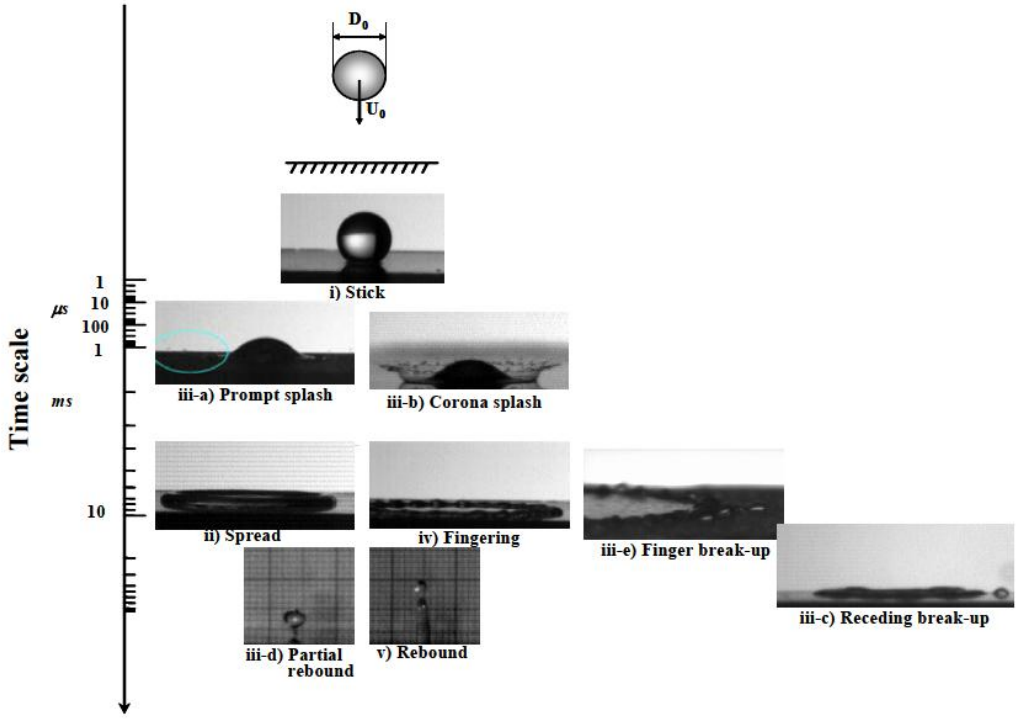

Figure I-3: Possible outcome of single droplets impacting onto non-heated dry surfaces. The classification is in accordance with the characteristic time scale, as in Rioboo et al. (2001). (Moreira et al., 2010)

The *fingering regime* takes place at moderate impact velocities, when the rim of the lamella destabilize during the spreading phase at a dry surface (Yarin, 2006). Those regular structures may grow ahead of the contact line and further breakup during the last stages of spreading. In the presence of a rough surface, small portions of the lamellas fail to transpose those asperities and, consequently, the surface tensions don't succeed in preserve the cohesion of the lamella – this mechanism is called as *receding break-up*.

2.1.2. Effect of Heat Transfer

The surface temperature is an important parameter that affects the outcome of the spray impingement phenomenon. However, the consideration of the surface temperature factor introduces further complexity in the analysis of the interaction between the drops and the surface, making it more difficult to an accurate description of the spray impingement

phenomenon. Depending on the surface temperature, diverse heat transfer mechanisms may develop when a droplet impacts onto a heated surface. Bai and Gosman (1995) have identified the following characteristic temperatures that are used to identify the impingement regimes on hot solid surfaces:

T_B Liquid boiling point temperature;

T_{PA} Pure adhesion temperature: below this temperature an impinging droplet adheres at low impact energy;

T_N Nukiyama temperature: temperature of maximum evaporation for a specific liquid (CHF – critical heat flux), also known as critical temperature (Nukiyama, 1966);

T_{PR} Pure rebound temperature: above this temperature bounce occurs at low impact energy;

T_{Leid} Leidenfrost temperature: temperature of minimum evaporation for a specific liquid (Leidenfrost, 1966).

The relation for the characteristic temperatures defined above is as follows:

$$T_B < T_{PA} < T_N < T_{PR} < T_{Leid}$$

Four main heat transfer regimes can be identified during spray impingement and heated surface interaction, as depicted in Figure I-4. These regimes are usually associated with temperature dependence of the heat removed by droplet gently deposited onto a hot surface, or conversely, by the droplet lifetime (Moreira *et al.*, 2010):

I) Single phase/film evaporation ($T_w < T_{sat}$): heat transfer occurs mainly by conduction and free convection, without phase change. This regime is upper limited by the saturation temperature of the liquid;

II) Nucleate boiling ($T_{sat} < T_w < T_{CHF}$): as the surface temperature overcomes the saturation temperature of the liquid and the heat transfer from the surface to the liquid is large enough to cause phase transition, vapour bubbles are formed close to the wall (region IIa) and move through the liquid by buoyancy up to the liquid–air interface (region IIb). The heat is removed by vaporization and increases with the surface temperature up to a maximum at the Critical Heat Flux Temperature (T_{CHF});

III) Transition ($T_{CHF} < T_w < T_{Leidenfrost}$): as the vaporization rate increases, an insulating vapour layer forms at the liquid–solid interface and the heat flux decreases down to a local minimum at the Leidenfrost temperature.

IV) Film boiling/Leidenfrost regime ($T_w > T_{Leidenfrost}$): a stable vapour layer forms, which precludes contact between the droplet and the surface and through which heat is transferred by conduction. Radiation starts to play a non-negligible role only at higher temperatures (region IVb), and in the case of fuel droplets, ignition may also occur, after which a slight decrease in droplet lifetime curve occurs (region IVc in Figure I-4b).

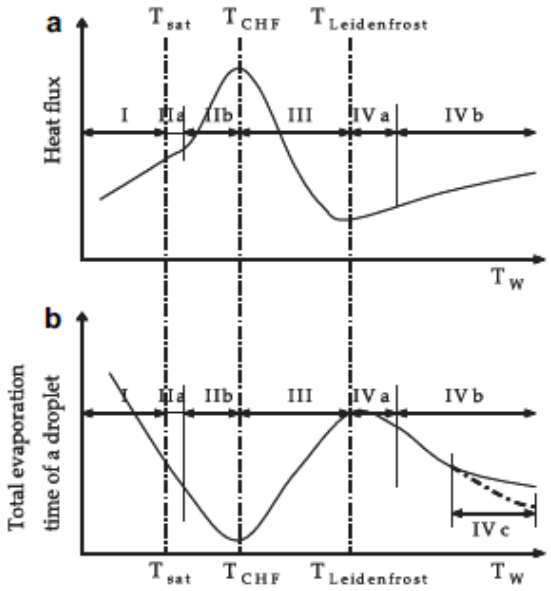

Figure I-4: Boiling and lifetime curves of a droplet gently deposited on a heated surface. (Moreira et al., 2010)

However, Wang *et al.* (2000) showed that this association is not so straightforward but, for ease of analysis, it is convenient to follow the picture given by Naber and Farrel (1993) that the film evaporation and nucleate boiling regimes are related with a wetting regime (region I and II) while the film boiling regime is associated with a non-wetting regime (region IV). In the transition regime, the liquid is in contact with the surface only intermittently, with partial contact only, due to separations from the surface caused by vapour expelled from the liquid (region III).

As said before, above the temperature corresponding to the local minimum in the boiling curve, the Leidenfrost phenomenon occurs, which is characterized by the appearance of a thin vapour layer, or vapour cushion, between the liquid and the surface (why referred as a non-wetting regime). With fuel drops and at high wall temperatures, auto-ignition of the fuel occurs (Rein, 2002a). Since it only takes place with liquid fuel, this doesn't appear in Figure I-4. Based on these observations, Habachi *et al.* (1999) made an assumption that the piston does not have any significant fuel film when the surface temperature exceeds the average between the boiling point and Leidenfrost temperature. When the wall temperature is above T_{Leid} the wall is assumed to be dry.

Notwithstanding the universality of the previous heat transfer regimes for impacting droplets and sprays, the critical points of the boiling curves are influenced by impacting conditions (Panão and Moreira, 2005). In fact, the Leidenfrost temperature depends not only on the materials and wall properties but also on various other parameters such as the initial mass, size and temperature of the droplet; the impact velocity and angle of impact; and the pressures in the ambient gas (Baumeister and Simon, 1973; Bernardin and Mudawar, 1999; Nishio and Hirata, 1978; Yao and Cai, 1978; Emmerson, 1975). In addition, extensive researches have been developed to observe the influence of the fluid properties, surface roughness, and surface contamination on the Leidenfrost temperature, e.g. Bernardin and

Mudawar (1999). On the other hand, some authors prefer to define the Leidenfrost temperature as a dynamic property (Gottfried *et al.*, 1966) which can be obtained experimentally as the temperature at which the vapour layer rebounds the droplets (Naber and Farrel, 1993). This is the so-called "pure rebound temperature" which is, in fact, the boundary considered in the majority of the studies reported in the literature, since the identification of the different heat transfer regimes is often based on the observation of droplet morphology.

Different representations of the impinging regimes, for a dry heated wall, have been proposed by Bai and Gosman, 1995; Lee and Ryu, 2006; and Rein, 2002 (Figure I-5). These representations offer a good qualitative description of the heat induced phenomena despite the difference in the criteria used to define the boundary temperatures: they can be based on the observations of the droplet morphology (for the case of the first two authors above mentioned) or on the variation of the Leidenfrost temperature with impact conditions (Rein, 2002).

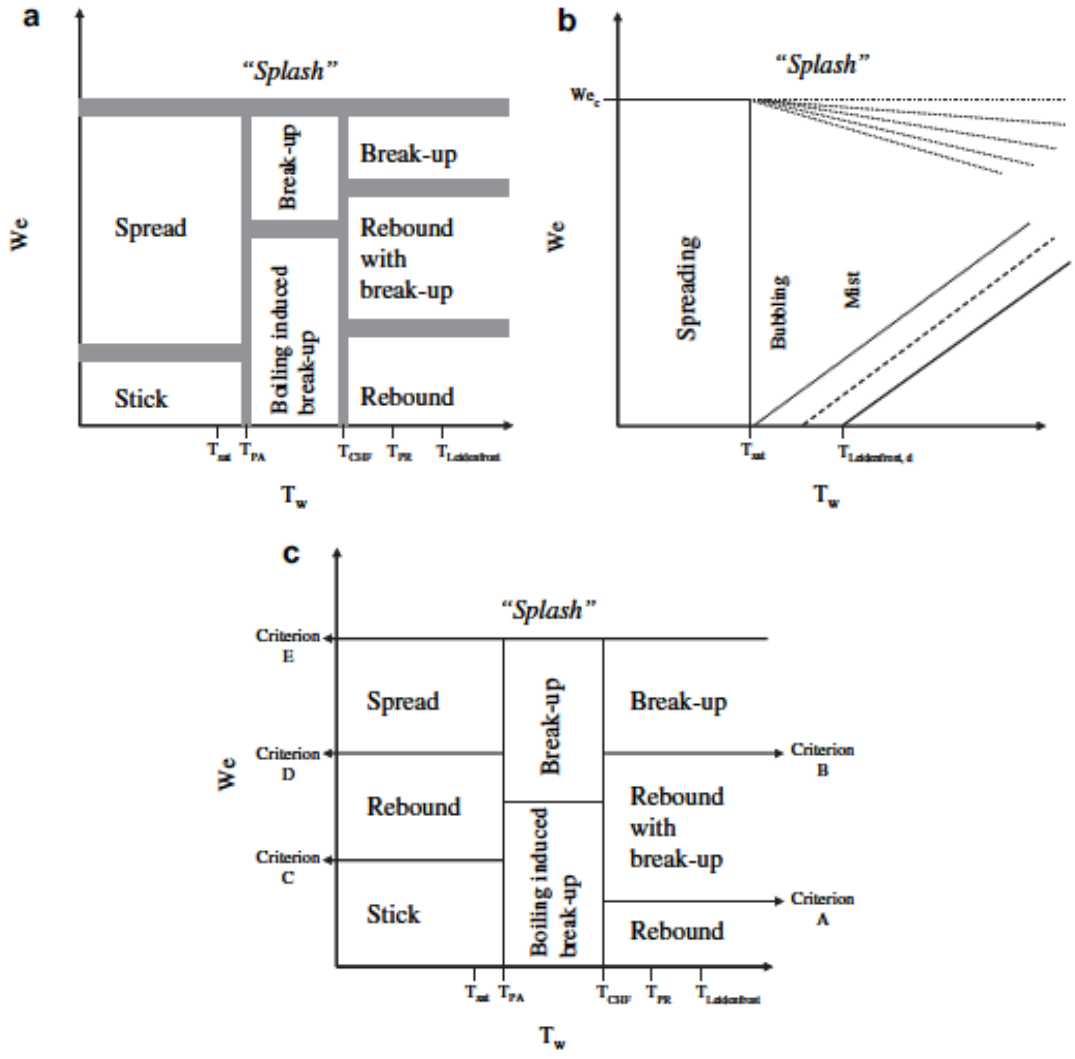

Figure I-5: Overview of droplet global representations of the impact regimes and transition conditions for a dry heated wall. a) Bai and Gosman, 1995; b) Rein, 2002; c) Lee and Ryu, 2006.

In turn, Senda *et al.* (1999) identified six different types of break-up when a droplet impinges on a heated surface (see Figure I-6), which are function of the surface temperature and the incoming droplet Weber number. For these experiments water was used as liquid and it is assumed that when a droplet impacts on the surface it deforms to a radial film on the surface. The most common regimes are:

N type: At a surface temperature above *200 ºC*, the radial film breaks up since vapour blows through the centre of the film. This "*N type*" is characterised by the fact that small droplets are blown upward with the vapour. After the vapour blow-through process, a radial film remains on the surface in a separated form.

H type: When the droplet diameter or impinging velocity increases for *N* type impingement, the *H* type appears and the number of spots where vapour blows through the film increases compared with the *N* type. The small droplets attributed to blow-through are distributed over the film, but the blow-through of vapour is weak compared to the *N* type. The separated films which remain on the surface after vapour blow-through are the *N* type.

V type: In this state the radial film does not decrease. The *V* type appears at surface temperatures of *300 ºC - 400 ºC*. No partial blow through of vapour is observed, which is different from the *N* type, and the radial film breaks up after or when the film leaves the surface. The radial film does not remain on the surface, which dries in a short time. As the droplet diameter or impinging velocity increases further from that of the *V* type, break up droplets disperse in the radial direction and transition is made to the *F* type.

F type: In this type, the radial film leaves the surface the film state because vapour underneath the film is blown out in the radial direction. Thereafter, as the diameter of the film further increases, the radial film is torn and broken up into droplets. In the *F* type, vapour passes under the radial film. The behaviour of this vapour can be confirmed in those small droplets dispersed from under radial film in the radial direction, and the dispersing velocity is faster than the film velocity.

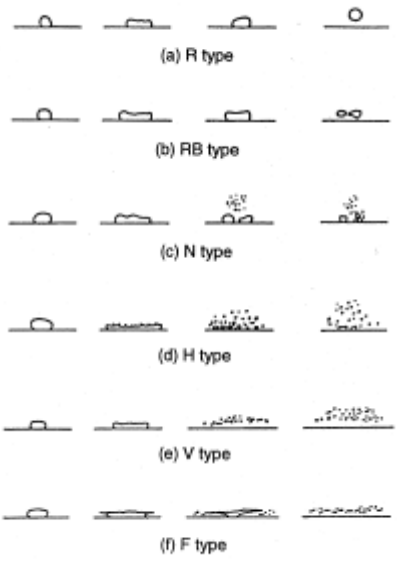

Figure I-6: Model of break-up form (Senda et al., 1999)

2.1.3. Incident angles

The impingement angle, θ_I, formed by the droplet trajectory and the surface of impact, is also an important parameter influencing the dynamic behavior of the impacting droplet, as the fine-tuning of injector position and inclination in an IC engine plays a fundamental role on engine performance (e.g., Wang *et al*. 2004)

Jayaratne and Mason (1964) investigated the impact of a water droplet on a liquid surface with low collision energy. The authors observed that the droplets would either coalesce or bounce with the water surface. In the latter case, the outgoing velocity and the mass exchange between the impinging droplet ant the liquid film were found to be function of the impact angle. Senda *et al*. (1999) observed that the normal incident droplet led to a larger amount of liquid on the wall than the droplet with other impact angles. In fact, the authors found that with smaller impingement angles the droplet slide along the surface and the fuel film changed from circular to elliptic form.

Meanwhile, Mundo *et al*. (1995) found that in contrary to the fluid properties, the incident angle and the ratio between the normal and tangential momentum had a strong influence on the reflected droplet. A small impingement angle led to a large ratio between tangential and normal momentum of the primary droplet, which led to a narrow distribution, both in front of and behind the point of impact, for both momentum components of the reflected droplet. Experimental data from the study showed that the ratio between the tangential momentum of the reflected droplet and the primary incoming droplet was greater than one. This indicates that the momentum in the normal direction is partially transformed into tangential momentum.

Okawa (2008) conducted an experimental study to investigate the effect of impingement angle on the total mass of secondary droplets produced during the collision of single water drops onto a plane water surface. From available experimental data (Okawa, 2006), the approximate deposition-splashing limit was expressed by $K = We.Oh^{-0.4} \approx 2100$. The range of impingement angles and drop diameter tested was within $11° - 75°$ and $0.15 - 1.21\,mm$, respectively. In fact, the primary drop diameter was rather small and consequently the range of dimensionless film thickness (δ) was within $1.7 - 52$. The authors proposed a correlation for the number of secondary droplets, based on their own experimental results.

2.1.4. Wall Roughness

Several authors (Engel, 1955; Levin and Hobbs, 1971; Mundo *et al.,* 1994; Mundo *et al.,* 1995; Mundo *et al.,* 1998; Mutchler, 1970; Stow and Hadfield, 1981; Stow and Stainer, 1977) have observed that the surface roughness is an important parameter in droplet impingement dynamics. In fact, changes in surface roughness affect the number, the total volume and the size distribution of secondary droplets but also alter the local incidence angle of the impingement droplet. This effect becomes important when the droplets are small compared to the surface roughness. In addition, rough surfaces dramatically lower the critical

threshold for splash that is observed for a smooth surface (Randy *et al.*, 2006a). Mundo *et al.* (1994) showed that the mass of the splash seems to decrease with increased surface roughness, which was later confirmed by Mundo *et al.* (1998). The latter study identified that high surface roughness makes it impossible for the fluid from an impinging droplet to be redirected in a direction normal to the surface. The splash mass is referred to by Mundo *et al.* (1994) as a non-dimensional quantity defined by the ratio between the splashed and the incoming droplet mass.

For droplets with high kinetic energy, the deformation of the droplet upon impact is much more irregular in rough surfaces than in the case of the smooth surfaces. In this latter case, a corona is formed in the deformation process around the point of impingement. When the wall is rough, the high tangential momentum of the incident droplet leads to a sudden and rigorous disintegration into secondary droplets. A corona and the associated instabilities before atomization are no longer identifiable. A number of secondary droplets appear behind the impact location as a result of the surface roughness (Mundo *et al.*, 1995).

On the other hand, there are no great differences between droplets with low kinetic energy impacting on the rough surface and those impacting on smooth surfaces because the surface roughness, in this range, does not promote the splashing of the primary droplet. The droplet deposits on the surface and the liquid flows out over the wall forming a wall film.

Mundo *et al.* (1995) observed in their experiments that while in smooth surfaces, the diameter distribution of the secondary droplets depends on the fluid properties (viscosity and surface tensions) and kinematic parameters (velocity and size of the primary droplets), in the case of rough surfaces, the diameter distribution of the secondary droplets becomes narrower with smaller mean diameter. The influence of liquid properties was also found to be less important in the case of a rough surface. From Mutchler (1970) and Ghadiri (1978) experimental observations, the ejection angle of secondary droplets have sub ranges with higher probabilities exist dependent on the surface roughness. For instance, Ghadiri (1978) found that angle θ_S varies in a range of $[20°; 60°]$ in situations where droplets splash on a rough soil surface; Mutcher (1970) found that the high probability for θ_S was $[5°; 50°]$ for the case of smooth hard walls.

The Leidenfrost temperature increase with surface roughness for impacting droplets (Bernardin and Mudawaar, 1997) but decrease for sessile droplets (Avedisian and Koplik, 1987). Using a three dimensional numerical code, Bussman *et al.* (2000) found that the effect of surface roughness was to initially decrease the number of fingers at early times, suggesting that the magnitude of the surface roughness is related to the strength of the perturbation of the advancing fluid.

2.1.5. Liquid Film

Roisman *et al.* (2006) presented the possible outcomes of droplets impact onto a liquid film: float over the film, deposition and coalescence with the film, bounce or rise of a droplet ejection cascade (impacts at small Weber numbers); formation of a crater on the

liquid film at the droplet impact region (impacts at moderate Weber numbers); corona splash (symmetric and/or asymmetric); splashing crown destruction by film fluctuations; uprising central jet breakup, which is often associated with the entrainment of a single bubble in the leading front of the film; and film jetting with subsequent breakup. However, depending on the wettability of the surface by the liquid film, the crown splash may also result in the dewetting of the surface, as the liquid sheet lifts up.

The wall film thickness is often described as a non-dimensional thickness, δ_{non}, calculated as the ratio between wall film thickness, δ, and the droplet initial size before impingement, d_I:

$$\delta_{non} = \frac{\delta}{d_I} \qquad \textbf{(I-1)}$$

The presence of a liquid film over the surface alters the boundary conditions, as the impingement phenomenon involves liquid/liquid interactions. However, surface characteristics may still have a significant influence depending on the thickness of the film (Randy *et al.*, 2006c). Experimental evidence showing the effect of a liquid layer depth, δ, on droplet impingement dynamics is available mainly for the case of droplet splashing (Hobbs and Osheroff, 1967; Stow and Stainer, 1977). The dependence splashing limit on the depth of a liquid film has been reported by Mutchler (1970), Ghadiri (1978), Marengo *et al.* (1996), Cossali *et al.* (1997). Tropea and Marengo (1999) considered four categories of impact onto wetted surfaces, based on the dimensionless film thickness, δ_{non}, and on the dimensionless roughness, $R_{ND} = R_a/d_I$:

- very thin film ($L_R/d_I < \delta_{non} < 3R_{ND}^{0.16}$): droplet behaviour depends on surface topography (in the absence of other parameters to quantify the effect of surface roughness besides R_a, Tropea and Marengo (1999) define a ''length scale of roughness'' - L_R);
- thin film ($3R_{ND}^{0.16} < \delta_{non} < 1.5$): the dependence of droplet behavior on surface topography becomes weaker;
- thick film ($1.5 < \delta_{non} < 4$): droplet impact is no longer dependent on surface topography but only on the film thickness;
- deep pool ($\delta_{non} > 4$): impact does not depend on surface topography nor on film thickness.

Single-drop impacts on pre-existing films of the same liquid were studied by Cossali *et al.* (1997), Wang and Chen (2000), and Rioboo *et al.* (2003). In all these cases, crown formation, i.e., splashing was recorded at sufficiently high impact velocities. In turn, Yarin and Weiss (1995) established the experimental threshold velocity for drop splashing in thin liquid layer in a train of frequency f:

$$V_{0S} = 18\left(\frac{\sigma}{\rho}\right)^{1/4} \nu^{1/8} f^{3/8}$$

which can stand for single impact when substituting f by V_0/D.

While drop spreading occurs at the impact velocities $V_0 < V_{0S}$, splashing and formation of a crown and multiple secondary droplets occur at $V_0 > V_{0S}$. From the previous equation, it is seen that the drop diameter D has no effect on the splashing threshold. This implies that the crown originates from the liquid lamella at the surface long after the memory of the squashed primary drop has faded. Due to the small scales involved, only inertia and surface tension are significant factors (with viscosity involved only via the film thickness) whereas the role of gravity is negligible.

An increase in film thickness leads to an increase in the dissipation of kinetic energy during the deformation process, and therefore the kinetic energy of the incoming droplet must be increased to cause break up (Mundo *et al.,* 1998). There is also additional fluid available for forming a corona. This leads to larger size of the secondary droplets (Coghe *et al.,* 1994; Mundo *et al.,* 1998; Stow and Stainer, 1977) and smaller number of the secondary droplets. The liquid film can also influence the splashing process so the ratio of splashed mass becomes greater than one; liquid from the layer is incorporated into the jet wall and crown, so that the jet wall may be expected to thicken. As a consequence of this, larger jets will be formed which give rise to large droplets, yielding in some cases a secondary size distribution with double peaks (Ozdemir, 1991).

If the thickness of the film is much larger than the drop diameter, the drop impact creates a crater in the liquid layer. When this crater recedes it can lead to bubble entrapment in the liquid and to the formation of an uprising central jet. Such impacts can also lead to splash when this central jet breaks up and creates a single or several secondary droplets. A condition for this central jet splash has been given by (Oguz and Prosperetti, 1990) as: $We \geq 48.3\, Fr^{0.247}$. In order to define two asymptotic conditions describing the central jet phenomenon, Fedorchenko and Wang (2004) have used dimensionless parameter called the capillary length ($l_C^* = [2\sigma/\rho g]^{1/2}$). The authors conclude that, for spray impact phenomena, the gravity does not play an important role in the formation of uprising control jets contrary to what happens with normal single droplets impingement.

Studying the break-up influence, Al-Roub and Farrell (1997) and Senda *et al.* (1999) identified three different location-based types: *rim*, *cluster*, and *column*. All of these break-up types have the same tangential Weber number, but the *cluster* type has the largest normal Weber number. The *rim* type of break-up is associated with thin liquid films; characteristically the break-up occurs at the edges of the film and often results in one or a few big droplets. For *cluster* type more film is required on the wall, i.e. it has to be a little thicker. The break-up occurs in the centre of the liquid film where a column first arises that breaks up into a cluster of droplets when it reaches maximum height. This type creates the smallest size secondary droplets. The *column* case is observed when the non-dimensional thickness is above *1*. This type is very similar to the *cluster* type, with creation of a liquid

column that breaks up. The big difference is that the *column* break-up results in one big droplet.

2.1.6. Multi Droplet Interactions

The impact of individual droplets provides a useful understanding of the fundamental mechanisms and behaviour of the spray impact but it is not an exact representation of a spray impact. Sivakumar and Tropea (2002) pointed out clearly that the splash created by a drop in a spray differs significantly from that of an isolated single drop impact or from the impact of a train of drops on a stationary liquid film (see Figure I-7).

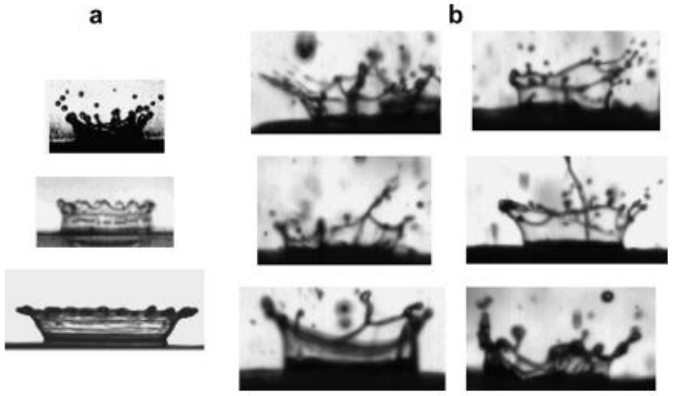

Figure I-7: Morphological comparison between splashes created by: (a) an isolated single drop, and (b) by a drop in a spray, time interval between frames is 62.5 μs. (Kalantari and Tropea, 2007)

These differences can be easily seen in Figure I-7a and b, indicating that splash of a droplet in spray impact is much more irregular and non-symmetric in comparison to the symmetric propagation of a crown in the case of an isolated single droplet impact onto an undisturbed liquid layer. In fact, very different hydrodynamic structures are found in a spray impingement comparing with the splash and rebound observed at the impact of single droplet. Roisman *et al.* (2006) depicted those structures as asymmetric corona splash, uprising central jet breakup, splash from an uprising lamella resulting from multiple drop interactions, and film jetting with subsequent breakup.

Break-up due to multiple droplet impingements can be characterized with different parameters, such as: the ratio of the distance between droplets in the parcel and the droplet diameter (L/d); the time it take the second droplet to reach the surface after the first has collided with the surface (Δt); the elapsed time between the droplet impingement and until it leaves the surface τ_{res}; and the ratio $\Delta t/\tau_{res}$ (TR).

The length scale L can be expressed as:

$$L = |r_{i+1} - r_i| \qquad \text{(I-2)}$$

while the normalized time scale (Δt) can be expressed as:

$$\Delta t = \frac{t_{i+1} - t_i}{t_{i+2} - t_i} = \frac{l_{i+1,i}}{l_{i+1,i} + l_{i+2,i+1}} \frac{\left|\overline{V}_{I_{i+2}}\right| \cos(\theta_{I_{i+2}})}{\left|\overline{V}_{I_{i+1}}\right| \cos(\theta_{I_{i+1}})} \qquad \text{(I-3)}$$

where i corresponds to the droplet striking the wall, $(i+1)$ and $(i+2)$ corresponds to the subsequent droplets which are expected to follow (see Figure I-8).

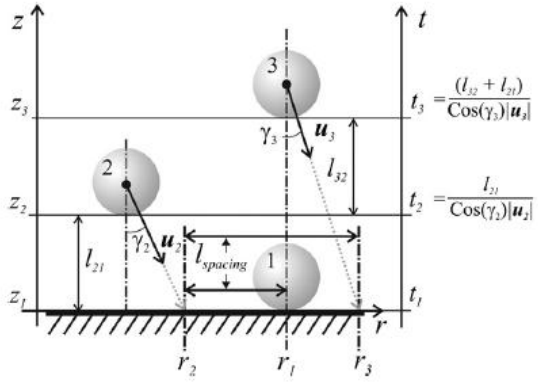

Figure I-8: Scale parameters involved in multiple drop impact (Moreira et al., 2010).

Droplet Spacing Number (*DSN*) is another way to describe the spacing between two droplets in a parcel. Comparing to the time ration, TR, Al-Roub and Farrell (1997) showed that DSN is the most convenient parameter to use. Whether or not an impinging droplet pair or parcel will cause break-up is estimated using the concept of breakup probability, ψ. This parameter is defined as the ratio between the number of impacts causing break-up, N_{IB}, and the total number of impacts, N_{IT}. The break-up probability is influenced by spray and wall film parameters including the number of droplet impinging in a sequence, droplet spacing and incoming Weber number for the droplets, and also by surrounding conditions such as the liquid film thickness.

Experiments have shown that there is a critical value for *DSN* where the break-up probability reaches a maximum value. The *DNS* at which ψ reaches a maximum is increased with increased Weber number for the impinging droplet (Al-Roub and Farrel, 1997). Considering that all droplets have the same residence time on the surface and if the break-up probability is plotted as a function of time ratio, TR, instead of the *DNS* number, the curves for ψ for different Weber numbers merge into one curve. This results in a maximum break-up probability for a certain TR. According to Al-Roub and Farrell (1997) it can be concluded that the time ratio between the droplets may be a more important parameter than the Weber number for multiple droplet interactions.

2.1.7. Droplet-Wall Impingements Models

The spray impingement phenomenon is influenced by various parameters related with both the impact conditions and the liquid and surface properties. Depending on these parameters, as well as kinematic conditions, different outcomes are verified giving rise to diverse secondary droplets characteristics. Therefore, there are two key issues that need to be addressed in the modelling of spray impingement processes. The first is to establish regime

transition criteria for predicting which regime occurs under specific given conditions. The second is to quantitatively estimate post-impingement characteristics, notably the fraction of the mass deposited on the wall and the size and velocity distributions of the secondary droplets for the splash/breakup regime. Thus, both topics are presented in the following sections.

i. Transition Criteria

Extensive effort was made to study the liquid droplet impacting on solid or liquid surfaces. Based on these experimental data, several empirical threshold criteria were developed to define to establish the boundaries between the four regimes. Those transition criteria are used in all models in order to describe how an impinging droplet behaves on the surface. Transition criteria include combinations of different dimensionless parameters, for instance the Weber number, We, the Reynolds number, Re, the Laplace number, La, or the Ohnesorge number, Oh. However, care must be taken to assure that viscous effects are negligible (e.g., Roisman *et al.*, 2009) otherwise the Weber number alone does not describe the phenomenon. Stow and Hadfield (1981) introduced the "splashing parameter", which is a parameter used in most correlations reported to predict the onset of splash and is defined as follow:

$$K_c = A.Oh^a.We^b \qquad \textbf{(I-4)}$$

The transition between different regimes occurs when the dimensionless parameter becomes critical. This numerical value depends on parameters such as size, velocity, temperature, incident angle and fluid properties, as well as different wall conditions: wall temperature, relative film thickness, surface roughness. It is worth noting that, for particular impact conditions for which the Ohnesorge number can be neglected, the threshold parameter can be simply related to the Weber number. This approach is very easy to interpret in terms of energy balance, since disregarding energy dissipation by viscous forces, the Weber number provides an immediate relation between the kinetic energy of the impacting droplet and the stabilizing surface energy required to keep the shape of the droplet.

The transition criteria for the various impingement models are summarized in Annex 1, which includes the equations, their application, and some reference works. To note that the accurate description of the boundary conditions are of great importance in the development of the disintegration criteria proposed in the literature. In fact, in the case for example of impact onto dry targets, it is unlikely to find a unique general criterion K_c for all the disintegration mechanisms because of the nature of the surface, which introduces significant modifications on those correlations. This is probably the main reason for the discrepancies observed when the various criteria are compared and fitted to a diversity of experimental results. Most authors, like Stow and Hadfield (1981) include the effect of the surface roughness with the mean roughness amplitude. Others, like Bai and Gosman (1995)

simply include the effect of surface roughness by varying the fitting parameters of the correlation. Preliminary results were reported by Rioboo *et al.* (2001) who observed a stronger influence of the roughness amplitude when compared to the fundamental wavelength. However, a deeper investigation is still required to describe more accurately the role of the nature of the surface, in the context of the pioneering investigations of these authors. On the other hand, interactions onto wetted surfaces occur mainly at the liquid-liquid interface so that the effect of the nature of the surface is less important (though may not be negligible). Instead, the thickness of the film should be taken into account as seen above. However, a different approach has been proposed by Bai and Gosman (1995), who did not include the effect of the film thickness, but altered the fitting constant A, by taking the analogy of the liquid film as a very rough surface. This analogy must be carefully considered since the film thickness may have an opposite effect to that of augmenting roughness amplitude (it depends on the range of δ_f, as seen in Section I.2.1.4). Thus, more investigation is required to describe more accurately the role of the nature of the surface.

Taking advantage of some work already engaged by Silva (2007), the following paragraphs are dedicated to the exposition of the conditions under which the transition criteria have been applied in the spray impingement models.

The first known attempt to model spray impingement on walls of internal combustion engines was made by Naber and Reitz (1988) using the KIVA code. The principal limitations of this model was the conditions for the occurrence of each regime which was not specified in relation to experimental data and to ignore the phenomenon of droplet shattering occurring at high collision energy and the loss of momentum and energy of the impinging droplets. Later, Watkins and Wang (1990) established the transition criteria between the rebound and scattering regimes by Weber number of 80, deduced from experimental data of Wachters and Westerling (1966) on water drops impinging with a hot plate, whose temperature was above the Leidenfrost temperature of the fuel. However, the criterion used in the models was not applicable to a wall whose temperature was below the fuel boiling temperature. Nevertheless, Nagaoka *et al.* (1994) utilized the same transition criteria for sprays impinging on hot walls in gasoline engines, where the wall temperature was below the fuel boiling point. Later, Park and Watkins (1996) also employed the data of Wachters and Westerling (1996) to build a wall impaction model, but for impact on a cold surface.

Senda *et al.* (1994a; 1994b) proposed an impinging spray model for diesel engines based on experimental data obtained by the authors. In this model, the authors divided the impact into two cases, with the surface temperature as the critical criterion. If the surface temperature was above the fuel boiling temperature the liquid film would boil and would cause vapour to blow upward and the liquid film would break-up.

The Bai and Gosman (1995) work applied to cases where the wall temperature was below the boiling temperature of the droplet liquid - typical in DI Diesel engines. Different impinging regimes were identified for dry and wetted walls depending on the Webber number

and wall roughness. Experimental results showed that for a wetted wall the stick regime occurred only at very low impact energy, which rarely occurs in a diesel engine. In a dry surface, the transition criterion between deposition and splash regimes was derived from the data of Stow and Hadfield (1981), where the coefficient *A* depended on the roughness surface. For the same transition criteria, but for a wet wall, it was assumed that a liquid surface behave like a very rough dry wall. In a model derived by Gavaises *et al*. (1996) only rebound, with or without break-up, or stick was considered. This model was derived from a diesel spray impact and the droplet behaviour on the surface depended on Weber number of normal component velocity, like in Senda *et al*. (1994), Bai and Gosman (1995) and Bai *et al*. (2002) models. If the incoming droplet's Weber number was below the critical value, droplets bounced away from the wall. One interesting thing is that the authors suggest that the critical Weber number is not a universal constant but in the range of *80* to *300*.

The model presented by Stanton and Rutland (1996) was validated for droplet impingement on a wetted wall with a temperature below the fuel boiling point. The impingement regimes considered were *stick, rebound, spread* and *splash*. The splash transition criterion was taken from Yarin and Weiss (1995), and they established a correlation describing the transition from spread to splash which took into account the droplet impingement frequency f - a parameter characterising a group of impinging droplets. All the transition criteria between the impinging regimes were based on the experimental results of various investigations (Jayaratne and Mason, 1964; Rodriguez and Mesler, 1985; Stow and Hadfield, 1981; Yarin and Weiss, 1995). Later, Cossali et al (1997) investigated the transition from coalescence to splashing by analyzing a large number of pictures. Their correlation was based on the Weber and Ohnesorge numbers, and the liquid film thickness was normalized with the droplet diameter.

In 1999, Senda *et al*. (1999) presented an impinging model to port-injection spark-ignition engine. The authors divided the impingement phenomenon into two cases, one for droplets with low impact energy and another for droplets with high impact energy. The two cases were limited by a critical value: $We = 300$. When the Weber number was below 300, a liquid film could form on the dry surface. In the second case, $We > 300$, a droplet impinging on the wall could stick to the wall and spread out to form a liquid film or it could splash from the surface. The criterion for *deposit* or *splash* followed the experimental data of Cossali *et al*. (1997).

In the model presented in Mundo *et al*. (1998; 1997) the transition criteria used were based on a dimensionless variable *K*. This dimensionless parameter was a function of the Reynolds number and Ohnesorge number. Experiments performed by Mundo *et al*. (1994, 1995) showed that the critical point, i.e. when transition from *deposit* to *splash* occurred, was *K*=5.77 for an impinging droplet. So, when *K* was below 57.7 the droplet would deposit on the surface and when *K* was above 57.7 the droplet would splash. In the experiments underlying this model, influences of wall roughness on the impingement process were also included. These experiments showed that roughness influenced the outcome of splashing,

while the transition condition for *deposit* or *splash* remained unchanged with increasing wall roughness (Mundo *et al.,* 1994, Mundo *et al.,* 1955).

Lee and Ryou (2000) proposed a model for impinging droplets on a cold and wetted wall below the fuel boiling temperature. The Lee and Ryou model (2000) consisted on three representative regimes such as *rebound*, *deposition* and *splash*. The transition criteria between deposition and rebound were given from the work Bai and Gosman (1995). The regime transition criterion between deposition and splash was determined by the empirical correlation proposed by Mundo *et al*. (1994, 1995).

Grover Jr. and Assanis (2001) proposed an impinging model to study the splash regime on direct-injection stratified charge (DISC) engine. The impingement model used different splash criteria for dry or wet wall impacts. For dry wall parcel collisions, the splash criterion of Mundo *et al*. (1995) was used while in the case of wet wall impact it was used the splash criterion of Cossali *et al*. (1997).

The Bai *et al*. (2002) was an improvement of Bai and Gosman (1995) model and was applied to gasoline engines. The quantitative criteria for the regime transitions for both the dry and wet wall situations were refined. The transition criteria between rebound and spread regimes was extracted from experimental data of Lee and Hanratty (1988) for water droplets impinging on deep water.

Lemini and Watkins (2002) presented a model based on Eulerian-Eulerian approach to study the phenomena of a spray impinging on a wall. This method didn't require the discretization of droplets into size classes to capture the polydisperse nature of spray flow. Instead, it solved both the liquid and gaseous phases in an Eulerian manner. The transition criteria proposed by Mundo *et al*. (1995) was used for splash and for the deposition limit was assumed K=15.

Randy *et al*. (2006a), who studied the disintegration for a large number of liquids, mostly hydrocarbon fuels (heptane, nonane and hexadecane) and alcohols (ethanol, methanol and buthanol), defended that the results were better described by the correlations which did not neglect the viscous effects. Even though Randy *et al*. (2006a) identified different disintegration mechanisms in their work (e.g. Randy *et al.,* 2006b,c), they tried to fit all their results according to a single threshold correlation establishing a binary splash/no splash condition. Consequently, the correlation fitted very well their experimental results for large Reynolds numbers, i.e. when the flow is dominated by inertial forces, but there was a significant scattering of the data, which were not well fitted to the correlation as the Reynolds number decreased (particularly for Re<4000), when viscous and the wetting effects become more important and may promote the occurrence of diverse break-up mechanisms.

Huang and Zhang (2008) conducted experimental observations for droplet impingements with different fluids, droplet sizes and velocities, and film thicknesses. High-speed video recording is shown to be an effective technique for identifying the transition boundaries between bouncing, coalescence, jetting and splashing. For the impingement on a liquid film surface, the Cossali *et al*. (1997) model and the Marengo and Tropea, (1999) model

for the splashing-coalescence transition were compared with oil film and water film (1 mm) data. The comparison showed good results with the oil film but not so good with the water film. Good agreements were observed for impingements on both oil and water films.

ii. Post-Impingement Characteristics

The spray impingement phenomenon is influenced by various parameters, which are associated to the impact condition and liquid and surface properties. These parameters will influence the outcome of the droplets impingement, and, consequently, the impact regime under which each droplet fits. Thus, it is essential to determine the post-impingement characteristics of the secondary droplets for an adequate modelling of the spray impingement phenomenon. Numerous approaches have been adopted in the different spray impingement models presented. The most important for this work are presented in the following chapter (Chapter II.6.2) but a thorough analysis of the post-impingement characteristics of the numerous models available in the literature has been presented by Silva (2007). This analysis is presented and completed with some new data in Annex 2.

3. Objectives

The present work is devoted to the numerical study of the impingement of sprays onto a solid wall through a crossflow. The major purpose of the thesis is to improve the accuracy of the base model of Bai *et al.* (2002) through the employment of both new correlations – for the deposition/splash transition criteria – and new relationships – for the energy dissipation loss. The numerical predictions were then compared with the experimental data of Arcoumanis *et al.* (1997) for two crossflow rates (5 and $15\ m/s$).

4. Overview

This Thesis is organized in four chapters. In the first chapter, an introduction to the subject has been made mainly through the extensive literature review regarding the wall impingement theme. The Chapter 2 is dedicated to the mathematical model. This section describes all the procedure adopted in both continuous and dispersed phase (and their interaction) to attain the solution, as well as the boundary conditions. The following chapter presents the results of the simulations made. Beyond the study of the mesh independence, two studies are presented: the study of the transition criteria and the study of the energy dissipation loss. The main conclusion and the future work suggestion are summarized in the Chapter 4. In addition to these chapters, two other sections are also presented, which correspond to the references used along the entire work and the Annexes.

II. Mathematical Model

1. Introduction

The modelling of turbulent multiphase flows is of great importance to better understand the phenomena found inside a spray combustion engine. In this sense, several mathematical techniques have been developed to predict dilute two-phase flows. The accurate prediction of these kinds of flows requires the effective modelling of both continuous gas and dispersed phases.

Used in this work, the Eulerian-Lagrangian hybrid model computes the collisions in a natural way – despite considering the droplet-droplet interaction negligible – but it is also currently preferred due to its easy handling of droplet-size discrimination. In this method, the particle phase is described using a Lagrangian approach while an Eulerian frame is used to describe the effects of both interphase slip and turbulence particle motion using a random sampling technique called Monte Carlo (Barata *et al.,* 2002).

Therefore, this chapter presents the mathematical model used to predict the droplet spray impinging onto a solid surface under crossflow conditions. Presented in the Section II.2, the continuous phase, or gas phase, is based on the solution of the equation of energy, momentum and mass, while the turbulence is modelled by mean of the "$k-\varepsilon$" turbulence model (Launder and Spalding, 1974). Then, in the subsequent section, the turbulence particle dispersion and vaporization, or dispersed phase, is presented assuming that the particles are sufficiently dispersed so that particle-particle interaction is negligible as well as the stochastic separated flow (SSF) model used to characterize the droplet behaviour, where anisotropy is taken into account. In the section II.4, the interaction between the continuous three-dimensional phase and dispersed phase is described using an Eulerian frame. To note that for both continuous and dispersed phases it is assumed that the material properties are constant and the mean flow is steady. The section II.5 outlines the general procedure necessary for modelling, and the last section is devoted to the boundary conditions employed in the model.

2. Continuous Phase

2.1. Introduction

This fluid phase is treated as a continuum by solving the partial differential equations in a fixed reference frame, which represent each particle and its properties of interest.

2.2. Governing differential equations

The basic set of partial equations solved in the carrier phase, as well as the transport equations introduced with the turbulent model are presented in this section.

The time-averaged partial differential equations governing the steady, uniform-density isothermal three-dimensional flow may be written in Cartesian coordinates as

$$\rho \bar{U}_j \frac{\partial \bar{U}_i}{\partial X_j} = -\frac{\partial \bar{P}}{\partial X_i} + \frac{\partial}{\partial X_j}\left(\mu \frac{\partial \bar{U}_i}{\partial X_j} - \rho \overline{u_i' u_j'}\right) + S_{u_i,d} \qquad \textbf{(II-1)}$$

Based on the second-moment closure, the equations of continuity, enthalpy, and vapour mass fraction are written as

$$\rho \frac{\partial \bar{U}_i}{\partial X_j} = S_{m,d} \qquad \textbf{(II-2)}$$

$$\rho \bar{U}_j \frac{\partial \bar{H}}{\partial X_j} = \frac{\partial}{\partial X_j}\left(\frac{\mu}{Pr}\frac{\partial \bar{H}}{\partial X_j} - \rho \overline{u_j' h}\right) + S_{H,d} \qquad \textbf{(II-3)}$$

$$\rho \bar{U}_j \frac{\partial \bar{F}}{\partial X_j} = \frac{\partial}{\partial X_j}\left(\frac{\mu}{Sc}\frac{\partial \bar{F}}{\partial X_j} - \rho \overline{u_j' f}\right) + S_{m,d} \qquad \textbf{(II-4)}$$

where the overbars represent averaged quantities. These equations shall be applied to a single-phase fluid. Interactions between the fluid and any suspended particulate material of a different phase are accounted for through the source terms $\left(S_{u_i,d}, S_{H,d}\ and\ S_{m,d}\right)$ that appear in each equation.

The required additional equations are available from the two-equation $k-\varepsilon$ model, which has become the workhorse of practical engineering flow calculations since it was proposed by Launder and Spalding (1974). This model employs the Boussinesq hypothesis to model the Reynolds-averaged Navier-Stokes (RANS) and relates the Reynolds stresses to the mean velocity gradients:

$$\overline{u_i' u_j'} = -\nu_T \left(\frac{\partial \bar{U}_i}{\partial X_j} + \frac{\partial \bar{U}_j}{\partial X_i}\right) + \frac{2}{3} k \delta_{ij} \qquad \textbf{(II-5)}$$

where ν_T is the turbulent kinematic viscosity. This property is a space and time dependent quantity – and not an intrinsic property of the fluid – whose value depends entirely on the local turbulent characteristics of the flow. Based on simple dimensional arguments concerning the relationship between the size and the energetic of individual eddies in fully developed isotropic turbulence, the model employs the following equation for the turbulence kinematic viscosity (Launder and Spalding, 1974):

$$\nu_T = C_\mu \frac{k^2}{\varepsilon} \qquad \textbf{(II-6)}$$

where C_μ is a dimensionless model constant and k and ε are the turbulent kinetic energy (SI units: m^2/s^2) and the turbulent kinetic energy dissipation rate (SI units: m^2/s^2), respectively. These quantities are, in turn, computed using a pair of additional transport equations of the form

$$\overline{U}_j \frac{\partial k}{\partial X_j} = \frac{\partial}{\partial X_j}\left(\frac{\nu_T}{\sigma_k}\frac{\partial k}{\partial X_j}\right) - \overline{u_i' u_j'}\frac{\partial \overline{U}_i}{\partial X_j} - \varepsilon + S_{k,d} \qquad \textbf{(II-7)}$$

$$\overline{U}_j \frac{\partial \varepsilon}{\partial X_j} = \frac{\partial}{\partial X_j}\left(\frac{\nu_T}{\sigma_\varepsilon}\frac{\partial \varepsilon}{\partial X_j}\right) - C_1 \frac{\varepsilon}{k}\overline{u_i' u_j'}\frac{\partial \overline{U}_i}{\partial X_j} - C_2 \frac{\varepsilon^2}{k} + S_{\varepsilon,d} \qquad \textbf{(II-8)}$$

where C_1 and C_2 are additional dimensionless model constants, σ_k and σ_ε are the turbulent Prandtl numbers for kinetic energy and dissipation, and $S_{k,d}$ and $S_{\varepsilon,d}$ are interphase source terms for the kinetic energy and turbulent dissipation.

Each of the equations presented above could be written separately in a discretized form and solved individually to produce a solution. However, careful observation reveals that these equations all have a similar form, indicating that each dependent variable solved obeys to the same generalized conservation principle. In particular, letting Φ to denote the dependent variable, it turns out that all of the governing equations can be reduced to a single convective-diffusive conservation equation of the form

$$\frac{\partial(\rho U_i \Phi)}{\partial X_i} = \frac{\partial}{\partial X_i}\left(\Gamma_\Phi \frac{\partial \Phi}{\partial X_i}\right) + S_\Phi \qquad \textbf{(II-9)}$$

where Γ_Φ is the effective diffusion coefficient for quantity Φ. The term on the left-hand side is the convection term, whilst the first and the second terms on the right-hand side are the diffusion term and the source term, respectively.

The source term S_Φ can be divided into two parts, which yields the following expression:

$$S_\Phi = S_{\Phi,\mathrm{g}} + \mathrm{S}_{\Phi,\mathrm{d}} \qquad \textbf{(II-10)}$$

where $S_{\Phi,g}$, specifies the source term of the gas and $S_{\Phi,d}$, specifies the source term of the droplet. The source terms of the gas phase, $S_{\Phi,g}$, and the effective diffusion coefficient are summarized in Table II-1 for different dependent variables.

Table II-1: General form of the terms of the differential equations.

Φ	$\boldsymbol{S_{\Phi,g}}$	$\boldsymbol{S_{\Phi,d}}$	Γ_Φ
1	-	$\overline{S_{\rho,d}}$	-
$\boldsymbol{U_i}$	$-\frac{\partial}{\partial X_i}\left(P+\frac{2}{3}k\right)-\frac{\partial}{\partial X_j}\frac{2}{3}\mu_t\frac{\partial \overline{U}_j}{\partial X_i}+\rho g_i$	$\overline{S_{U,d}}$	$\mu+\mu_T$
$\boldsymbol{T}$	0	$\overline{S_{T,d}}$	$\frac{\mu}{Pr}+\frac{\mu_T}{Pr_T}$
$\boldsymbol{Y_d}$	0	$\overline{S_{Y_k,d}}$	$\frac{\mu}{Sc}+\frac{\mu_T}{Sc_T}$
K	$G-\rho\varepsilon$	$\overline{\mathrm{S_{k,d}}}$	$\mu+\frac{\mu_T}{\sigma_k}$
ε	$C_1\frac{\varepsilon}{k}G-C_2\rho\varepsilon$	$\overline{S_{\varepsilon,d}}$	$\mu+\frac{\mu_T}{\sigma_\varepsilon}$

where *G* is the usual turbulence energy production term defined as:

$$G = \mu_T\left[\frac{\partial \overline{U}_i}{\partial X_j}+\frac{\partial \overline{U}_j}{\partial X_i}\right]\frac{\partial \overline{U}_i}{\partial X_j} \qquad \textbf{(II-11)}$$

and

$$\mu_T = C_\mu \rho \frac{k^2}{\varepsilon} \qquad \text{(II-12)}$$

The standard values (Launder and Spalding, 1974) for each of the various dimensionless constants used in the turbulence equations are given in table below:

Table II-2: Turbulence model constants.

C_μ	C_1	C_2	C_3	σ_k	σ_ε	Pr_T	Sc_T	Pr	Sc
0.09	1.44	1.92	1.1	1.0	1.3	0.6	0.85	$\mu C_p/k_g$	$\mu/\rho D$

These values are based on an evaluation of several plane turbulent free jets and mixing layer simulations. They have been found to work fairly well for a wide range of turbulent flow, and can be assumed to provide model accuracy in the range from about 10% to 50%, depending on the flow (Launder and Morse, 1979).

2.3. Finite-difference equations

The resolution of the differential equations for turbulent flows requires the employment of a finite-difference method to obtain a system of algebraic equations that can be solved numerically. Those algebraic equations are converted from the general scalar transport Equation II-9 using a control-volume-based technique. The discretization of the differential equation involves the integration of the transport equations over each elementary control volume surrounding a central node with a scalar value Φ_P. The volume integrals are converted into surface integrals for the control volume using Green's theorem; the convection flux for each variable at the cell face has then to be estimated based on the value of the variable Φ at the neighbouring cell centre. All the quantities (i.e. *p,k, ε, T, etc*.) are located at the grid nodes excluding the velocities, which are located at the boundaries of the control volume for scalar quantities. That "manoeuvre" allows the direct determination of the velocities from the pressure gradients and mass fluxes through each face of the control volume (Patankar, 1980).

In this stage, a numerical method must be used for a proper accuracy of the solution. In fact, numerical methods allow interpolating the face values, which are required for the convection terms in the discretization process, from the discrete value of the scalar Φ at the cell center.

2.4. Numerical Method

In order to reduce the numerical diffusion several higher order schemes have been developed. The QUICK scheme proposed by Leonard (1979) is free from artificial diffusion and gives more accurate solutions with coarser grid than that required by the hybrid scheme. This

is achieved by utilizing quadratic upstream-weighted interpolation to calculate the cell face values for each control volume.

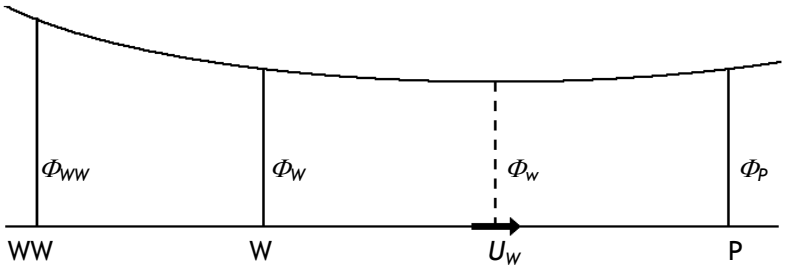

Figure II-1: Nodal configuration for the west face of a control volume (Barata, 1989).

The Figure II-1 shows the west face of a control volume surrounding a central node with a value Φ_P. For this face, using a uniform grid for simplicity, the value of Φ_w is expressed by

$$\Phi_w = \frac{1}{2}(\Phi_P + \Phi_W) - \frac{1}{8}(\Phi_P + \Phi_W + \Phi_{WW}) \qquad \textbf{(II-13)}$$

when the convective velocity component U_W is assumed to have the direction shown in Figure II-1. In the case of negative value of U_W, then Φ_E would be involved rather than Φ_{WW}. The first term in Equation II-13 is the central difference formula, and the second is the important stabilizing upstream-weighted normal curvature contribution. Expressing the values of Φ at each cell face with the appropriate interpolation formula and writing gradients also in terms of node values, the finite-difference equation corresponding to Equation II-9 may be written in the general form as

$$A_P^{\Phi}\Phi_{\mathrm{P}} = \sum \mathrm{A}_{\mathrm{i}}^{\Phi}\Phi_{\mathrm{i}} + \mathrm{S}_{\mathrm{U}}^{\Phi} \qquad \textbf{(II-14)}$$

where

$$\mathrm{A}_{\mathrm{P}}^{\Phi} = \sum \mathrm{A}_{\mathrm{i}}^{\Phi} + \mathrm{S}_{\mathrm{P}}^{\Phi} \qquad \textbf{(II-15)}$$

Here, the summation occurs over the 12 nodes neighbouring *P* (see Figure II-2).

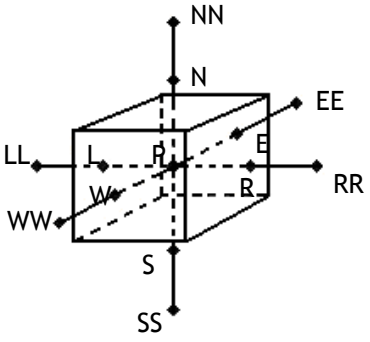

Figure II-2: Nodal configuration for a control volume (Barata, 1989).

The resolution of the set of equations for the complete field by the original QUICK method can lead to the A_i^{Φ} coefficients become negative and stable solutions cannot be obtained. In the present work, diagonal dominance of the coefficient matrix is ensured and enhanced by rearranging the difference equation for the cells where the coefficients A_i^{Φ} become negative. This rearrangement consists in subtracting $A_i^{\Phi}\Phi_P$ from both sides of Equation II-14, eliminating the negative contribution of A_i^{Φ} and simultaneously enhancing the diagonal dominance of the coefficient matrix (Barata *et al.,* 2002a; Barata *et al.,* 2002b; Barata *et al.,* 1989; Silva *et al.,* 2002). The source term S_U^{Φ} becomes

$$S_U^{\Phi} = S_U^{\Phi} - \mathrm{A_i^{\Phi}}\Phi_{\mathrm{P}}' \qquad \textbf{(II-16)}$$

where $\Phi_P^{'}$ is the latest available value of Φ at node P.

2.5. Solution Procedure

The solution procedure for the continuous phase is based on the SIMPLE algorithm widely used and reported in the literature (Patankar and Spalding, 1972). This procedure is based on a "guess and correct" method in order to obtain a pressure field such that the solution of the momentum equations satisfy continuity. A solution for the gaseous field assuming no droplets is initially obtained, and the droplet trajectories and source terms are calculated. The gas field is then recomputed with the contribution of the droplet source terms. This process is repeated until convergence is achieved.

3. Dispersed phase

3.1. Introduction

Currently, the particle dispersion models can be classified based on their reference frame: the Lagrangian and the Eulerian reference frame. In the first formulation, which is the one used in this work, the dispersed phase is solved by tracking a large number of particles through the calculated flowfield. Here, the reference frame moves along with the particles through space and time, processing the instantaneous position of the droplets as function of the location from where it was originated and the corresponding time elapsed. On the other hand, the Eulerian reference frame is stationary and the droplets pass through fixed differential control volumes. Unlike the Lagrangian formulation, this model treats the particles as a continuum – similar to the fluid phase – and the solution is obtained by solving the Navier-Stokes equations. Eulerian models are very popular when particle loading is high – for example fluidized combustion systems – but have certain limitation in modelling simplified dilute flows, in which the particle-particle interaction can be neglected (Shirolkar *et al.,* 1996). Thus, and since this chapter is limited to the dispersed phase of a dilute two-phase flow, the following section is dedicated only to the Lagrangian Dispersion Model.

3.2. Particle Tracking – Lagrangian Particle Dispersion Model

The main difficulty in Lagrangian computations is to define the instantaneous gas field, since the time-averaged Eulerian equations only provide the gas mean properties (Chen and Pereira, 1995). Several models have been proposed to account for the effect of the turbulence on the particle trajectory, such as deterministic separated flow (DSF) model, "particle diffusional velocity" model and stochastic separated flow (SSF) model (Faeth, 1987). Among them the SSF model has been widely used. In that model the turbulent dispersion of a particle is considered based on the concept of energy containing eddies and the particle trajectories are obtained by solving the particle momentum equation through the Eulerian fluid velocity field. To note that the droplets are divided into representative samples, with equal dimension and initial conditions, in order to reduce the computation required to characterize satisfactorily the droplet behaviour. On the other hand, the number of trajectories must be high enough to provide a representative statistics.

When the particles move through the turbulent flow field, they are assumed to interact with the local turbulent eddies, which are represented by an instantaneous property consisting of a mean quantity and a fluctuating quantity. The mean quantity can be obtained directly from the Reynolds averaged equations, while the fluctuating quantity is selected from a Gaussian distribution with a variance related to the turbulent kinetic energy. The key point in this model is to determine the interaction time of the particle and the turbulent eddy. To note that the initial droplet size distribution of the spray is selected according to the given experimental probability density function (PDF) to obtain an adequate number of discrete parcels, each of which represents a set of droplets having the same size and initial conditions.

Therefore, the equations of motion of the particles can be deduced from Newton's Second Law of Motion if all the forces acting on a droplet immersed in a turbulent flow are mathematically quantified. However, assuming the usual simplification for dilute particle-laden flows, the droplet momentum equation can be greatly simplified. In fact, in most practical dilute flow applications, the static pressure gradient is small, so it can be assumed that the droplets, whose characteristic dimension is smaller than Kolmogorov scale, are spherical, the droplet-to-fluid density ratio is greater than 200 and the effect of Basset, virtual mass, Magnus, Saffman and buoyancy forces are negligible. Thus, in the simplified droplet momentum equation, the steady-state drag term is the most important force acting on the particle. Under these assumptions, the simplified particle momentum equation is:

$$\frac{\partial u_{p,i}}{\partial t} = \frac{1}{\tau_p}\left(u_{f,i} - u_{p,i}\right) + g_i \qquad \text{(II-17)}$$

where g_i are the external forces (i.e., gravity, centrifugal and Coriolis forces) and τ_p is the droplet relaxation time, defined as the rate of response of droplet acceleration to the relative velocity between the droplet and the carrier fluid. In fact, if the droplet is dense ($\rho_d > \rho_f$), the inertial force at the fluid-droplet interface will decrease the velocity fluctuations

comparing to the fluctuations observed for the surrounding fluid; this reduction in the droplet root mean square (*rms*) fluctuating velocity is known as inertia effect, and it is characterized by the particle (droplet) relaxation time. The mathematical expression for the relaxation time, τ_p, is:

$$\tau_p = \frac{24\rho_p d_p^2}{18\mu_f C_D Re_p} \quad \textbf{(II-18)}$$

where the Re_p is the particle Reynolds number,

$$Re_p = \frac{\rho_f |\vec{V}_p - \vec{V}_f| d_p}{\mu_f} \quad \textbf{(II-19)}$$

and C_D is the drag coefficient,

$$C_D = \left(\frac{24}{Re_p}\right)\left(1 + 0.15 Re_p^{0.687}\right) \quad \textbf{(II-20)}$$

for $Re_p < 10^3$. Substituting Equations II.19 and II.20 in Equation II.18, we obtain a new expression for the droplet relaxation time:

$$\tau_d = \frac{m_d}{3\pi d_p \mu_f} \frac{1}{1 + 0.15 Re_d^{0.687}} \quad \textbf{(II-21)}$$

Equation II.17 along with Equation II.21 is most commonly used in Lagrangian models to generate the droplet trajectories (Chen and Pereira, 1995; Gosman and Ioannides, 1981).

The particle momentum equation can be analytically solved over a small time steps, Δt, in which the instantaneous fluid velocity and the droplet relaxation time are assumed to be constant. Thus, by knowing the new droplet velocity at the end of each time step, a droplet trajectory can be constructed as shown by the equations given below:

$$u_{p,i}^{NEW} = u_{f,i} + \left(u_{p,i}^{OLD} - u_{f,i}\right) e^{-\Delta t/\tau_p} + g_i \tau_p \left[1 - e^{-\Delta t/\tau_p}\right] \quad \textbf{(II-22)}$$

$$x_{p,i}^{NEW} = x_{p,i}^{OLD} + \frac{\Delta t}{2}\left(u_{p,i}^{NEW} + u_{p,i}^{OLD}\right) \quad \textbf{(II-23)}$$

The critical issues are to determine the instantaneous fluid velocity and the evaluation of the time, Δt, of interaction of a particle with a particular eddy. The time step is obviously the eddy-particle interaction time, which is the minimum of the eddy lifetime, τ_{FL}, and the eddy transit time, t_c. The eddy lifetime is estimated assuming that the characteristic size of an eddy is the dissipation length scale isotropic flow:

$$l_e = B\frac{k^{3/2}}{\varepsilon} \approx C_\mu^{3/4}\frac{k^{3/2}}{\varepsilon} \quad \textbf{(II-24)}$$

$$\tau_{FL} = A\frac{k}{\varepsilon} \approx 0.2\frac{k}{\varepsilon} \quad \textbf{(II-25)}$$

where A and B are two dependent constants (Shirolkar *et al.*, 1996).

The transit time, t_c, is the minimum time a particle would take to cross an eddy with characteristic dimension, l_e, and given by

$$t_c = \frac{l_e}{|\vec{v}_{drift}|} \quad \text{(II-26)}$$

where $\vec{v}_{drift}$ is the relative velocity between the particle and the fluid (drift velocity). A different expression for the transit time is also recommended in the literature (Gosman and Ioannides, 1981; Shirolkar *et al.,* 1996), and has been used in the present work:

$$t_c = -\tau_p \ln\left(1 - \frac{l_e}{\tau_p|u_{f,i} - u_{p,i}|}\right) \quad \text{(II-27)}$$

where the drift velocity is also estimated at the beginning of a new iteration.

This equation has no solution when $l_e > \tau_p|u_{f,i} - u_{p,i}|$, that is, when linearized stopping distance of the particle is smaller than the eddy size. In such a case, the particle can be assumed to be trapped by the eddy. In short, at each particular droplet location, the eddy-droplet interaction time can be determined from the eddy lifetime and eddy size, which in turn are estimated from the local turbulence properties available from a turbulence model.

The instantaneous velocity at the start of a particle-eddy interaction is obtained by random sampling from an isotropic Gaussian pdf having standard deviations of $\sqrt{2/3k}$ and zero mean values. The fluctuating velocity associated with a particular eddy is assumed to be constant over the interaction time.

Knowing the interaction time and the randomly sampled fluctuating fluid velocity, it is possible to solve both Equation II.22 and Equation II.23 for the droplet trajectory. The time step is again the eddy-droplet interaction time. At the end of each time step, a new fluctuating fluid velocity is sampled from a new *pdf*, which is generated using local turbulence properties. The next interaction time is determined from the local properties at the new droplet location.

The above isotropic model was extended in the present work to account for cross-correlations and anisotropy. To obtain the fluctuating velocities u_f' and v_f', two fluctuating velocities, u_1' and u_2', are sampled independently, and then correlated using the correlation coefficient R_{uv}, which was obtained from measurements:

$$u_f' = u_1' \quad \text{(II-28)}$$

$$v_f' = R_{uv}u_1' + \sqrt{1 - R_{uv}^2}u_2' \quad \text{(II-29)}$$

$$R_{uv} = \frac{\overline{u_f'v_f'}}{\sqrt{u_f'^2}\sqrt{v_f'^2}} \quad \text{(II-30)}$$

4. Interaction between Continuous and Dispersed Phase

The interactions between the continuous and the dispersed phases are very complex physical processes. Due to the exchanges of mass, momentum and energy between the two phases, both gas flow and droplets behaviour are modified. These exchanges are modelled treating droplets as sources of mass, momentum and energy to the gaseous phase. The source terms due to the droplets calculated for each Eulerian cell of the continuous phase are summarized in Table II-3. Those terms can be divided into two parts:

$$S_{\phi d} = S_{\phi i} + S_{\phi m} \qquad \text{(II-31)}$$

where $S_{\phi i}$ specifies the source term due to inter-phase transport and $S_{\phi m}$ takes into consideration the transfer caused by evaporation. Chen and Pereira (1992) used the following equations to represent the temporal changes of droplets size and temperature:

$$\frac{d(d_d)}{dt} = -\frac{4k_g}{C_{p_g}} \ln\left(1 + \frac{C_{p_g}}{L(T_s)}(T_\infty - T_s)\right)\left(1 + 0.23Re^{1/2}\right) \qquad \text{(II-32)}$$

$$\frac{dT_d}{dt} = 12k_g\left(\frac{T_\infty - T_s}{\rho_F C_{P_F} d_d^2}\right)\left(1 + 0.3Re^{1/2}\mathrm{Pr}^{1/3}\right) \qquad \text{(II-33)}$$

In the last equation is assumed that the prevailing mode of heat transfer is forced convection, no evaporation occurs during the preheating period and the temperature is uniform across the droplet radius. For the forced convection the Ranz and Marshall (1952) correlation has taken the place of the Nusselt Number.

Table II-3: Dispersed phase source terms (Sommerfeld, 1998).

$S_{\Phi d}$	$S_{\Phi i}$	$S_{\Phi m}$
$\overline{S_{\rho,d}}$	0	$\sum_d \frac{\dot{m}_d N_d}{V_{i,j}}$
$\overline{S_{U,d}}$	$-\sum_d \frac{\dot{m}_d N_d}{V_{i,j}}\left[\left(u_{j,d}^{t+\Delta t} - u_{j,d}^{t}\right) - g_i \Delta t\right]$	$\sum_d \frac{\dot{m}_d N_d u_{i,a}}{V_{i,j}}$
$\overline{S_{T,d}}$	$-\sum_d \frac{N_d}{V_{i,j}}\left(\frac{L_{tbn}\dot{m}_d + Q_L}{C_{P_A}}\right)$	$\sum_d \frac{\dot{m}_p N_d}{V_{i,j}}\left(\frac{C_{P_{vap}} T_s \times (T_r - T_s)}{C_{P_A}}\right)$
$\overline{S_{Y1,d}}$	0	0
$\overline{S_{Y2,d}}$	0	$\sum_d \frac{\dot{m}_d N_d}{V_{i,j}}$
$\overline{S_{k,d}}$	$\overline{U_J S_{UJi}} - \overline{U_J}\ \ \overline{S_{UJi}}$	$\overline{U_J S_{UJm}} - \overline{U_J}\ \ \overline{S_{UJm}} + \frac{1}{2}\overline{U_J}\ \ \overline{U_J}\ \ \overline{S_m} - \frac{1}{2}\overline{U_J U_J S_m}$
$\overline{S_{\varepsilon,d}}$	$C_{\varepsilon 3}\frac{\varepsilon}{\mathrm{k}}\overline{S_{ki}}$	$C_{\varepsilon 3}\frac{\varepsilon}{\mathrm{k}}\overline{S_{km}}$

The source terms due to the particles are presented in Table II-4 where $C_{\varepsilon 3} = 1.9$ is an empirical constant (Mostafa and Mongia, 1987; Shuen *et al.*, 1985).

Table II-4: Dispersed phase source terms (Chen and Pereira, 1992).

$S_{\Phi d}$	$S_{\Phi i}$	$S_{\Phi i}$
$\overline{S_{\rho,d}}$	0	$\sum_d \frac{N_d}{V_{i,j}}\left(\dot{m}_d^t - \dot{m}_d^{t+\Delta t}\right)$
$\overline{S_{U,d}}$	$-\sum_d \frac{\dot{m}_d N_d}{V_{i,j}}\left[\left(u_{j,d}^{t+\Delta t} - u_{j,d}^t\right) - g_i \Delta t\right]$	$\sum_d \frac{N_d}{V_{i,j}}\left(\dot{m}_d^t u_{j,d}^t - \dot{m}_d^{t+\Delta t} u_{j,d}^{t+\Delta t}\right)$
$\overline{S_{T,d}}$	$-\sum_d \frac{N_d}{V_{i,j}}\left(\frac{\dot{m}_d{}^t C_{P_F}^t T_S^t - \dot{m}_d{}^{t+\Delta t} C_{P_F}^{t+\Delta t} T_S^{t+\Delta t}}{C_{P_A}}\right)$	
$\overline{S_{Y1,d}}$	0	0
$\overline{S_{Y2,d}}$	0	$\sum_d \frac{N_d}{V_{i,j}}\left(\dot{m}_d^t - \dot{m}_d^{t+\Delta t}\right)$
$\overline{S_{k,d}}$	$\overline{U_J S_{\mathrm{U}Jl}} - \overline{U}_J \quad \overline{S_{\mathrm{U}Jl}}$	0
$\overline{S_{\varepsilon,d}}$	$C_{\varepsilon 3}\frac{\varepsilon}{k}\overline{S_{kl}}$	0

5. Implementation and Procedure of the Model

There are of course several ways to implement computationally the model. The concise numerical procedure implemented in this work to obtain a converged solution for both phases is described as follow (see Figure II-3):

1. The initial conditions are settled up; the grid is modelled and the diameter of the initial drops are defined;
2. A converged solution of the gas flow field is calculated without the source terms of the dispersed phase;
3. The discrete parcels are traced through the flow field in the dispersed phase and the values of the source terms are calculated;
4. The gas flow is again modelled considering now the source terms (S.T.) of the dispersed phase;
5. The steps 2 and 3 are repeated until convergence is reached;
6. Post-processing of the data.

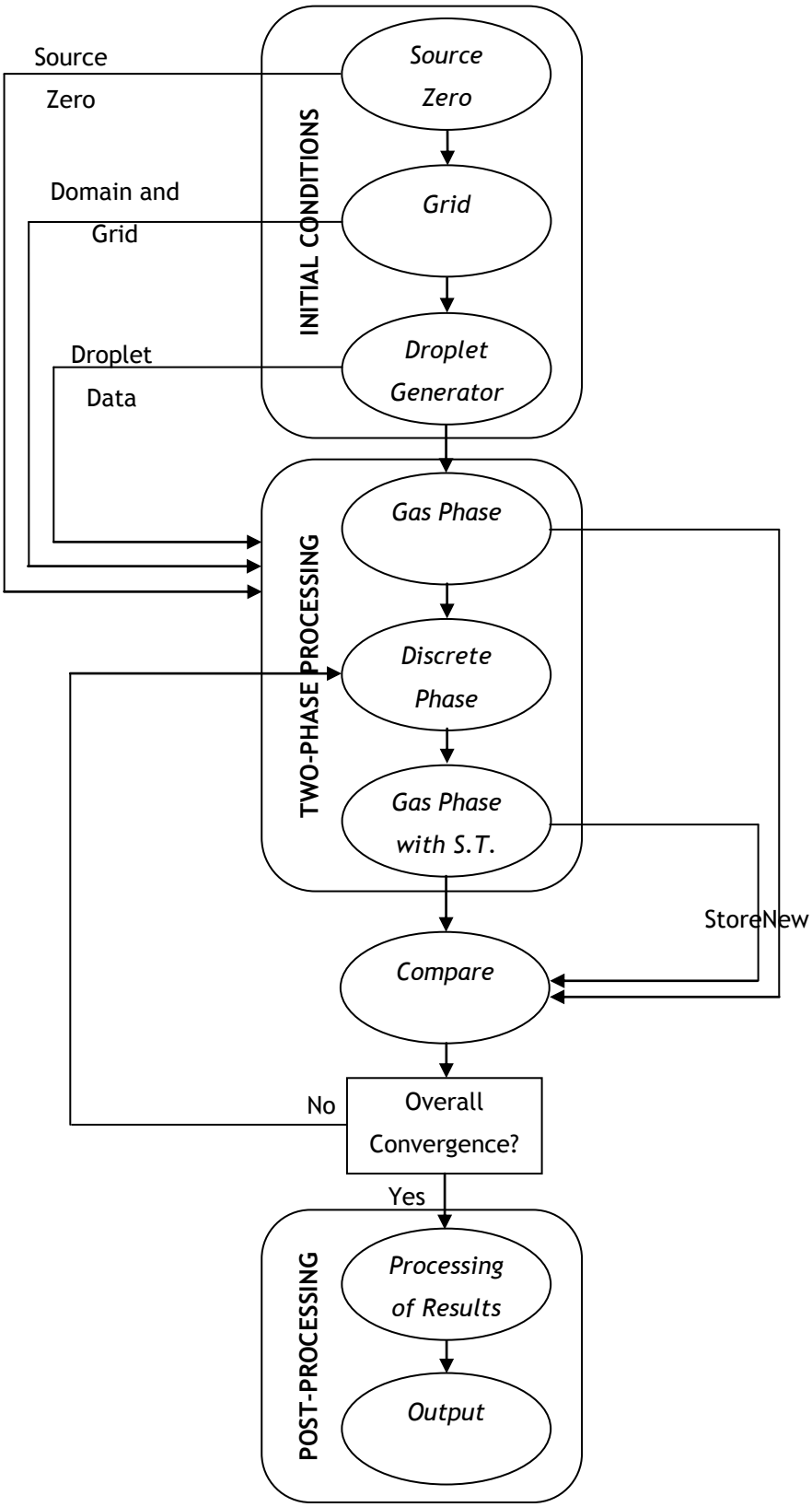

Figure II-3: Flowchart illustrating the iterative procedure of the model.

6. Boundary Conditions

The numerical study of turbulent flows demands the resolution of differential equations in the domain under consideration. This computational domain corresponds to the representation of the experimental rig of the work of Arcoumanis *et al.* (1997). The authors performed experiments with oblique gasoline sprays impinging on a solid wall inside a wind tunnel which had a rectangular cross section of $32 \times 172\ mm$. The injector was positioned at the top along the centreline of the tunnel $0.05\ m$ far from the inlet plane, and the injector direction was $20°$ inclined in relation to the vertical, in the downstream sense. The geometry is illustrated in Figure II-4. The air was at atmospheric pressure and room temperature.

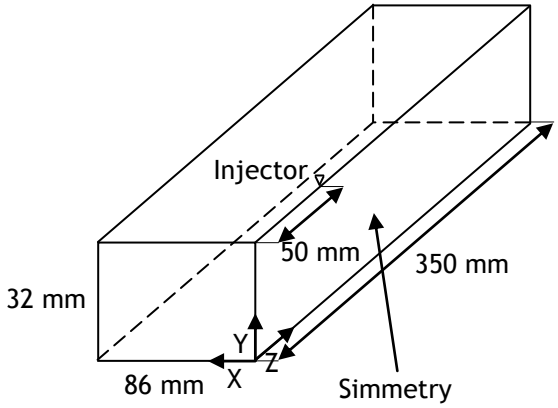

Figure II-4: Domain of solution.

The computational domain has six boundaries: an inlet and outlet plane of the crossflow, a plane of symmetry and three solid walls at the top, bottom and side of the channel.

6.1. Continuous Phase

At the inlet boundary, it is assumed that the crossflow has a constant horizontal velocity component through the entire cross-section while the other two velocity components are set to zero. At the outlet plane, there is a free boundary and no action for transport equation is required. At the symmetry plane, the normal velocity component vanishes as well as the gradients of the other variables in the normal direction. At the three solid surfaces, the normal components of the velocity are set to zero whilst in the other directions wall functions described by Launder and Spalding (1974) are employed for the velocity and turbulence quantities.

6.2. Dispersed Phase

In this phase, it is assumed that the particles are sufficiently dispersed so the interaction between droplets is negligible. The outcomes of an impinging droplet after impacting on a solid surface and the resulting secondary droplets are influenced by various

parameters related with the impact conditions and the liquid and surface properties. These parameters affect the regime transition criteria, which are defined in terms of dimensionless numbers, and in turn lead to different secondary droplets characteristics.

6.2.1. Atomization Conditions

The accurate modelling of spray impinging on a solid surface strongly depends on the pre-impingement conditions and the characteristics of the spray at the early stage after being generated. Since there is no reliable atomisation mode yet available, an empirical procedure is used for estimating the effective conditions at the exit of the injector. Those initial values have been estimated using the data from the free spray measurements that were given by Posylkin (1997) and described in Arcoumanis *et al*. (1997) and Bai *et al*. (2002). In the free spray experiment, the ensemble-averaged droplet size and velocity characteristics of the spray were obtained at a horizontal plane with circular region (with radius of $32\ mm$), $80\ mm$ downstream of the injector (Figure II-5).

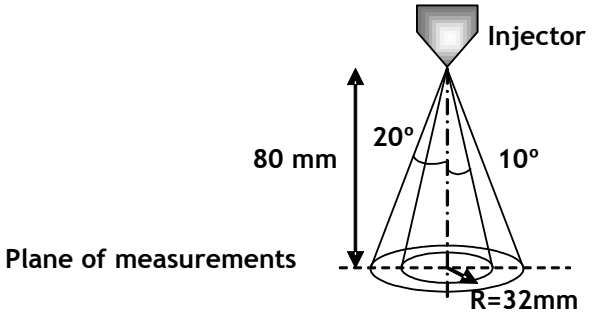

Figure II-5: Diagram illustrating the free spray experiment and the plane of measurements.

However, to use these data it is necessary to assume that the droplet parcel keeps the same size as assigned at the injector throughout the pulse duration, and the whole size range observed at the measured plane corresponds to that encountered in the near-nozzle region. These major simplifications can be ascribed since the hollow cone sprays are normally well-dispersed and, thus, the probability of collision is small.

Therefore, both the initial droplet sizes and velocities must then be estimated. The procedure to estimate these initial conditions rely on a *pdf* for the droplet sizes, a droplet velocity-size correlation and an average droplet mass flux as a function of radius. A detailed explanation is given in the reference of Bai *et al*. (2002).

6.2.2. Impingement Regimes

The original Bai *et al*. (2002) model – the one used in this work – considers four impingement regimes (*stick, rebound, spread* and *splash*), which depends on the properties of the impinging droplets and the impingement surface, but neglect the effects of neighbouring impinging droplets and gas boundary layer on the impingement dynamics. The model considers both dry and wetted wall conditions, below the fuel boiling point.

i. Deposition

This regime corresponds to the combination of the *stick* and *spread* phenomena. In both regimes the droplet adheres to the wall and coalesces to form a local film, i.e., no secondary droplets are ejected.

ii. Rebound

This regime can be observed in either dry or wetted wall as stated before. The rebound velocities components are determined from the relationship developed for a solid particle bouncing on a solid wall (Matsumoto and Saito, 1970):

$$\vec{V}_{RT} = 5/7\,\vec{V}_{IT} \quad \textbf{(II-34)}$$

$$\vec{V}_{RN} = -e\vec{V}_{IN} \quad \textbf{(II-35)}$$

where $\vec{V}_{IT}$ and $\vec{V}_{IN}$ are the tangential and normal incident velocity components, and $\vec{V}_{RT}$ and $\vec{V}_{RN}$ are the tangential and normal rebound velocity components, respectively. The quantity e is the "restitution coefficient", which has been obtained by Grant and Tabakoff (1975) and is as follow:

$$e = 0.993 - 1.76\theta_I + 1.56\theta_I^2 - 0.49\theta_I^3 \quad \textbf{(II-36)}$$

where θ_I is the incident angle, i.e., it is the angle (in radians) between the incident particles and the wall surface (see Figure II-6). To note that it is considered that the rebounding droplets have a negligible rotation effects (Bai and Gosman, 1995).

iii. Splash

Splashing occurs when the incident particles collides with the solid surface with high impact energy giving rise to secondary droplets. Those secondary droplets are organized into up to six parcels with equal mass and different size and velocities. The ejection angle (θ_S) of those secondary particles falls randomly into a cone but not uniformly. In fact, there are sub-ranges into which there will be a greater probability to find droplets. The bounds of such sub-ranges depend on the surface roughness and the liquid layer thickness. Mutchler (1979) found that θ_S varies in the range of $[5°; 50°]$ in situations where droplets splash on a smooth hard wall.

These assumptions will help to determine the total secondary to incident droplet mass ratio (m_S/m_I), and the size, velocities and ejection angles of the secondary droplets.

Mass ratio

Since there is no available general correlation to determine the mass ratio in terms of its influencing parameter (We, La, δ/d_I), the following approximations (established from the existing experimental data) have been made for both dry and wetted wall:

$$r_m = \frac{m_S}{m_I} = \begin{cases} 0.2 + 0.6\alpha & for\ dry\ wall \\ 0.2 + 0.9\alpha & for\ wetted\ wall \end{cases} \quad \textbf{(II-37)}$$

where α is a random number distributed uniformly between the interval $[0;\ 1]$, which make r_m to take random value evenly distributed in the experimentally-observed range $[0.2;\ 0.8]$ for a dry wall and $[0.2;\ 1.1]$ for a wetted wall.

Secondary Droplets Sizes

There are three available methods for modelling droplet size distributions in sprays: the maximum entropy method, the discrete probability function method and empirical method. The latter is an approach in which the distributions are obtained by curve fitting the data collected for a wide range of experimental conditions. In the other two cases, it is assumed that the droplet are generated by a non-deterministic process (maximum entropy) or composed of both deterministic and non-deterministic parts (Discrete Probability Function).

The empirical models, such as the chi-square, Rosin-Rammler and Nukiama-Tanasawa distributions, can be generally expressed as:

$$f(d) = \left[\frac{q}{\bar{d}}\left(\frac{d}{\bar{d}}\right)^p\right]\exp\left[-\left(\frac{d}{\bar{d}}\right)^q\right] \quad \textbf{(II-38)}$$

where p is a shape parameter, $\bar{d}$ and q are scale parameters. While $\bar{d}$ influence the size distributions, q seems to affect the size range of the distribution. In their model, Bai *et al*. (2002) assumed that the secondary droplets sizes distribution – derived from experimental data (Stow and Stainer, 1977; and Levin and Hobbs, 1971) and measurements (Yarin and Weiss, 1995; and Mundo *et al.,* 1995) – could be fitted by a Chi-square distribution function (substituting $p = 0$ and $q = 1$ in the previous equation):

$$f(d) = \frac{1}{\bar{d}}\exp\left(-\frac{d}{\bar{d}}\right) \quad \textbf{(II-39)}$$

where $\bar{d}$ denotes the number mean diameter, which is related to the volumetric mean diameter d_v:

$$\bar{d} = \frac{d_v}{6^{1/3}} = \frac{1}{6^{1/3}}\left(\frac{r_m}{N_s}\right)^{\frac{1}{3}} d_I \quad \textbf{(II-40)}$$

Here, d_I is the incident droplet diameter and $r_m = m_s/m_I$ is the total splashing to incident droplet mass ratio, which is randomly determined, thus introducing some non-determinism into the formulation.

Number of Secondary Droplets:

Bai *et al*. (2002) obtained a correlation for the total number of secondary droplets by fitting the data of Stow and Stainer (1977) as:

$$N_s = a_0\left(\frac{We}{We_c} - 1\right) \quad \textbf{(II-41)}$$

in which $a_0 = 5$ and We_c is the critical Weber number for splashing. The number of droplets n_i in each secondary parcel (in this case, until 6 droplet parcels could be considered) is determined through mass conservation:

$$n_i d_i^3 = \frac{r_m d_j^3}{p} \quad \textbf{(II-42)}$$

However, some others approaches haves been used meanwhile. In the Senda *et al.* (1999) study, an impingement model for droplet impacting on wetted surface has been developed. The droplet-wall interaction process is classified into two cases and is separated by a Weber number of 300. In the lower Weber number case, the authors considered three type of fuel film breakup based on the non-dimensional film thickness (δ). For δ between 0.6 and 1.35, i.e. rim type breakup, it is assumed that the number of outgoing droplets N_s is 4; otherwise ($\delta < 0.6$ and $\delta < 1.35$ for Rim and Column type breakup, respectively) $N_s = 1$. With Weber number greater than 300, the post-splash droplet number is given by:

$$N_s = r_m \frac{d_i^3}{d_s^3} \quad \textbf{(II-43)}$$

with r_m assumed to be 80% by referring experimental results of Yarin and Weiss (1995).

Recently, Okawa *et al.* (2006) fitted a correlation for the number of secondary droplets to their own experimental results and to that reported by Stow and Stainer (1977), valid for normal impacts:

$$(N_s)_{wet} = \max[4.97 \times 10^{-6}; 7.84 \times 10^{-6}(\delta)^{-0.3}]\, K^{1.8} \quad \textbf{(II-44)}$$

where δ is the dimensionless film thickness (h/d_l) and $K = Oh^{-0.4}We$.

Velocity of Secondary Droplets

There are also different ways to predict the velocity of the secondary droplets generated from the impact of a drop. In the Bai *et al.* (2002) and Senda *et al.* (1999) models, the velocity is assessed from energy conservation, which balance the energy of incoming droplets before impacting on the surface and the splashing droplets moving away from the wall. Therefore, the surface and kinetic incident droplet energy must equalize the kinetic splashing droplet energy and the dissipative loss due to the action of viscosity. Since both the kinetic and surface energy are easily known, attention must be given to the energy dissipation. In fact, recent research efforts have been applied in this field in order to improve the accuracy of the method.

In the Bai *et al.* (2002) model, the secondary droplets velocities resulting from oblique impingement are analysed as a superposition of those arising from normal

impingement and wall-tangential component. Thus, the splash velocity vector, $\overrightarrow{V_S}$, of secondary droplets is composed by two component resulting from the normal and tangential component of the incident velocity:

$$\overrightarrow{V_S} = \vec{V}_{ST} + \vec{V}_{SN} \quad \textbf{(II-45)}$$

It is assumed that the component $\vec{V}_{ST}$ is a directly proportional to the tangential component of the incident velocity:

$$\vec{V}_{ST} = C_f \vec{V}_{IT} \quad \textbf{(II-46)}$$

where the constant of proportionality (C_f) is the friction coefficient, which has been estimated experimentally (Wright, 1986) to be in the range $[0.6;\ 0.8]$ for a water drop splashing on soil surface.

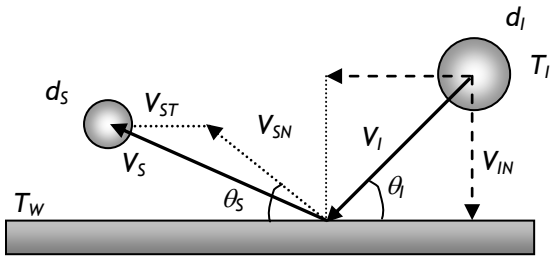

Figure II-6: Diagram illustrating droplet impingement on to a wall (Bai et al., 2002).

The other component of the velocity ($\vec{V}_{SN}$) comes from the normal component of the incident velocity, which is the component in the origin of the disintegration process of a splashing event. In other words, the impact energy imparted to the disintegration phenomenon depends solely on $\vec{V}_{IN}$, while $\vec{V}_{IT}$ simply transfers a portion of its tangential momentum to each secondary droplets. To note that $\vec{V}_{SN}$ is not in general normal to the surface – the secondary particles come with an ejection angle after the splash phenomenon (Figure II-6). The normal component of the splashing droplets must then be estimated by considering energy conservation law as follow:

$$\frac{1}{2}\frac{m_s}{p}\left[\left(\vec{V}_{SN,1}\right)^2 + \cdots + \left(\vec{V}_{SN,p}\right)^2\right] = E_{KS} \quad \textbf{(II-47)}$$

where E_{KS} is the splash kinetic energy due to $\vec{V}_{IN}$ only, and is given as:

$$E_{KS} = E_{KI} + E_{I\sigma} - E_D - E_{S\sigma} \quad \textbf{(II-48)}$$

in which $E_{KI} = 1/2\, m_I \vec{V}_{IN}^2$ is the incident kinetic energy based on the normal velocity; $E_{I\sigma} = \pi\sigma d_I^2$ is the incident droplet surface energy; $E_{S\sigma} = \pi\sigma \sum_1^p N_S d_S^2$ is the total surface energy of splashing droplets, and E_D is the dissipative energy loss. This last parameter is perhaps the most critical quantity to determine accurately. There have been several approaches taken until now.

Bai *et al.* (2002) deduced their own relationship for the dissipated energy in terms of the critical Weber number, but due to the under-estimation of the values in certain ranges of application, the parameter was then limited by a postulated value of 80% of the kinetic incident energy based on the normal incident velocity of the droplets:

$$E_D = \max\left(0.8E_{KI}; \frac{We_c}{12}\pi\sigma d_I^2\right) \quad \textbf{(II-49)}$$

Lee and Ryou (2000) determined the total velocity of droplets after impingement by using a dissipated energy correlation deduced from their own experimental consideration. The authors assumed that the splash occurred at the moment of the crown emergence and, then, from observations of Yarin and Weiss (1995), adopted a value for the dimensionless parameter of the disc when splashing occurs $(\beta_{max} = d_{max}/d_I = 2)$. The corresponding dissipated energy relationship of the droplet when the incident droplets impinge on the wall has the form:

$$E_D = \left(\frac{4.5C_w We_{IN}\beta_{max}^4}{r_m Re_{IN}} - \frac{12C_w}{r_m}\right) \quad \textbf{(II-50)}$$

where C_w is given as $(r_m/N_s)^{1/3}$ from mass conservation law and $N_s = 0.187We_{IN} - 4.45$.

Another approach has been taken by Mao *et al.* (1997) who approximated the flowfield of a droplet impinging on a surface by a stagnation point-flow, which led to a theoretical viscous dissipation model characterized by the liquid viscosity, impact velocity and maximum spread.

However, the principal study available related with this parameter has been conducted by Chandra and Avedisian (1991), which concluded that the dissipation energy is directly proportional to viscosity. In fact, this study was focused on estimating the maximum diameter of liquid which spreads on the surface. The authors found that the viscosity largely controls the post-impact occurrences, which in turn rules the splash phenomena. That specific energy can then be estimated as:

$$E_D = \int_0^{t_c}\int_V \phi dV dt \approx \phi V t_c \quad \textbf{(II-51)}$$

where the dissipation function ϕ is given by:

$$\phi = \mu\left(\frac{\partial v_i}{\partial x_j} + \frac{\partial v_j}{\partial x_i}\right)\frac{\partial v_i}{\partial x_j} \approx \mu\left(\frac{U}{h}\right)^2 \quad \textbf{(II-52)}$$

and t_c is estimated as:

$$t_c \approx d_I/U \quad \textbf{(II-53)}$$

which is a time scale characteristics of convection. The volume of the liquid in the drop, after flattened out in a regular disc shape, is:

$$\mathrm{V} \approx \frac{1}{4}\pi d_{max}^2 h \qquad \textbf{(II-54)}$$

Combining all those equations yields the relationship for dissipation energy:

$$E_D \approx \frac{1}{4}\pi\mu\frac{U}{h}d_I d_{max}^2 \qquad \textbf{(II-55)}$$

Since then, several investigators took the assumptions of Chandra and Avedisian (1991) to estimate the dissipation energy and tried to improve the accuracy of the theoretical model. Pasandideh-Fard *et al.* (1996) replaced the splat film thickness h in the dissipation function ϕ, which they found that it was overestimated to values up to 40% the maximum extend of the film d_{max}, by the boundary layer thickness δ_{bl} at the solid-liquid interface. This length scale, which appears to be more appropriate to estimate the magnitude of viscous dissipation, is given by:

$$\delta_{bl} = \frac{2d_i}{\sqrt{Re}} \qquad \textbf{(II-56)}$$

In addition, the authors (Pasandideh-Fard *et al.*, 1996) assumed a new time t_c, taken for the droplet to spread until its maximum extension, dependent on the impact velocity of the incident droplet, i.e., $t_c = 8/3\,(d_I/U)$.

After modelling the dissipation energy loss, it is possible to determine the splash kinetic energy, and consequently the "normal" component of the secondary droplets. Therefore, for the Bai *et al.* (2002) dissipation energy relationship and for only one secondary parcel ($p = 1$), replacing Equation II-48 and II-49 in Equation II-47 enable to determine $\vec{V}_{SN}$. Otherwise ($1 < p \leq 6$), the following size-velocity correlation of secondary droplets provided by Ghadiri (1978) is used as a supplemental equation:

$$\frac{\vec{V}_{SN,1}}{\vec{V}_{SN,i}} \approx \frac{\ln\left({}^{d_1}/_{d_I}\right)}{\ln\left({}^{d_i}/_{d_I}\right)}, \qquad (i = 2 \ldots p) \qquad \textbf{(II-57)}$$

which, upon substitution into Equation II-47 yields $\vec{V}_{SN,1}$. The latter velocity is then substituted into II-57 to obtain $\vec{V}_{SN,i}$.

6.2.3. Regime Transition Criteria

The Bai *et al.* (2002) model considers four impingement regimes: *stick*, *rebound*, *spread* and *splash*. The existence of these regimes depends on the properties of the impinging droplets and the impingement surface, including whether the latter is dry or wetted. The authors did not include the effect of the film thickness on the wall, but instead, took the assumption that a wetted surface behaves as a very rough dry wall and, consequently, the effect of a liquid film is accounted in the fitting constant A (of the deposition/splash

transition criteria). For either dry or wetted wall, the spread-splash regime transition conditions were derived from the Stow and Hadfield (1981) data, giving rise to a Critical Weber number dependent on the Laplace number. The stick-rebound and rebound-spread (derived from the data of Lee and Hanratty, 1988) transitions for wetted walls were set with the critical Weber number of 2 and 20, respectively.

The first objective of this thesis is to study the influence of the transition criteria between the deposition and splash regimes in the outcomes of the impingement droplet for a specific three-dimensional configuration. Then, in addition to the transition criteria applied in the model also the transition criteria between deposition and splash of Mundo *et al. (1995),* Cossali *et al. (1997),* Senda *et al. (1999)* and Huang and Zhang (2008) have been assessed in the same model for the configuration of the experimental work of Arcoumanis *et al.* (1997). The characteristics and the conditions under which the correlations were proposed are presented next, and are outlined in Table II-5.

Mundo *et al. (1995)* have investigated multi-droplet impingement on rough surfaces with the aim of identify the deposition-splash regime criterion. The experiments involved a wide range of Weber and Ohnesorge numbers by using different droplets fluids (water, sucrose, ethanol and a water-sucrose-ethanol mixture), diameters (from 60 to $150\ \mu m$) and injection velocities (from 12 to $18\ m/s$). The droplets were generated with a frequency between 27.2 and $64.3\ kHz$ in a plate with two different surface roughness (2.7 and $78\ \mu m$) at $25°C$. The empirical correlation, which determines the transition between deposition and splash regimes, is based on droplet Reynolds number and Ohnesorge number and has been used in many models since then. Despite the correlation has been deduced for dry surfaces, it is considered the analogy of the liquid film as a very rough surface.

Cossali *et al. (1997)* investigated the same regime transition by analysing a large number of pictures of droplets impacting on an aluminium plate – characterized by a mean roughness of $0.14\ \mu m$ – with a non-dimensional film thickness between 0.08 and 1.2. To span a wide range of conditions, various mixtures of water and glycerol (i.e., pure water, 50%, 65%, 75% and 85% of Glycerin in Water) with different diameter were used. The droplet generator height ranged between 0.05 and $2\ m$ and produced falling drops with maximum velocities of $6.5\ m$/s. The authors found a correlation for the deposition-splash limit based on the Weber and Ohnesorge numbers, which produced good results for non-dimensional film thickness under the unity.

In the Senda *et al. (1999)* study, a spray-wall interaction sub-model has been developed in order to incorporate into the KIVA-II code. The droplet-wall interaction process is classified into two cases and separated by a Weber number of 300. In the lower Weber number case ($We < 300$), the authors take into account the droplet-liquid interaction (due to the film liquid formation on the surface) as well as the interaction between neighbouring droplets. At higher Weber number, the model focus on the splash type breakup of the liquid film. Here, rough surfaces are assumed to be smooth surfaces, and wetted surface are

treated as rough one. The conditions were based on experimental results for iso-octane (gasoline), at atmospheric pressure and room temperature. The computational results are taken for a wall temperature of $293\,K$, an impingement distance between the injector and the flat wall of $30\,mm$ and impingement angles of $90°$. The criterion for critical Weber number – function of the Laplace number and the non-dimensional film thickness – establishing a deposition-splashing limit had been proposed by Marengo in 1995.

Recently, experimental observations for droplet impingement with different fluids have been conducted by Huang and Zhang (2008) and a new correlation based on the Weber and Reynolds number has been proposed to predict the deposition-splashing transition. The transition between the two regimes was observed for the impingement of droplet of diverse diameters (1.8 to $4\,mm$) on water and oil liquid film with 1 and $3\,mm$ of thickness. The correlation proposed depends on the Weber and Reynolds number, as well as the non-dimensional film thickness.

Table II-5: Impingement Regimes and Transition Criteria.

	Authors	***Wall status***	***Regime transition state***	***Critical Weber number***
Original Model	Bai *et al.* *(2002)*	Dry	Deposition / Splash	$We_c \approx 2630\ La^{-0.183}$
		Wetted	Stick / Rebound	$We_c \approx 2$
			Rebound / Spread	$We_c \approx 20$
			Spread / Splash	$We_c \approx 1320\ La^{-0.183}$
New Transition Criteria Studied	Cossali *et al.* (1997)	Wetted	Coalescence / Splash	$K = Oh^{-0.4}\ We = 2100 + 5880\ \delta^{1.44}$
	Mundo *et al.* (1995)	Wetted*	Deposition / Splash	$K = Oh\ Re^{1.25} = 57.7$
	Senda *et al.* (1999)	Wetted	Deposition / Splash	$We = \left(2164 + 7560\delta^{1.78}\right) La^{0.2}$
	Huang and Zhang (2008)	Wetted	Coalescence / Splash	$(We\ Re)^{0.25} = 25 + 7\delta^{1.44}$

*Correlation derived for dry surface. May be used in wetted surfaces assuming that it behaves as a very rough dry wall.

III. Results

1. Introduction

This chapter presents the numerical predictions of the model for droplets impinging on a solid wall through a crossflow, which computational method has been described in the previous chapter, and the discussion of the results obtained.

After this section, the validation of the results, which is made through the mesh independence, is presented. Then, the section III.3 is devoted to the study of the transition criteria to attain the splash regime. Several transition criteria available in the literature are tested in the Bai *et al.* (2002) base model and the results are tested against the experimental data of Arcoumanis *et al.* (1997). Finally, in the section III.4, attention is given to the energy dissipation loss. Several relationships available in the literature are inserted in the same global model in order to assess its influence on the spray impingement modelling. Here, the work is divided into two parts in which the same base model is used but with two different transition criteria: in the first part, with the transition criteria of Bai *et al.* (2002), which is the original criterion of the base model; and in the second part, with the transition criteria of Cossali *et al.* (1997), which presented good results in some specific case (as stated in the section III-3). A third part is presented to make a comparison between the two cases studied and discuss the results.

2. Mesh Independence

The mesh independence is carried out to ensure that the discretization error lies in an appropriate level and, consequently, the solution does not depend on the grid size. The horizontal and vertical profiles of the horizontal velocity component, W, are tested in three different grid sizes. The coarser grid has 14 points in the X direction, 11 in the Y direction and 21 in the Z direction, while the following finer meshes are obtained multiplying the number of points in each direction – of the previous coarser grid – by the square root of two and rounded to the nearest integer, giving rise to meshes of $20x16x30$ and $28x22x42$ points. The grid spacing was increased with a factor of 1.08 in all directions of the domain.

The Figure III-1 and Figure III-2 show the horizontal and the vertical profiles, respectively, of the horizontal velocity component, W, at three different planes: $Z/H = 1.3$, 2.3 and 8.3. The horizontal profile is obtained in the horizontal plane placed at half the total height of the domain ($Y/H = 0.5$), while the vertical profile is obtained in the vertical plane located at $X/H = 0.05$. The horizontal component of the velocity, W, is dimensionless by the horizontal component of the velocity at the plane of symmetry, W_C, while the height of the domain, H, is used to dimensionless the position in the horizontal and vertical planes.

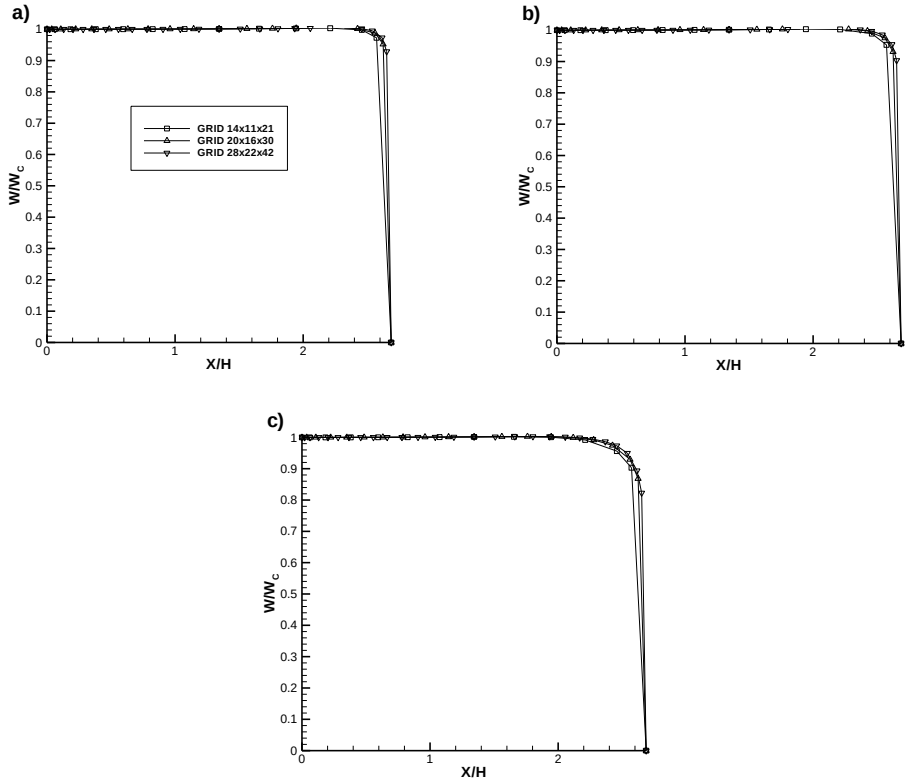

Figure III-1: Dimensionless horizontal profile, at Y/H = 0.5, of the horizontal velocity component, W, at a) Z/H = 1.3, b) Z/H = 2.3 and c) Z/H = 8.3.

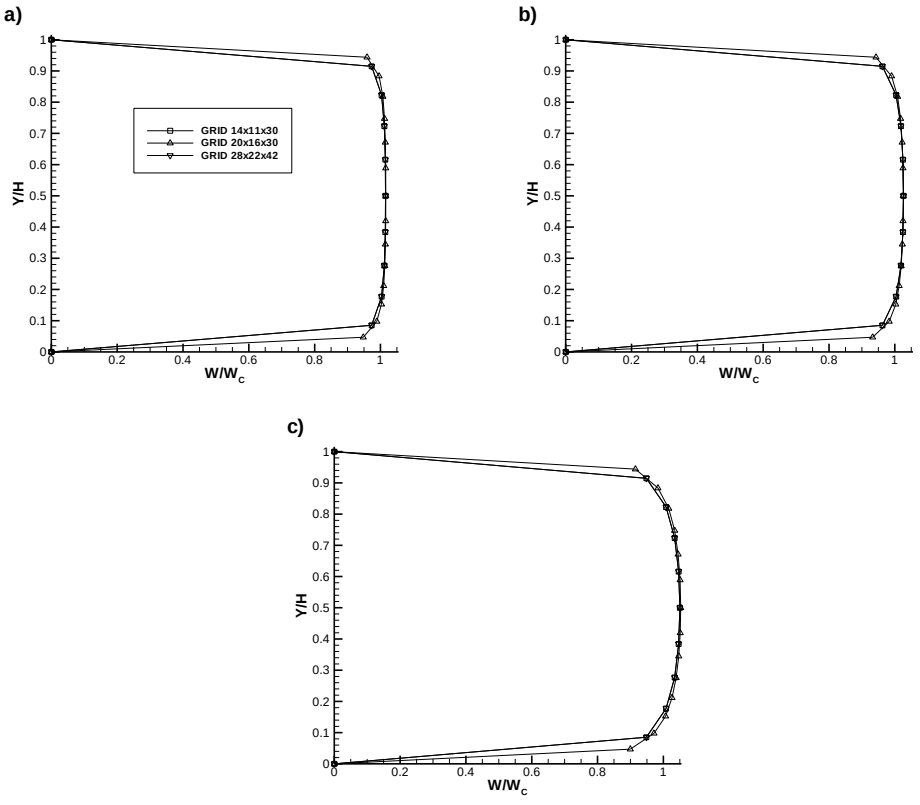

Figure III-2: Dimensionless vertical profile, at X/H = 0.05, of the horizontal velocity component, W, at a) Z/H = 1.3, b) Z/H = 2.3 and c) Z/H = 8.3.

The figures show that the results are independent of numerical influences since no significant variations are found for the three different meshes. In order to achieve an equilibrium between performance and time request, the middle mesh $20x16x30$ was adopted.

The comparison between the dimensionless vertical profile of the horizontal velocity – normalized by the maximum horizontal velocity component and the height of the solution domain – of the $5\,m/s$ air flow obtained numerically and the measured by Arcoumanis *et al.* (1997) are presented in Figure III-3. The velocity profile has been taken in the vertical plane at $X/H = 0.05$ and upstream of the injector ($Z/H = 1.3$). The Figure show that the numerical results are in agreement with the Laser Doppler measurements of the air flow.

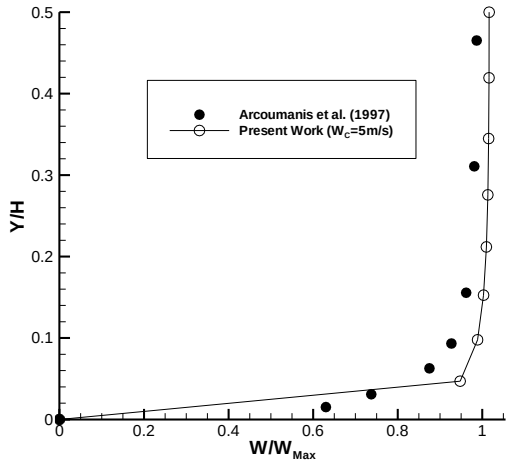

Figure III-3: Dimensionless vertical profile of the horizontal velocity component, W, at the position $X/H = 0.05$ *and* $Z/H = 1.3$.

3. Transition Criteria

The sizes and velocities – as well as the number – of the secondary droplets due to the impact of a drop on a solid wall depend strongly on the impingement conditions, which in turn depend on the initial conditions of the spray at the injector exit, geometry and characteristics of the system, and may also be associated with the crossflow velocity. In this section, it is presented a numerical study of a spray impinging on a surface through a crossflow in which the numerical predictions resulting from the Bai *et al.* (2002) base model for different transition criteria between the deposition and splash regimes are compared and assessed with the experimental data of Arcoumanis *et al.* (1997). Hence, the main purpose of this study is to evaluate the performance of the original model with other transition criteria for the representation of the spray impingement phenomena in a three-dimensional configuration. In fact, in addition to the improved transition criteria applied in the base model (Bai et al, 2002), also the transition criteria between deposition and splash deduced by Mundo *et al.* (1995), Cossali *et al.* (1997), Senda *et al.* (1999) and Huang and Zhang (2008) have been evaluated in the same model to test against the experimental data of Arcoumanis *et al.* (1997).

The splash transition criteria studied are presented in the Table III-1. In addition, a thorough analyses of the general conditions under which the transition criteria have been proposed are outlined in Annex 3.

Table III-1: Splash Transition Criteria studied in this work.

Authors	***Splash Transition Criteria***	***Criteria in terms of We***	***Boundary Conditions***	***Observations***
Bai et al. (2002)	$We_c = 1320La^{-0.18}$	$We_c = 1320La^{-0.18}$	Non-heated, takes into account θ_l and crossflow	The effects of the liquid film is accounted in the fitting constant A, by comparing the presence of the film to a rough surface
Cossali et al. (1997)	$K_c = (Oh^{-0.4}We)_c = 2100 + 5880\delta^{1.44}$	$We_c = \frac{2100+5880\delta^{1.44}}{Oh^{-0.4}}$	Non-heated, for $\delta < 1$	-
Mundo et al. (1995)	$K_c = (OhRe^{1.25}) = 57.7$	$We_c = \frac{3329.29}{Re^{0.5}}$	Non-heated, takes into account θ_l and frequency f	The droplets are generated with a precise frequency.
Senda et al. (1999)	$We_c = (2164 + 7560\delta^{1.78}).La^{0.2}$	$We_c = (2164 + 7560\delta^{1.78}).La^{0.2}$	Non-heated, frequency f, (movement of) fuel film	The droplet wall interaction is classified in two case: lower Weber number ($We \leq 300$) and higher Weber number ($We > 300$)
Huang and Zhang (2008)	$K_c = (We.Re)^{0.25} = 25 + 7\delta^{1.44}$	$We_c = \frac{(25+7\delta^{1.44})^4}{Re}$	Non-heated, Normal Impact	Good results were found for thin oil and water liquid film

It is assumed that the relative wall film thickness (δ) is the order of unity – as indicated by Bai and Gosman (1995). To note that the measurements data have size class of approximately $25\ \mu m$ while in this study a more precise size class of $15\ \mu m$ have been used, which can lead to some discrepancies. In Figure III-5 to Figure III-12 the dashed line with closed symbols correspond to the measurements of Arcoumanis *et al.* (1997), while the solid line with open symbols corresponds to the predictions results: the red triangle, the blue square, the green diamond, the pink gradient and the cyan rightward triangle corresponds to the transition criteria of Bai *et al.* (2002), Cossali *et al.* (1997), Huang and Zhang (2008), Mundo *et al.* (1995) and Senda *et al.* (1999), respectively, which are inserted into the same base model (Bai *et al.*, 2002).

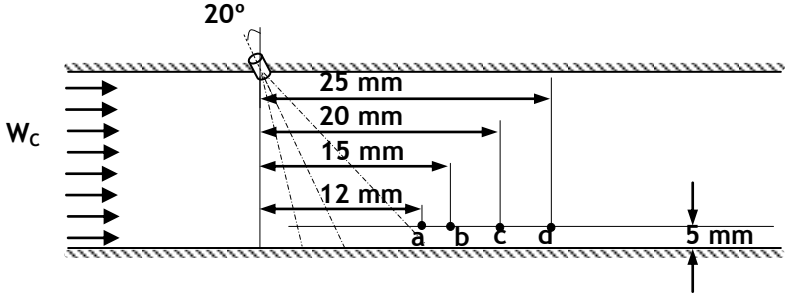

Figure III-4: Illustration of the four locations where the results have been taken.

The results have been taken at four different locations *a*, *b*, *c* and *d*, which are located in a horizontal plane $5\,mm$ above the impingement wall and 12, 15, 20 and $25\ mm$ downstream the injector, respectively, as seen in Figure III-4. These are the same positions where the measurements have been taken from the work of Arcoumanis *et al.* (1997) and, consequently, allow a direct comparison.

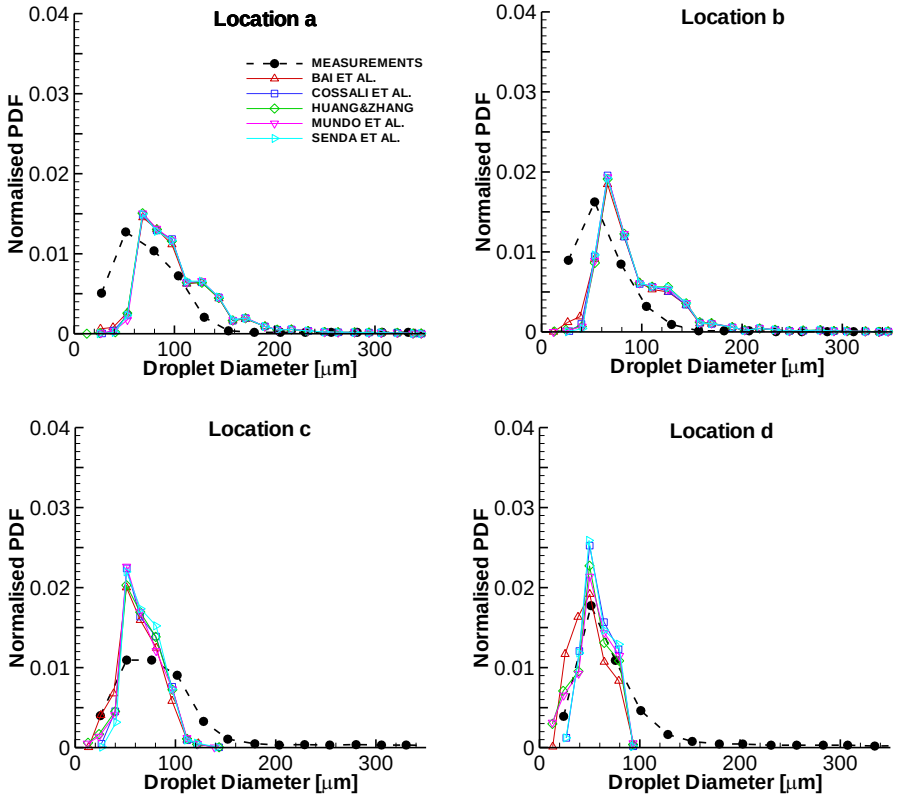

Figure III-5: Size distributions of downward-moving droplets at four locations for a cross flow velocity of 5 m/s.

The Figure III-5 shows the measured and predicted size distributions of droplets moving downward through a crossflow of $5\,m/s$. Despite the different deposition-splash boundaries evaluated, good concordance is verified for all the regime transition criteria considered (only the Bai *et al.*, 2002 case show a slight different behaviour for smaller and/or larger droplet diameters at locations *c* and *d*) but they still show over-predicted peak values at all the locations as well as a rightward shift of the mode of the droplet diameters (or more frequent droplet diameter) at the locations *a* and *b* in comparison with the measurements. These discrepancies may be related to the uncertainties with the expected initial characteristics of the spray as well as all the procedures used to estimate those initial conditions (in order to reproduce the spray at the early stage after being generated). In addition, it can be seen in the three locations closer to the injector that the number of smaller droplets is under-estimated, which makes either the increase of the mode value or the over-estimation of the larger droplet diameters. In the specific case of the location *c*, both smaller and larger droplet diameters are under-estimated, which causes a greater over-estimation of the peak value. Another observation is that for both location *c* and *d*, the

droplets with diameters larger than $120\,\mu m$ do not appear in the results contrary to what happens with the measurements.

For the normalized *pdf* of the upward-moving droplets, the results are presented in Figure III-6 with the presence of a $5\,m/s$ crossflow but in this case the results show very different behaviours. From the results, it is easily seen that the Senda *et al.* (1999) correlation shows difficulty to find upward-moving droplets. This is due to the fact that the critical threshold to reach the splashing regime is higher than in the other correlations, originating fewer secondary droplets and, consequently, altering the corresponding final outcome. In fact, it is seen at location *b* that one of the point estimated does not appears in the figure because it lies very far from the range limit introduced, while at location *c* the only two class observed are far from having a behaviour similar to the other correlations. At location *a* no upward moving droplets are found with this correlation and at the further location in relation to the injector (location *d*) it is found a completely distinct distribution. In contrast to the previous results, the Cossali *et al.* (1997) case presents predictions quite close to the measurements – despite still slightly over-predicting the droplet diameter peak value and under-estimating the droplets with a diameter of about $100\,\mu m$. For the other three cases, the peak-values are over-predicted and shifted to the left – in particular the correlations of Mundo *et al.*, 1995, and Huang and Zhang, 2008. The larger droplets found in the prediction are under-estimated, which may be one cause for the over-estimation of the most frequent droplet diameter.

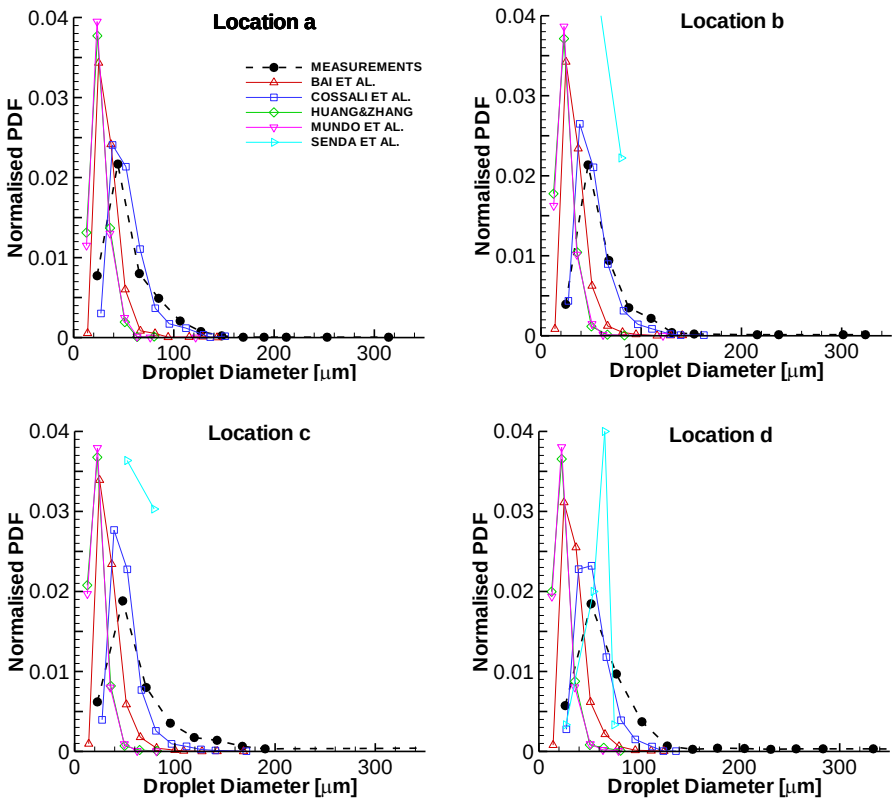

Figure III-6: Size distributions of upward-moving droplets at four locations for a cross flow velocity of 5 m/s.

In relation to the velocity-size correlations for droplets with downward and upward moving at the four locations with the presence of a $5\,m/s$ crossflow, the results are presented in Figure III-7 and Figure III-8. For the downward moving droplets, it is clear that further improvement must be done in order to minimize the difference between predicted and measured results. In general, the velocity profiles are under-estimated for the entire range of droplets diameters, except at the location *b* where there is a slight range (droplets with diameter around 200 μm) in which the predicted velocity is over-estimated in relation to the measurements. In addition, even the main behaviour of the velocity profile is different. At locations *c* and *d*, it is seen that the larger the droplet diameter the greater the upward velocity, whereas in the measurements the behaviour is not so straightforward. To note also that there are not found droplets class as large as those found in the measurements. In fact, this particular matter is more evident at locations *c* and *d* where the measured maximum size class are, respectively, 2.7 and 4 times greater than the estimated ones. On the other hand, good agreement is verified between all the different regime transitions evaluated at the four locations.

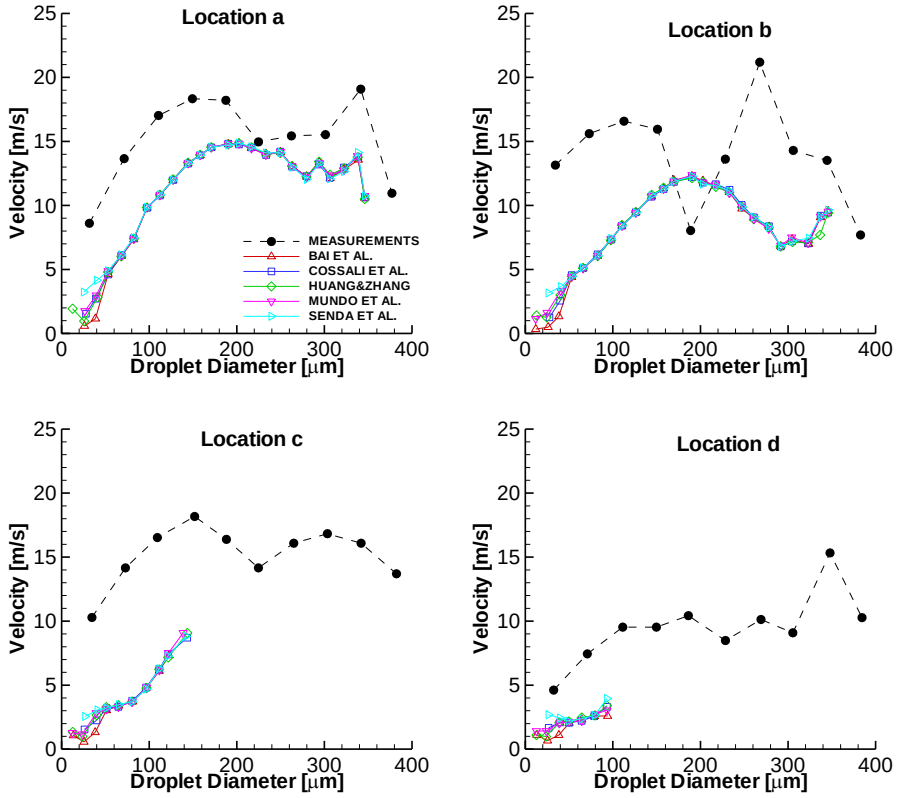

Figure III-7: Velocity-size correlation of downward-moving droplets at four locations for a cross flow velocity of 5 m/s.

The Figure III-8 presents the upward moving droplets and shows the difficulty of modelling the droplets resulting from rebound and splash regimes, which definitively calls for an improvement of this particular matter. The maximum class size found never exceeds $180\,\mu m$, while in the measured case they can extend until almost $400\,\mu m$. In addition, it can

be seen that the Cossali *et al.* (1997) results are somewhat overestimated. This may be due to the fact that the critical threshold is inversely proportional to the droplet diameter, which makes that only the larger droplets – and, thus, lower limit – can reach the splash regime. This fact leads to a slight increase in the splash kinetic energy and, consequently, a slight increase in the upward velocity. This combination between larger droplets splashing with greater velocity may make the difference in the results of the upward droplets.

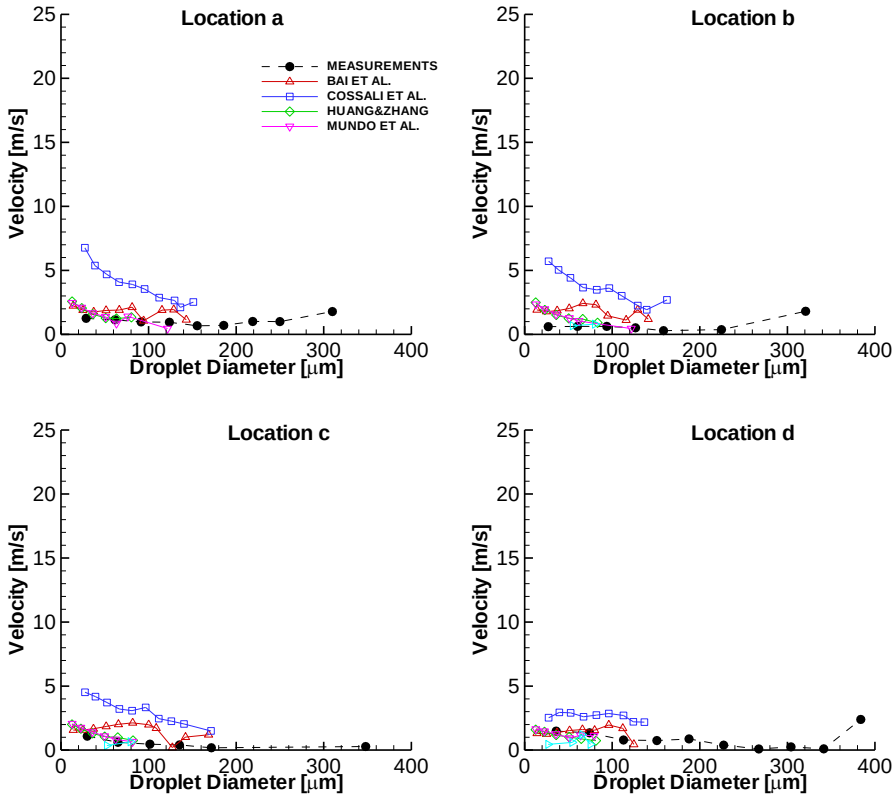

Figure III-8: Velocity-size correlation of upward-moving droplets at four locations for a cross flow velocity of 5 m/s.

Directing attention to the crossflow rate of 15 m/s, the measured and predicted size distributions of droplets moving downward and upward are presented in Figure III-9 and Figure III-10, respectively. Considering the normalized pdf with downward moving droplets, again great consistency is found for all the correlations considered but it still over-predicts the maximum frequency of the size-distribution at all the locations, and also present a rightward shift of the mode of the droplets diameters at location *c* and *d* and a leftward shift at location *b*. At locations *a*, *c* and *d* there is an under-estimation of the droplets with smaller diameters but it is balanced with the over-prediction and the rightward shift of the peak value – and consequent over-prediction of the larger droplets.

In the upward-moving case, there are again some differences between the predictions and the experimental data. The results show very specific behaviours dependent on the correlation considered. All have a leftward shift at all the location, except the Cossali *et al.* (1997) correlation at location *d*. In fact, this correlation is the one which is more similar to

the measurements at all the locations: besides the slight leftward shift at the locations *a*, *b* and c, it presents an insignificant under-estimation of the peak-value at location b and c and over-estimation at locations *a* and *d*. However, the Huang and Zhang (2008) and the Mundo *et al*. (1995) correlations present a more noticeable over-predicted mode of the droplet diameters at all the locations, while in the Bai *et al*. (2002) case this behaviour is only found at location *d*. Just as with the results presented with a crossflow of 5 m/s, the Senda *et al*. (1999) does not present satisfactory results possibly due to the reason presented above.

In the Figure III-11 and Figure III-12 it is presented the velocity-size correlations for droplets moving downward and upward, respectively. In the first case, the different transition criteria evidence good consistency between them but not with the measurements. In fact, the velocities verified are under-estimated at all the location and along the entire diameter range. To note also that the maximum size class estimated is still lower than the measured as seen in the results for a crossflow of $5\,m/s$. The Figure III-12 presents the upward-moving droplets and illustrates some discrepancies between the predictions and the measurements as stated also in Figure III-8. However, the maximum size class is now greater at the locations *b*, *c* and *d*, while at location *a* it can be said that there is a leftward shift of the results.

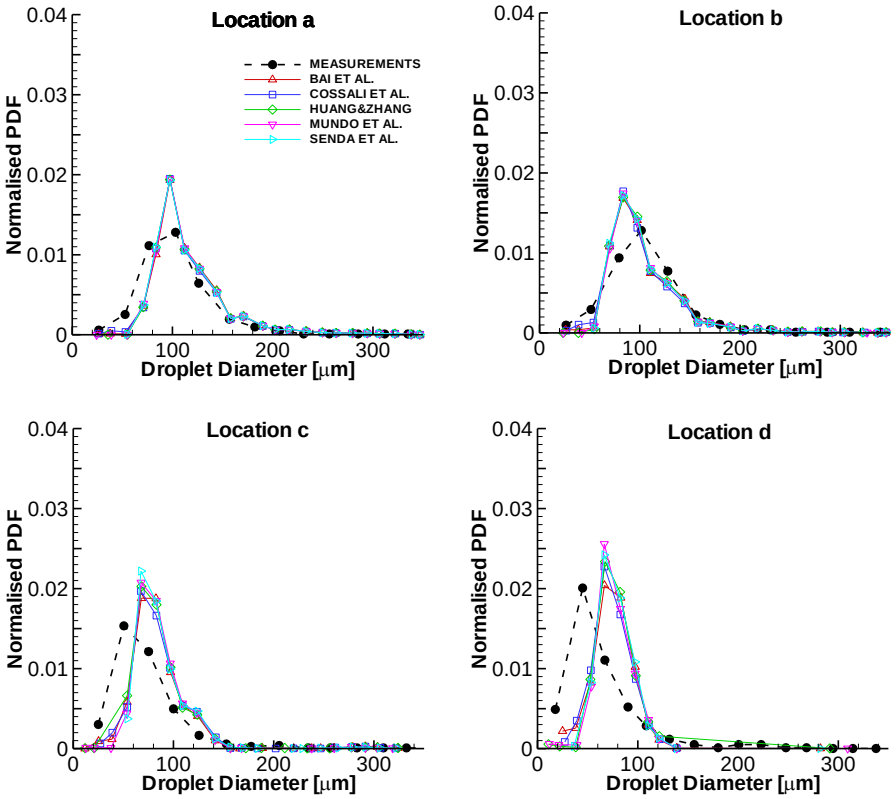

Figure III-9: Size distributions of downward-moving droplets at four locations for a cross flow velocity of 15 m/s.

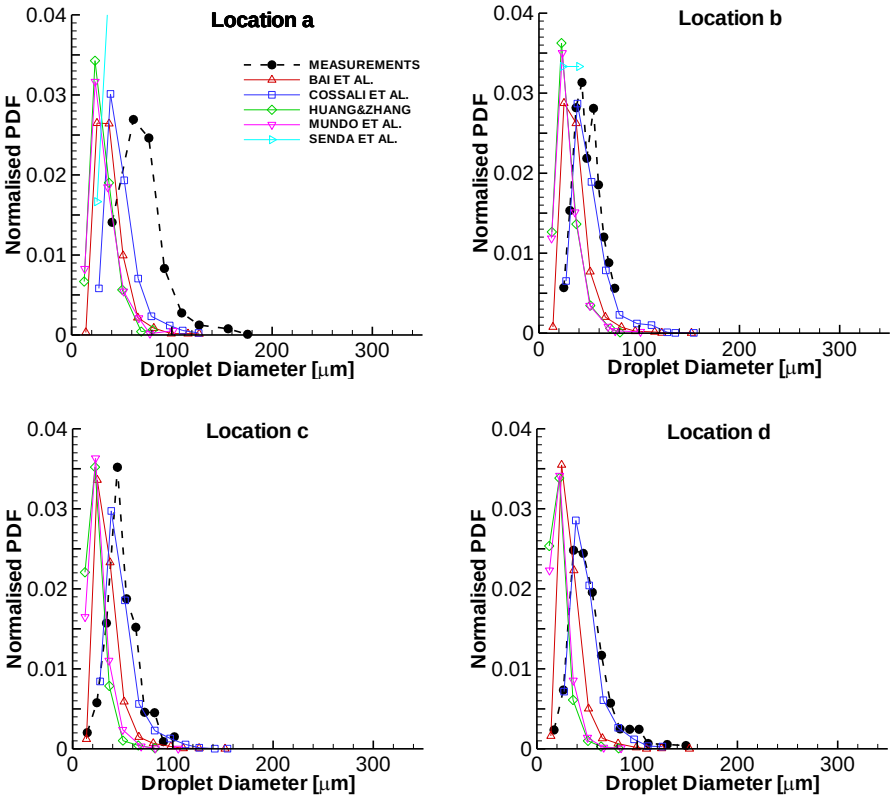

Figure III-10: Size distributions of upward-moving droplets at four locations for a cross flow velocity of 15 m/s.

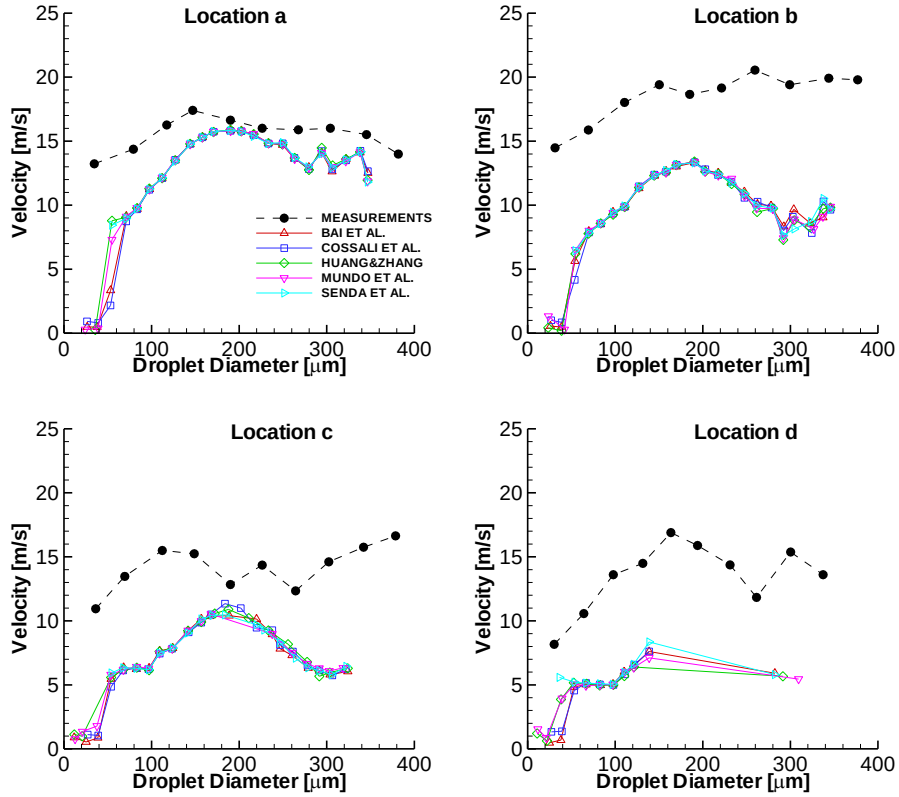

Figure III-11: Velocity-size correlation of downward-moving droplets at four locations for a cross flow velocity of 15 m/s.

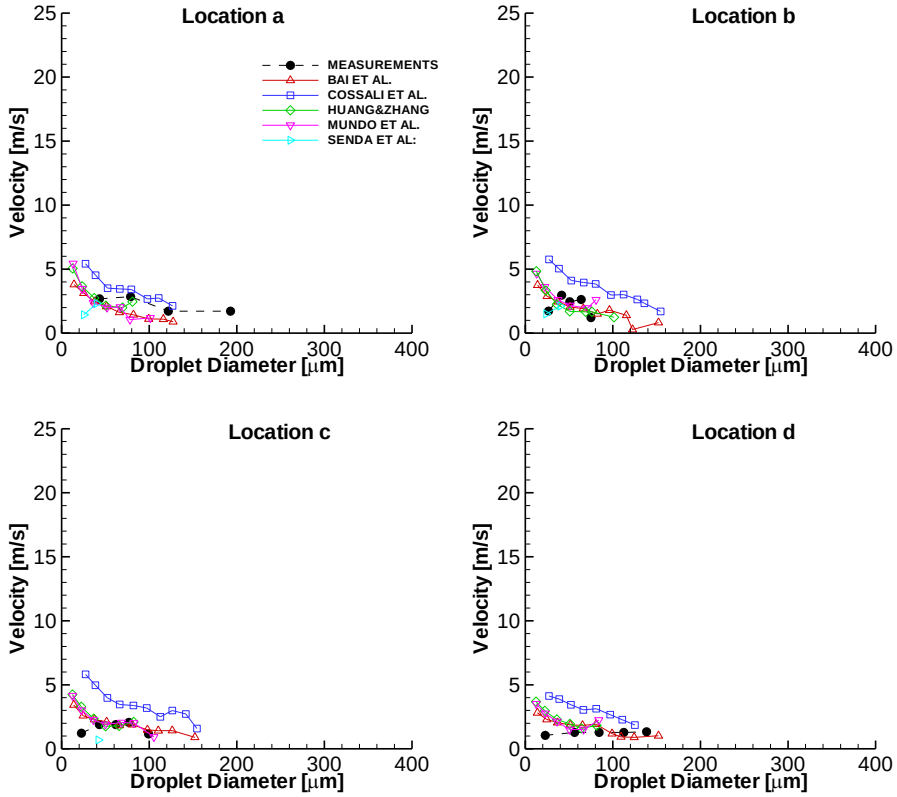

Figure III-12: Velocity-size correlation of upward-moving droplets at four locations for a cross flow velocity of 15 m/s.

In conclusion, and comparing the five transition criteria studied, as it would be expected the downward moving drops show great consistency between the results since the majority of the parcels come directly from the injector and deposit on the solid wall and, consequently, in this case the splash regime is not taken into account. However, all the correlations tested show some difficulty in predict adequately both smaller and bigger droplets, which in turn affect the overall distribution and, in particular, lead to an over-prediction of the peak value of the most frequent droplet. This situation reinforces the influence of the initial conditions. On the other hand, the upward moving droplets are due to the rebounding of the drops and the disintegration of the initial drops after impact in the splash regime. In this case, the Cossali *et al.* (1997) seems to have the better results, i.e., the predictions presents results closer to the measurements in the specific case of the normalised *pdf* with upward moving droplets for a crossflow of both 5 and $15\,m/s$. In the case of the velocity-size correlations, the picture changes completely: in the situation of the downward moving droplet, good agreement is seen between all the correlations tested; but for the upward-moving droplets, the correlation of Cossali *et al.* (1997) deviates from the results obtained with the other correlations and, in particular, deviates from the measurements. However, in general, the results of the five correlations tested for the velocity-size correlations of the downward and upward moving droplets do no present satisfactory results for both descending and ascending droplets.

The difficulty to reproduce the upward moving droplets may be due to the limitation of the model in relation to the transport of the liquid film deposited on the solid wall. Despite the base model considers up to 6 parcels resulting from the splash of the incident drops, it does not take into account the thickness of the liquid film in the secondary droplet characteristics as well as its possible movement with both the impact of incident drops and the influence of the crossflow. In fact, the crossflow may be responsible for a special phenomenon at the impingement local as it can be seen in Figure III-13. The figure shows a recirculation at the location of the incident drops impact, which alters the behaviour of the droplets after the impact. This phenomenon has already been reported by Silva (2007) and Barata and Silva (2010). To note that these results have been estimated with the base model of Bai *et al.* (2002) and for a small range of incident drop diameters (only 10 drops have been released from the injector).

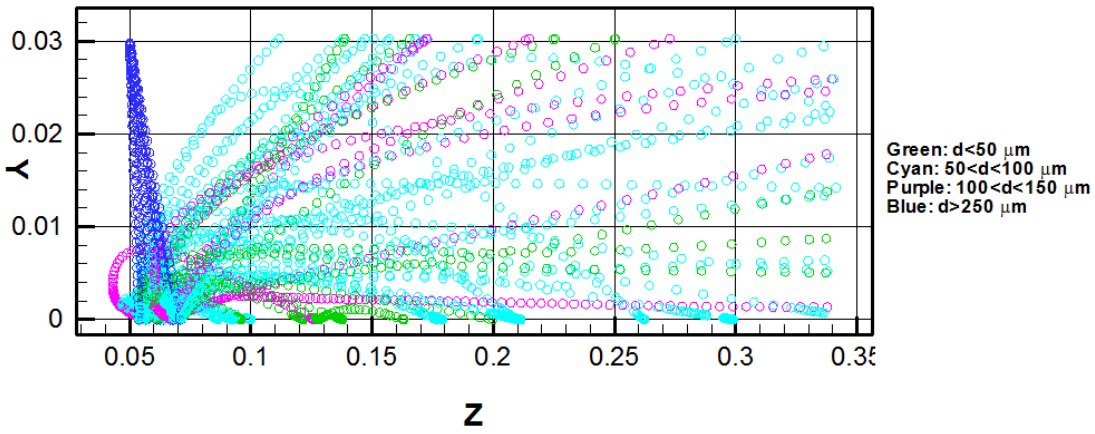

Figure III-13: Tracking of a number of drops during their trajectory through the simulation.

To conclude, none of the results show a special concordance at all the locations and for all the parameters studied, which call for further research in order to obtain new information that could bring accuracy to the modelling of the spray impingement phenomenon.

4. Energy Dissipation Loss

The spray impingement phenomenon is influenced by various parameters related with both the impact conditions and the liquid and surface properties. Depending on these parameters, as well as kinematic conditions, different outcomes are verified, which gives rise to diverse secondary droplets characteristics. As a result, the development of accurate empirical sub-models to predict the size, velocity and number of secondary droplets is essential. In this section, attention is given to the energy dissipation loss relationship, which is a fundamental parameter to estimate the post-impingement characteristics (specifically to evaluate the velocity of the secondary droplets) in the splash regime and, consequently, to model adequately the spray impingement process. The influence of the energy dissipation term is evaluated through the comparison of several relationships available in the literature,

which are inserted in the same global model of atomization. The selected base model is the model of Bai *et al.* (2002), which is tested against the experimental data of Arcoumanis *et al.* (1997).

In the original model, Bai and Gosman (1995) assumed their own relationship in terms of the critical Weber number. The equation was later revised and improved (Bai *et al.,* 2002). However, the origin of the approach used to define the energy dissipation is somewhat unknown.

There is little literature available related to this particular parameter as well as little agreement even for what it represents exactly in this regime. The principal study available related with the dissipative energy loss has been conducted by Chandra and Avedisian (1991), which concluded that the dissipation energy is directly proportional to viscosity. Later, Pasandideh-Fard *et al.* (1996) improved the accuracy of the theoretical model by replacing the splat film thickness, h, in the dissipation function, ϕ, by the boundary layer thickness, δ_{bl}, at the solid interface. The reason of such change lies in the fact that the use of the splat film thickness term would lead to an overestimation of the maximum extend of the film. In addition, the authors assumed a new time scale t_c, taken for the droplet to spread out until their maximum extension, which depends on the impact velocity of the incident droplet.

A thorough explanation of the dissipative energy loss relationships deduced by the investigators has been presented in the $Chapter\ II.6.2.2$ and is outlined in the Table III-2:

Table III-2: Dissipative energy loss relationship and corresponding observations.

	Bai *et al.* (2002)	Chandra and Avedisian (1991)	Pasandideh-Fard *et al.* (1996)
Dissipative Energy Loss Relationship	$E_D = \max\left(0.8E_{KI}; \frac{We_c}{12}\pi\sigma d_I^2\right)$	$E_D \approx \frac{1}{4}\pi\mu\frac{U}{h}d_I d_{max}^2$	$E_D \approx \frac{\pi}{3}\rho U^2 d_I d_{max}^2 \frac{1}{\sqrt{Re}}$
Observations	Defined as the critical kinetic energy below which no splashing occurs. The incident kinetic energy based on the normal incident velocity is: $E_{KI} = \frac{1}{2}m_I V_{IN}^2$	Estimated from $E_D = \int_0^{t_c}\int_V \phi dV dt \approx \phi V t_c$ Where the dissipation function is given by: $\phi = \mu\left(\frac{\partial v_i}{\partial x_j} + \frac{\partial v_j}{\partial x_i}\right)\frac{\partial v_i}{\partial x_j} \approx \mu\left(\frac{U}{h}\right)^2$ And $V \approx \frac{1}{4}\pi d_{max}^2 h$ $t_c \approx d_I/U$	Improvement of the Chandra and Avedisian (1991) theoretical model, by replacing h by: $\delta_{bl} = \frac{2d_i}{\sqrt{Re}}$ and assuming: $t_c = 8/3\,(d_I/U)$

In the relationship presented by Chandra and Avedisian (1991) the thickness (h) of the liquid drop after flattened out in a regular disc shape when splash occurs is estimated assuming that the incident drop keeps the same volume since the moments immediately before impact until the last instant of the spreading phase (there is no detachment of the drop liquid to the film). In addition, it is assumed that the splash regime only occurs at the moment of the crown emergence. Thus, from the work of Yarin and Weiss (1995), d_{max} is defined as being twice the incident drop diameter. Therefore, the equation defining the thickness of the disc is as follow:

$$h = \frac{d_I}{6} \quad \textbf{(III-1)}$$

However, Roisman *et al.* (2009) estimated the following disk thickness from the mass balance:

$$h = \frac{2}{3{d_{max}}^2} \quad \textbf{(III-2)}$$

which, admitting the previous value for the maximum spreading diameter ($d_{max} = 2d_I$), becomes:

$$h = \frac{1}{6d_I^2} \quad \textbf{(III-3)}$$

Both equations (III-1) and (III-3) for the disc thickness have been introduced in the relationship deduced by Chandra and Avedisian (1991) – called Model C and Model B, respectively –, which in addition to the correlation of Bai *et al.* (2002) – Model A – and Pasandideh-Fard *et al.* (1996) – Model D – constitute the four energy dissipation loss relationships tested in the Bai *et al.* (2002) model (see Table III-3).

Table III-3: The four relationships tested in this study.

	Model A (Bai et al.)	Model B	Model C	Model D
Dissipative Energy Loss Relationship	$E_D = \max\left(0.8E_{KI}; \frac{We_c}{12}\pi\sigma d_I^2\right)$	$E_D \approx 6\pi\mu U_{IN} d_I^5$	$E_D \approx 6\pi\mu U_{IN} d_I^2$	$E_D \approx \frac{4}{3}\pi\rho {U_{IN}}^2 d_I^3 \frac{1}{\sqrt{Re}}$

As seen in the previous section, the Cossali *et al.* (1997) transition criteria presented better results for the specific case of the *pdf* of the upward-moving droplets, but in contrast showed a greater deviation of the results in relation to the measurement in the velocity-size correlation of the upward-moving droplet case. Since the ascending velocity of the secondary droplets depends on the dissipation energy, testing the four energy dissipation loss relationship into the original model but assuming the transition criteria between deposition and splash of Cossali *et al.* (1997) seems to be a promising study. This study corresponds to the second part of the section 4. The first part corresponds to the same study (comparison of the different dissipative energy loss relationships) but with the original transition criteria of the base model (Bai *et al.,* 2002). Finally, in the third section, both results are compared and discussed.

4.1. Transition Criterion of Bai et al. (2002)

This section presents the results of the study about the influence of the energy dissipation term in the modelling of a spray impinging onto a solid surface. Hence, several relationships available in the literature are inserted in the same base model of atomization

(Bai *et al.*, 2002) and the results are compared with the experimental data of Arcoumanis *et al.* (1997).

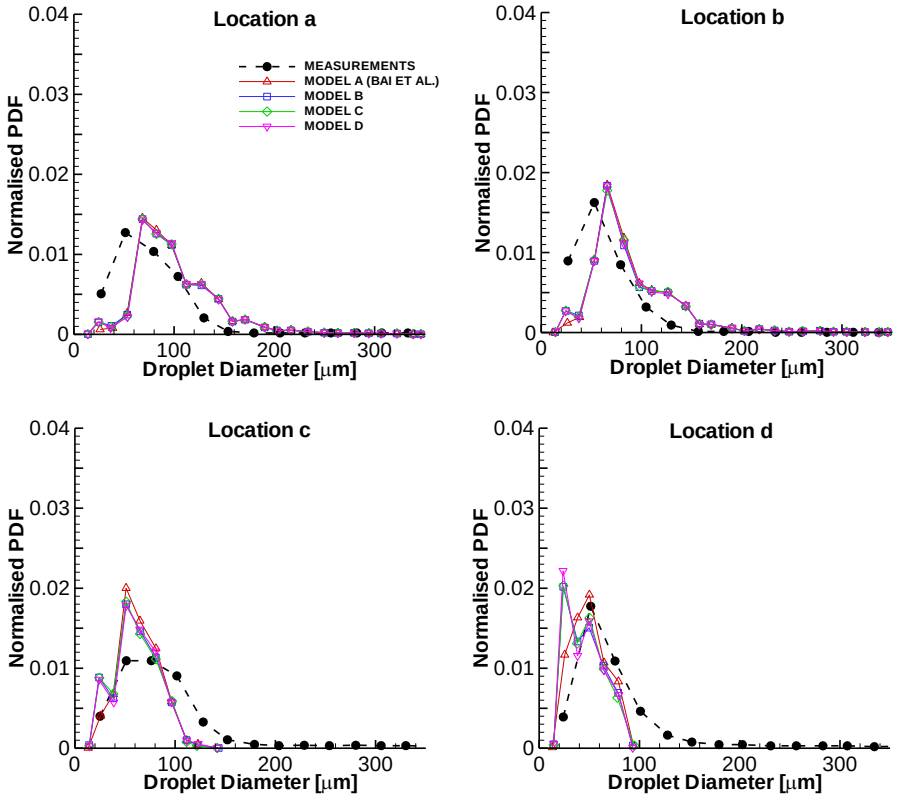

Figure III-14: Size distribution correlation of downward-moving droplets at four locations for a crossflow velocity of 5 m/s and transition criteria of Bai et al. (2002).

The Figure III-14 and Figure III-15 present the measured and predicted size distributions of droplets moving downward and upward, respectively, through a $5\,m/s$ crossflow. In the first case, and as it was expected, good agreement is seen between the results obtained for the four model studied. This concordance is less effective at the locations further away from the injection plane because it is more affected by the rebound and secondary droplets in their descending path – in particular for smaller droplets. The main difference between the results of the model A and the other three models' results (at location *c* and *d*) has to do with the difficulty of the newly-inserted models to reproduce the droplets with smaller diameters (first two size class). This situation alters the rest of the distribution of those models: the over-estimation of this range of droplets diameters is equilibrated by the under-estimation of the values after the mode (most frequent) of the droplet diameter. Comparing the predictions with the measurements, the figure show an over-estimation of the mode of the predicted droplet diameter at location *a, b* and *c*, as well as a rightward-shift at location *a* and *b*. Figure III-15 show the size distribution correlation of the upward-moving droplets, and again good agreement is seen between the four correlations. However, the estimated values have a peak value over-estimated and leftward shifted. This fact leads to an under-estimation of the droplets with greater diameters.

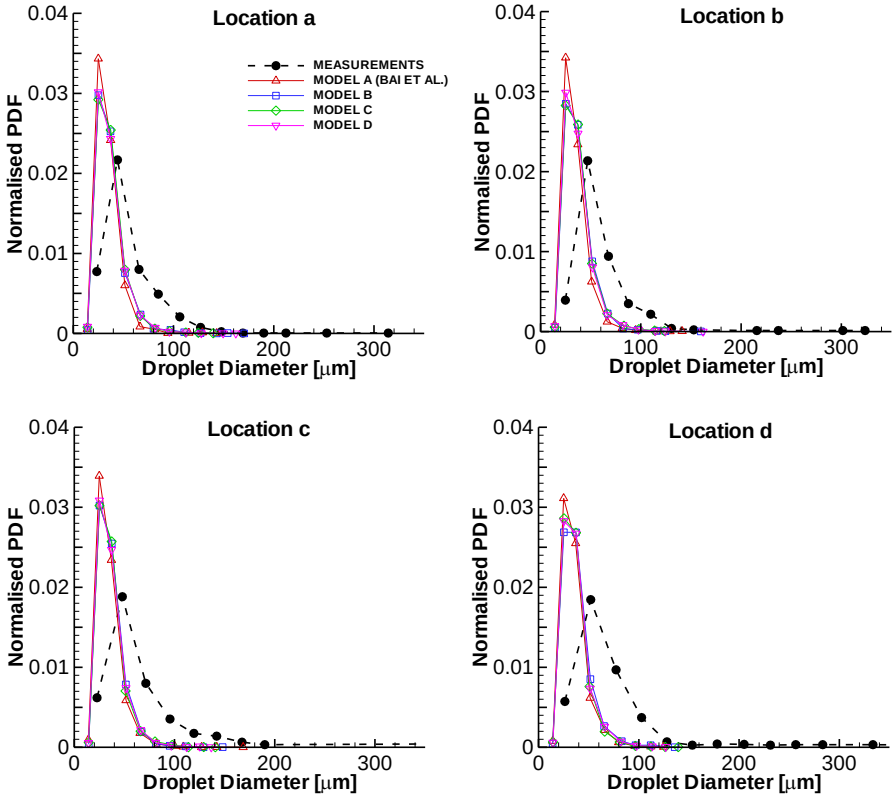

Figure III-15: Size distribution correlation of upward-moving droplets at four locations for a crossflow velocity of 5 m/s and transition criteria of Bai et al. (2002).

The measured and predicted velocity-size correlations for droplets moving downward and upward, for a crossflow of $5\,m/s$, are presented in Figure III-16 and Figure III-17. For downward moving droplets, the results of the four models show consistency between them but are still far from the ones expected. It can be seen that at location *c* and *d*, the maximum predicted size class does not exceed $160\,\mu m$, while the measurements reach $400\,\mu m$ at both locations. For droplets moving upward, firstly, it can be seen that the maximum size class predicted do not exceed $180\,\mu m$, while the measurements reach almost $400\,\mu m$ at location *d*. This situation does not seem to be affected by the dissipative energy loss since no considerable difference is seen between all the results. Secondly, the model A is the one that produce better results as far as the dissipative energy loss is concerned, i.e., it presents results closer to the measurements. The other three models, which include the different dissipative energy relationships, show reasonable agreements between them, but deviate somewhat from the results: they over-predict the velocity of the ascending droplets in the entire range.

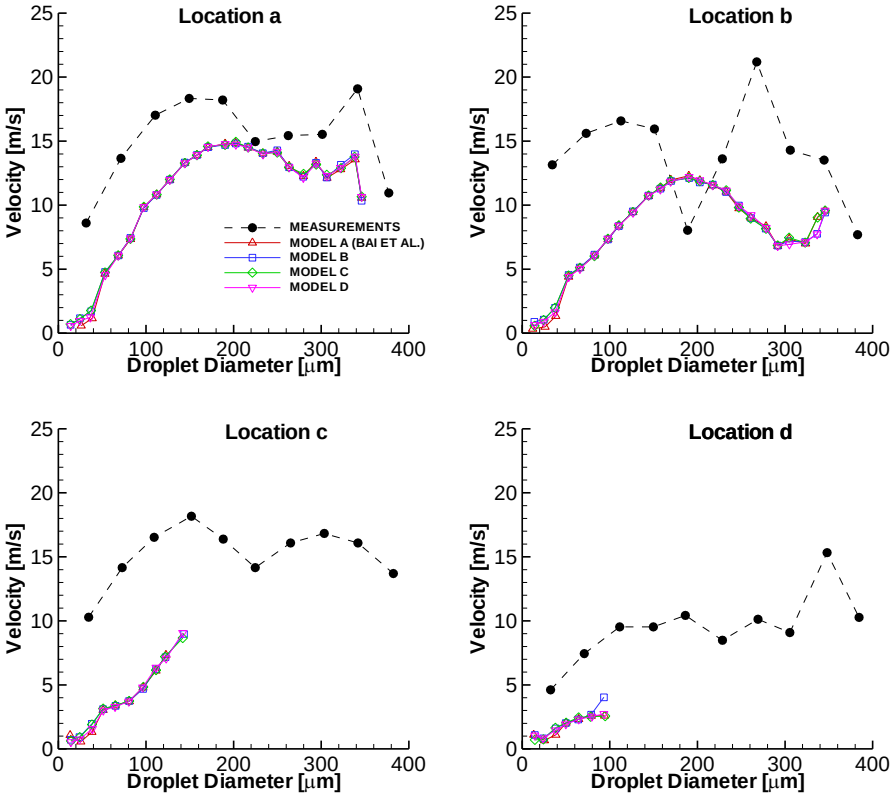

Figure III-16: Velocity-size correlation of downward-moving droplets at four locations for a crossflow velocity of 5 m/s and transition criteria of Bai et al. (2002).

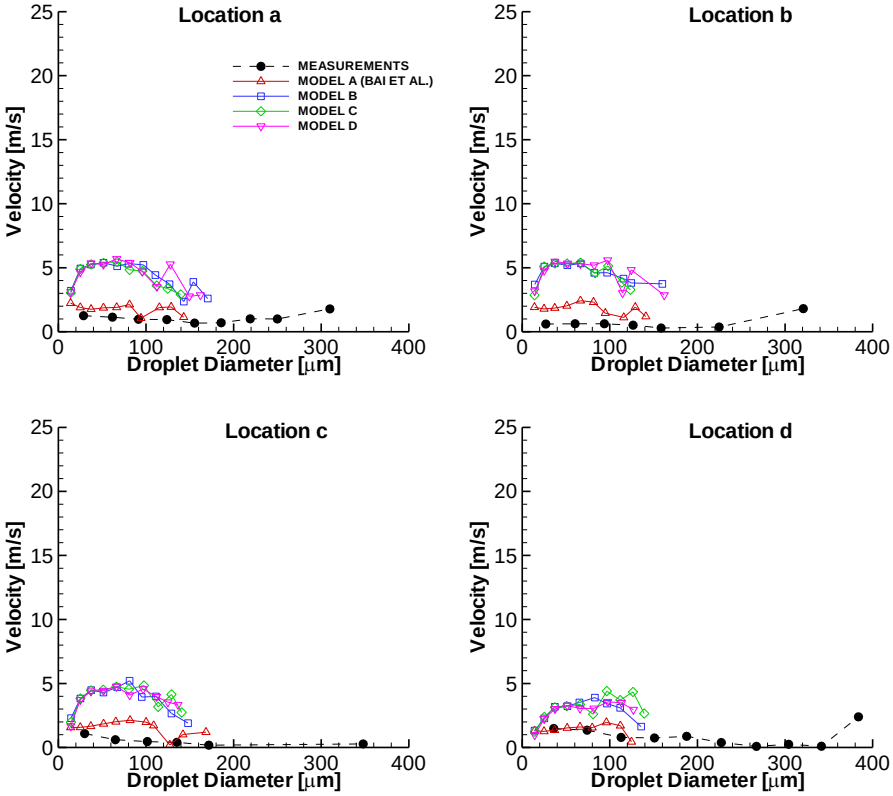

Figure III-17: Velocity-size correlation of upward-moving droplets at four locations for a crossflow velocity of 5 m/s and transition criteria of Bai et al. (2002).

The following figures present the results considering the presence of a crossflow of $15\ m/s$, instead of the $5\ m/s$ considered previously.

Figure III-18 presents the measured and predicted size distributions of droplets moving downward, for a crossflow of $15\ m/s$. As it was expected, and as verified in Figure III-14 for a crossflow of $5\ m/s$, good agreement is seen between the results obtained for the four models studied. The three newly-introduced models present a better capacity to predict the smaller droplet in the first two size classes. However, this fact leads to an under-estimation of the following size classes until reach the most frequent droplet diameter. Comparing the predictions with the measurements, it is seen that the mode of the droplet diameters is leftward shifted at location *b* and rightward shifted at locations *c* and *d*. In addition, the peak value is over-estimated at locations *a, b* and *c*.

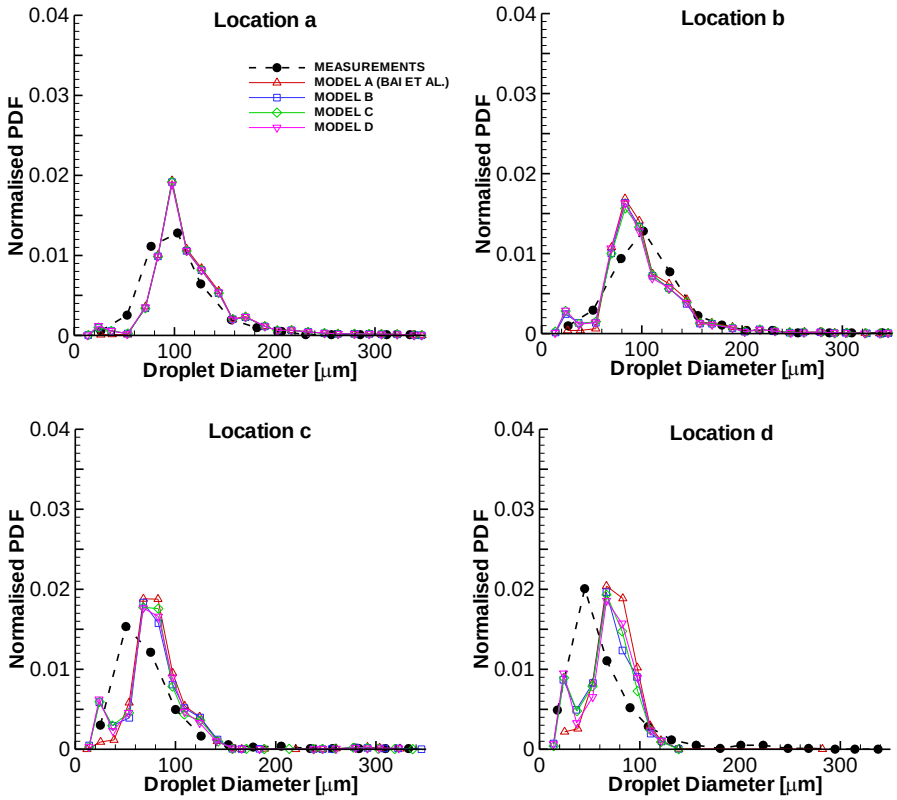

Figure III-18: Size distribution correlation of downward-moving droplets at four locations for a crossflow velocity of 15 m/s and transition criteria of Bai et al. (2002).

In the upward-moving case, there are again some differences between the predictions and the experimental data. The most frequent droplet diameter predicted is smaller than what it is seen in the measurements (leftward shift), but there are fewer droplets with greater diameter predicted. In addition, the mode of the droplet diameter is over-estimated at locations *a* and *d*. On the other hand, good consistency is verified between all the models assessed and, thus, it can be concluded that the energy dissipation relationship does not influence these specific results.

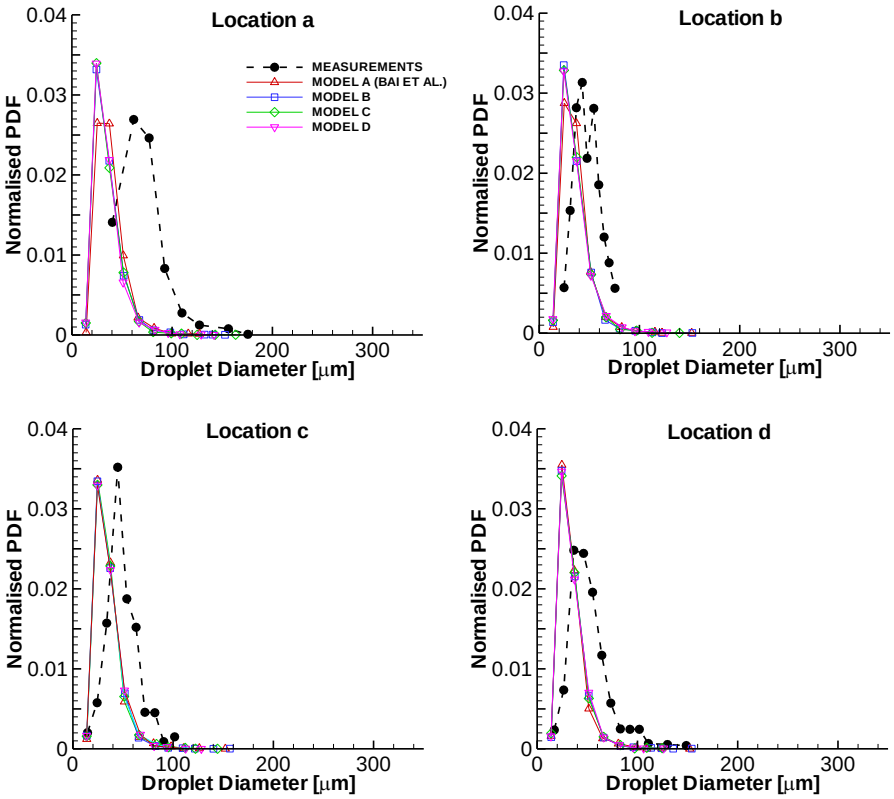

Figure III-19: Size distribution correlation of upward-moving droplets at four locations for a crossflow velocity of 15 m/s and transition criteria of Bai et al. (2002).

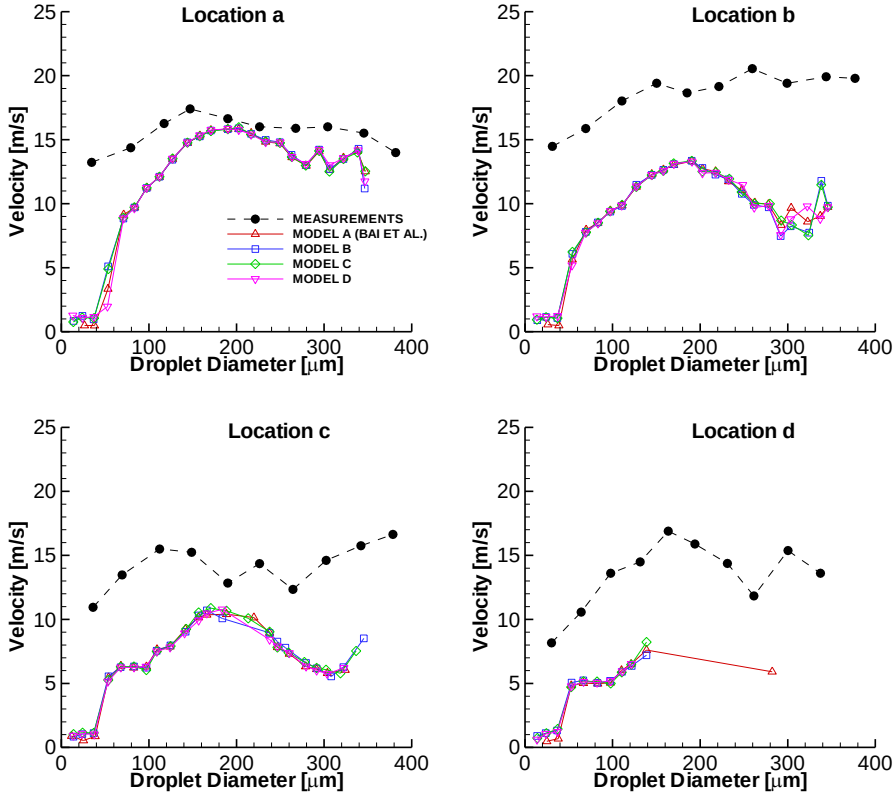

Figure III-20: Velocity-size correlation of downward-moving droplets at four locations for a crossflow velocity of 15 m/s and transition criteria of Bai et al. (2002).

Figure III-20 and Figure III-21 show the velocity-size correlation of the downward and upward-moving droplets, respectively. For droplets with descending velocity, the agreement between the predictions is good but still shows considerable difference between predictions and measurements. There is seen again some difficulties of the model to reproduce the greater size class at the farthest location from the injector. For ascending-moving droplet, the model A present results better than the other three models, which over-estimate the velocity along the entire range of droplet diameters at all the locations. In the case of the model A, good agreement is seen at the locations *d*, but at the other locations both the size class range and the velocity profile do not present satisfactory results.

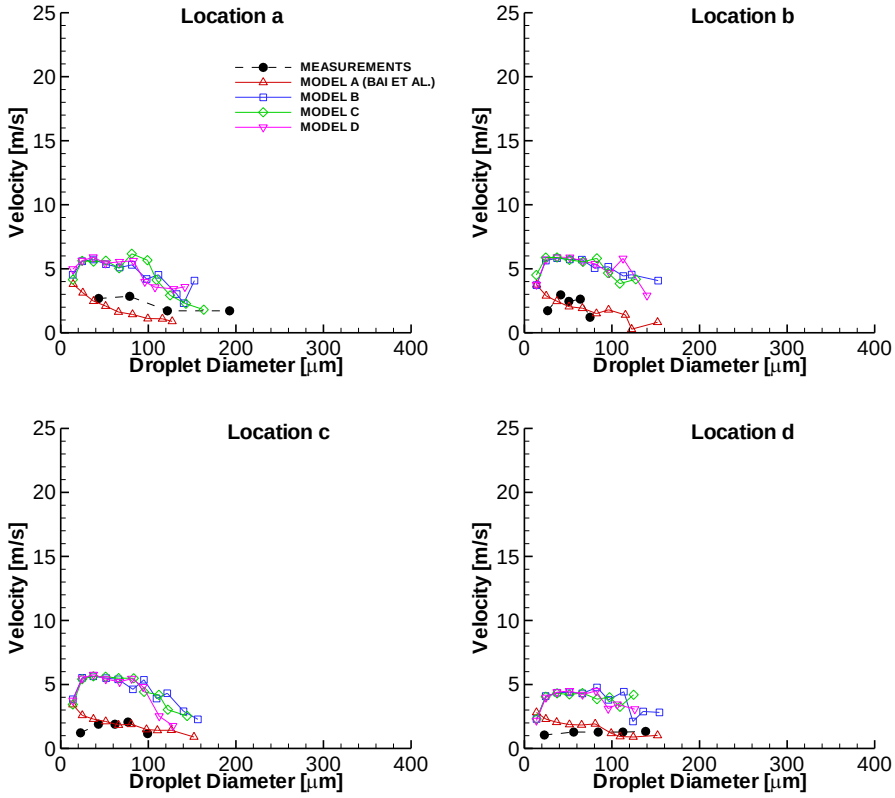

Figure III-21: Velocity-size correlation of upward-moving droplets at four locations for a crossflow velocity of 15 m/s and transition criteria of Bai et al. (2002).

4.2. Transition Criterion of Cossali et al. (1997)

This section presents the results of the study about the influence of the energy dissipation term in the spray impingement modelling. Several relationships available in the literature are inserted in the same global model of atomization. The selected base model is the model of Bai *et al.* (2002) but with the transition criteria of Cossali *et al.* (1997) instead of the original one of Bai *et al.* (2002).

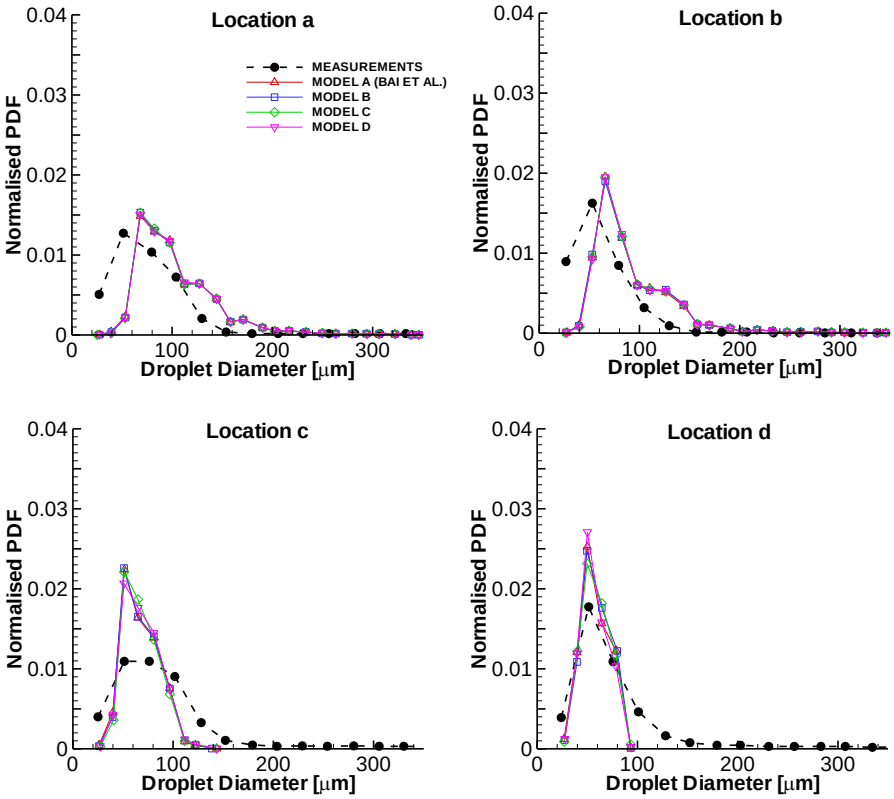

Figure III-22: Size distribution correlation of downward-moving droplets at four locations for a crossflow velocity of 5 m/s and transition criteria of Cossali et al. (1997).

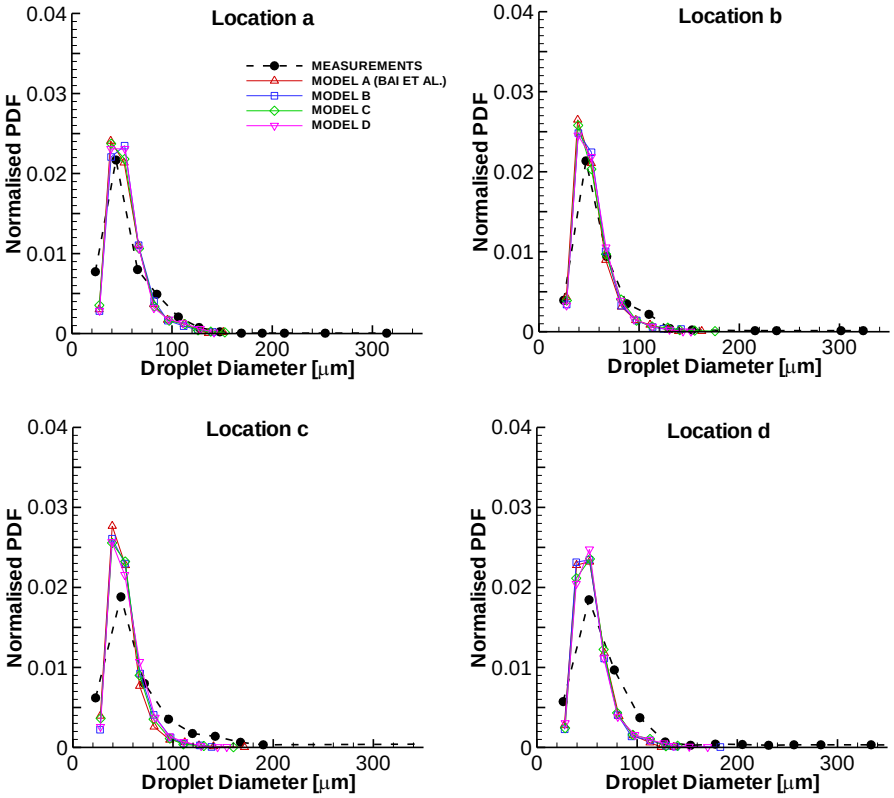

Figure III-23: Size distribution correlation of upward-moving droplets at four locations for a crossflow velocity of 5 m/s and transition criteria of Cossali et al. (1997).

The Figure III-22 and Figure III-23 show the measured and predicted droplet size distributions for a crossflow velocity of $5\,m/s$. In both case, the predictions are in good agreements between them but are still over-predicted in relation to the measurements. In the case of the descending moving droplets, it can be seen in the three locations closer to the injector that the number of smaller droplets is under-estimated which makes either the increase of the mode value or the over-estimation of the larger droplet diameters. In the specific case of the location *c*, both smaller and larger droplet diameters are under-estimated, which causes a greater over-estimation of the peak value. Another observation is that for both location *c* and *d*, the droplets with diameters larger than $120\,\mu m$ does not appear in the results contrary to what happens with the measurements. For the upward moving droplets, very good agreement is seen: the peak value is only slightly over-estimated at location *c* and *d*. From both previous results, and considering the transition criteria of Cossali *et al*. (1997), it can be conclude that the dissipative energy loss does not significantly influence the outcome of the spray impingement.

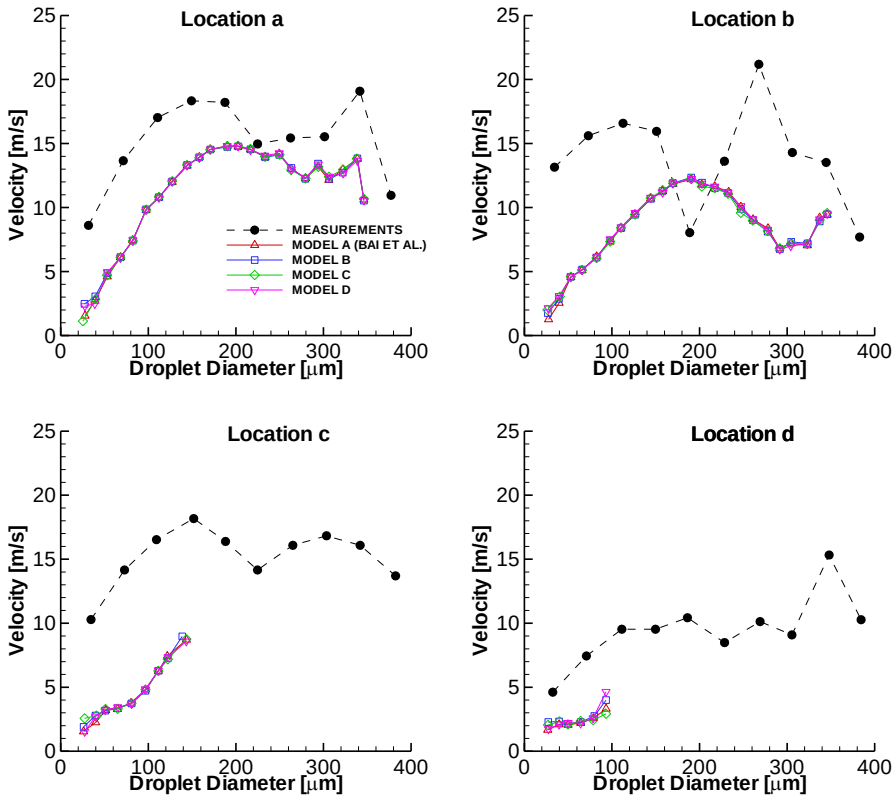

Figure III-24: Velocity-size correlation of downward-moving droplets at four locations for a crossflow velocity of 5 m/s and transition criteria of Cossali et al. (1997).

In relation to the velocity-size correlations for droplets with downward and upward moving at the four locations with the presence of a $5\,m/s$ crossflow, the results are presented in Figure III-24 and Figure III-25. For the downward moving droplets, the four models present good concordance between them but in general, the velocity profiles are under-estimated in the entire range of droplets diameters, except in a small range at location *b*. In addition, at location *c* and *d* the greater predicted class size is $140\,\mu m$ while the measurements extend up

to $400\ \mu m$. For the upward moving droplets the figure show different behaviour between the model A and the other three models: the latter are more over-estimated than the model A (which was already somehow over-estimated, as seen in the Chapter III.3) and this difference is more noticeable for smaller droplets. In addition, it is seen that the maximum class size found never exceeds $180\ \mu m$, while in the measured case they can extend until almost $400\ \mu m$.

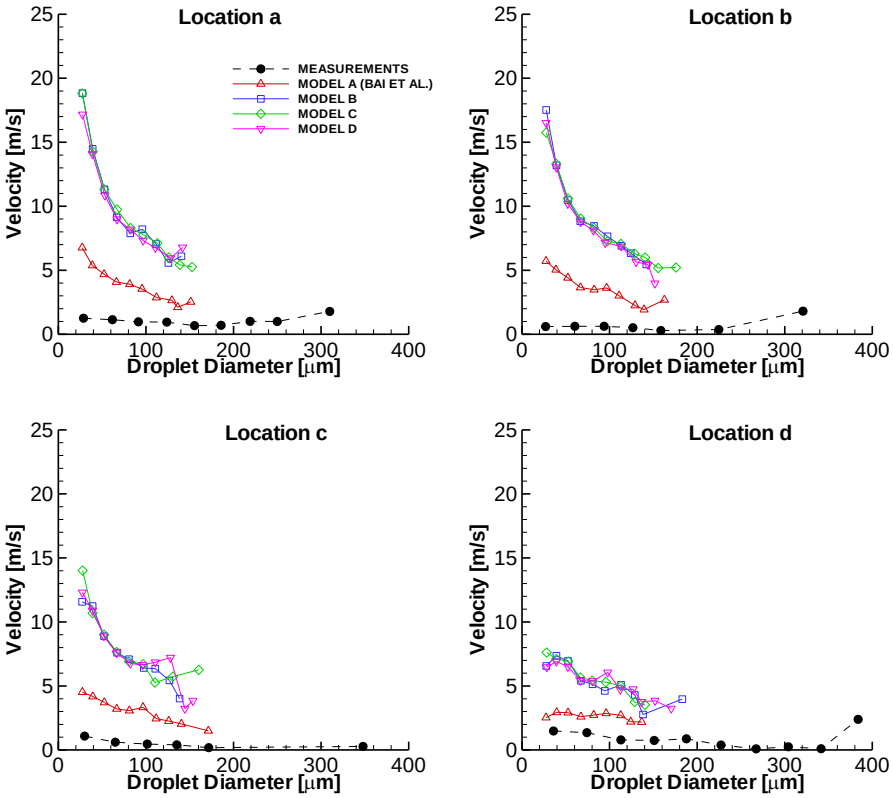

Figure III-25: Velocity-size correlation of upward-moving droplets at four locations for a crossflow velocity of 5 m/s and transition criteria of Cossali et al. (1997).

In relation to the results obtained considering the higher crossflow rate, the measured and predicted size distributions of droplets moving downward and upward are presented in Figure III-26 and Figure III-27, respectively. Considering the normalized *pdf* with downward moving droplets, again great consistency is found for all the correlations considered but it still over-predicts the maximum frequency of the size-distribution at all the locations, and also present a rightward shift of the mode of the droplets diameters at location *c* and *d* and a leftward shift at location *b*. At locations *a*, *c* and *d* the droplets with smaller diameter are under-estimated but, in contrast, the larger droplets are over-predicted. In the upward-moving case, there are again just small differences between the predictions and the experimental data, but in general, good agreement is verified for all cases at all locations (except at location *a*, where the leftward shift of the peak value is more evident).

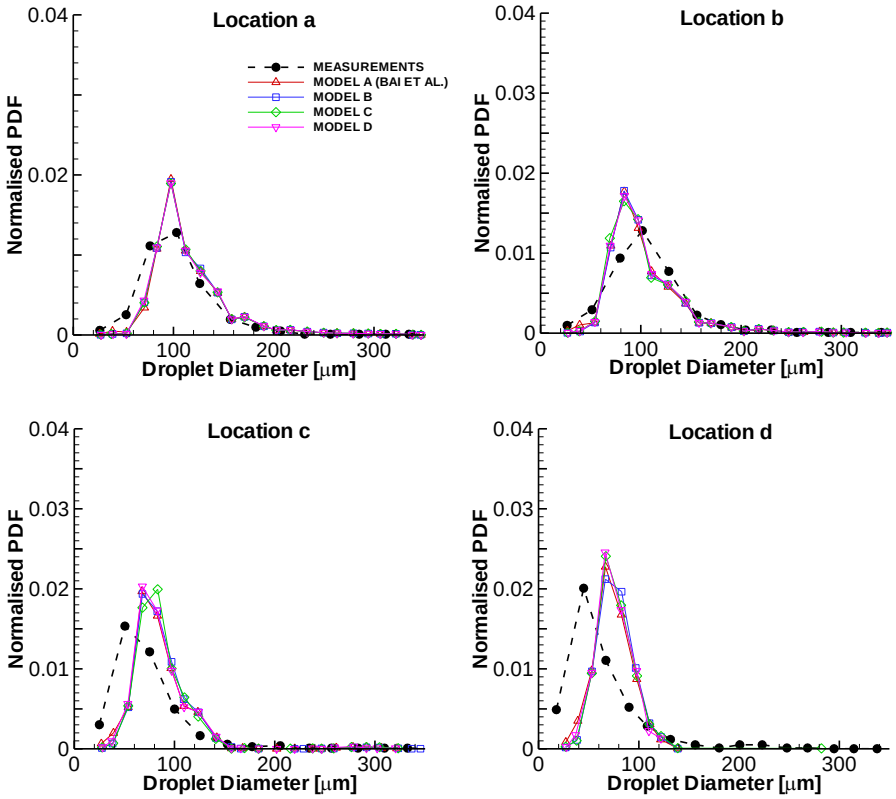

Figure III-26: Size distribution correlation of downward-moving droplets at four locations for a crossflow velocity of 15 m/s and transition criteria of Cossali et al. (1997).

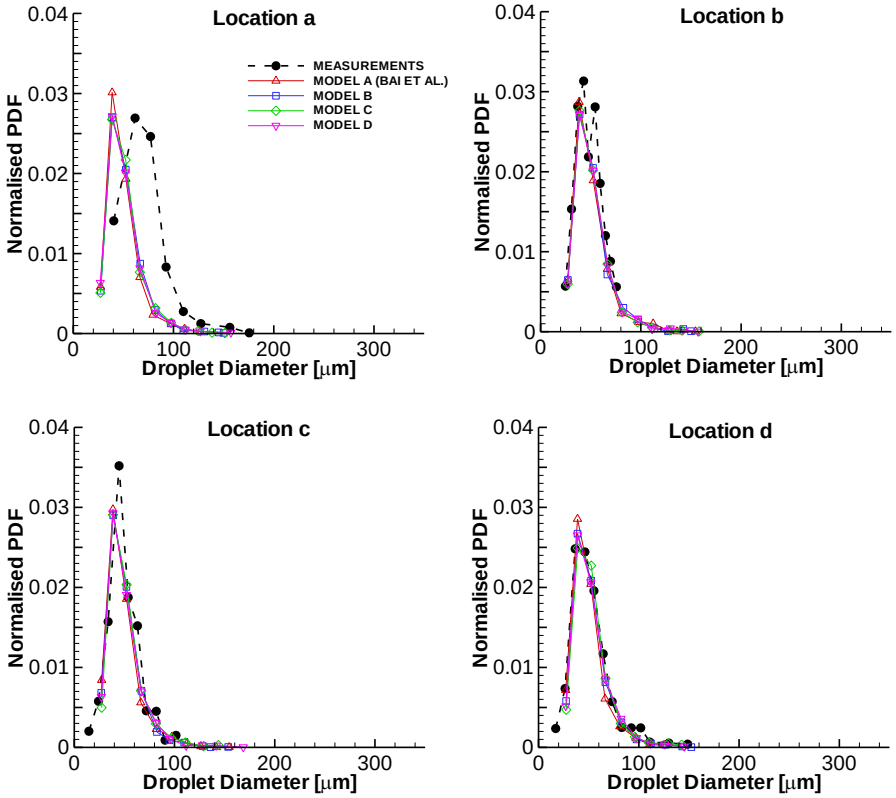

Figure III-27: Size distribution correlation of upward-moving droplets at four locations for a crossflow velocity of 15 m/s and transition criteria of Cossali et al. (1997).

In the Figure III-28 and Figure III-29 it is presented the velocity-size correlations for droplets moving downward and upward, respectively, considering the presence of a crossflow of $15\,m/s$. In the first case, the different transition criteria evidence good consistency between them but not with the measurements. In fact, the velocities verified are under-estimated at all the location and along the entire range of droplet diameters. To note also that the maximum size class estimated is still lower than the measured as seen in the results for a crossflow of $5\,m/s$. The Figure III-29 presents the upward-moving droplets and illustrates some discrepancies between the predictions and the measurements. In addition, the model B and C, which corresponds to the relationship deduced by Chandra and Avedisian (1991), over-estimate even more the results presented by the model A and D. The later results are very close but are still far from what it is expected. In addition, to note that the size class range of the predicted droplets does not corresponds to the measured size class range in any location. From this figure, it is seen that the dissipative energy loss relationship introduced in the base model of Bai *et al.* (2002) influence the velocity-size correlation of the upward moving droplet.

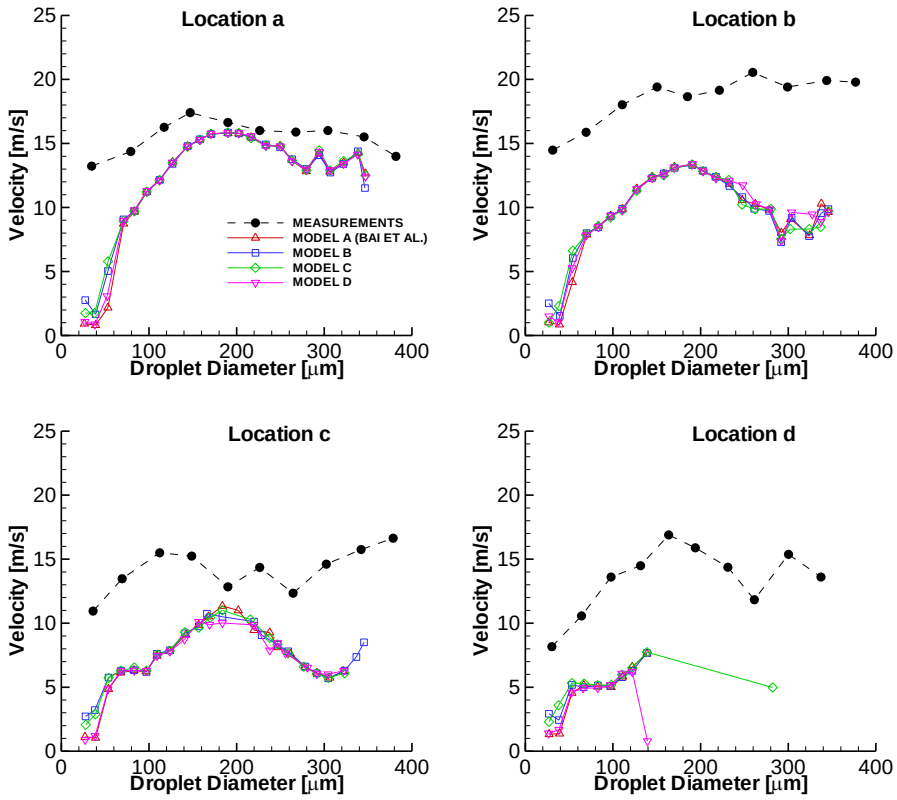

Figure III-28: Velocity-size correlation of downward-moving droplets at four locations for a crossflow velocity of 15 m/s and transition criteria of Cossali et al. (1997).

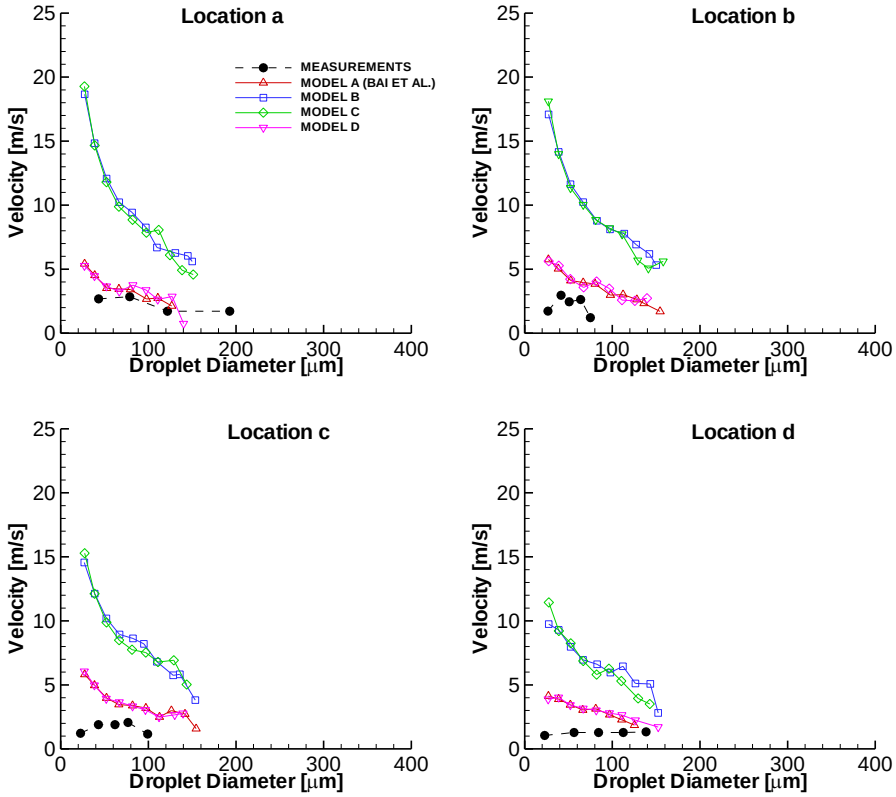

Figure III-29: Velocity-size correlation of upward-moving droplets at four locations for a crossflow velocity of 15 m/s and transition criteria of Cossali et al. (1997).

4.3. Comparison and Discussion

In the previous two sections, the influence of the dissipative energy loss has been evaluated in the spray impingement modelling through the comparison of the results of several relationships inserted in the base model of Bai *et al.* (2002) with the experimental data of Arcoumanis *et al.* (1997). However, in addition to the original transition criteria of the base model (Bai *et al.*, 2002), also the deposition/splash transition criterion of Cossali *et al.* (1997) has been tested in order to evaluate the influence of both parameters simultaneously.

Firstly, it can be said that the energy dissipation relationship of Bai *et al.* (2002) presents better results than the newly-introduced relationships in the velocity-size correlation results of the upward-moving droplets, both for Bai *et al.* (2002) and Cossali *et al.* (1997) transition criteria. This leads to admit that the assumptions taken to deduce the equations that define the dissipative energy loss as well as the assumptions taken to apply the equations, which were deduced to the spread regime, in the splash regime carry too much inaccuracy.

Secondly, despite its negligible influence on some parameters studied, it has been seen that the dissipative energy loss influence the outcome of the spray impingement and, in particular, the size-velocity correlations of the upward-moving droplets and the size distribution correlations of the downward moving droplets. However, it is seen in both case

that depending on the transition criteria chosen, the energy dissipation term plays different roles in the outcomes verified.

Third, it is curious to note that the diameter of the incident droplets does not bring many differences in the results of the parameters studied, although the models B and C being function of d^5 and d^2, respectively.

Thus, there is no clear evidence that the newly-inserted relationships improve the quality of the results. Despite allowing a better agreement with the measurements in some case (Figure III-18), in others it does not bring an increase in quality or even worsens the situation (Figure III-14). Thus, in general, the dissipative energy loss relationship that better approximates the experimental data of Arcoumanis *et al.* (1997) is the one of Bai *et al.* (2002) for both the case of the transition criteria of Bai *et al.* (2002) and Cossali *et al.* (1997).

This page has been intentionally left blank for double-sided copying.

IV. Conclusions

The present work is devoted to the numerical study of the impingement of sprays onto a solid wall through a crossflow. The major purpose of the thesis is to improve the accuracy of already existing models through the employment of new correlations and relationships. The selected base model was the model of Bai *et al.* (2002) and the numerical predictions were tested against the experimental data of Arcoumanis *et al.* (1997) for both crossflow rates of *5* and *15 m/s*. The effective initial conditions have been approximated by a specially-derived empirical procedure using the measured droplet size and velocity characteristics of a free spray. This approach may lead to some discrepancies between the predicted and the measured values.

The computational modelling of spray-wall impingement requires a deep knowledge of the numerous parameters affecting spray impaction and all the phenomena occurring in the near-wall region. However, the focus of this work was in defining the splash regime because of its importance in the modelling of impinging sprays. In a first phase of the work, several transition criteria between deposition and splash regimes have been tested in the same global model in order to evaluate the performance of the model. It has been seen that the employment of different transition criteria alters the outcome predicted in the simulation. However, only one correlation (Cossali *et al.,* 1997) presented better results than the original one for the particular case of the size distribution of the upward-moving droplets for both crossflow rates studied, but in the case of the velocity-size correlations the opposite is verified: the correlation of Cossali *et al.* (1997) deviates from the results obtained with the other correlations and, in particular, deviates from the measurements. Comparing the five transition criteria studied, as it would be expected the results of the downward moving droplets show good concordance between them (principally at the locations closer to the injector plane) since the majority of the parcels comes directly from the injector and the droplets are predicted in their descending path (before impact): the post-impingement characteristics under the splash regime do not have much influence. This situation reinforces the influence of the initial conditions on the outcome and, consequently, the necessity of an accurate atomization model to determine the initial condition in the near-nozzle region of the spray.

In the second phase of the thesis, the specific term of the energy dissipative loss has been the focus of the work. In fact, several energy dissipation relationships have been inserted in the Bai *et al.* (2002) base model in order to compare and evaluate the results for each correlation studied. However, in addition to the original transition criteria of the base model (Bai *et al.,* 2002) also the deposition/splash transition criterion of Cossali *et al.* (1997) has been tested in order to evaluate the influence of both parameters (transition criteria and energy dissipation) simultaneously. In this study, no improvements were seen by the employment of the new relationships in the base models for both Bai *et al.* (2002) and Cossali

et al. (1997) transition criteria. Some differences were seen in the figures presented but none showed advantages for both the crossflow rate considered. This may be due to the fact that the equations admitted were deduced for the spread regime, instead of the splash regime. Some assumptions were made in order to make possible the employment of the relationships. However, it is clear that further research is needed to define an equation that could represent adequately the energy dissipative loss during the splash regime.

The main challenge now lies in refining the model in some aspects in order to converge to a better solution. Besides the problems seen with the initial conditions, the influence of the liquid film is an aspect that needs further research whether regarding to the near-wall gas boundary layer (and attention must be paid to the presence of the crossflow) or in relation to the thickness of the liquid film and the exchange of liquid between the liquid film and the secondary droplets. Both situations may have a major influence on the post-impingement characteristics, which in turn are dependent on the energy dissipated during the splash event. In this regime, in addition to the viscous dissipation during the spread of the drop, finding the energy dispended in the raising of the liquid sheet and/or the detachment of the secondary droplets of the rim would be an important contribution. Recently, Roisman *et al.* (2009) found that the edge effect must be taken into account in the energy balance.

Another relevant aspect which requires a better understanding has to do with the methods to model the droplet size distribution in sprays. In fact, there are some methods available (as stated in Chapter II.6.2.2.iii) in the literature but it has not been yet investigated the influence of this parameter on the outcome. In addition, the correlation deduced by Okawa *et al.* (2008) for the number of secondary droplets may be another good investigation to undertake.

V. References

Al-Roub, M., and Farrell, P.V., "Atomization of Thin Liquid Films by Droplet Impact", *Atomization and Sprays*, Vol. 7, No. 5, pp. 531-547, 1997.

Amsden, A.A., O'Rourke, P.J., and Butler, T.D., "KIVA-2: A computer program for chemically reactive flows with sprays", *Technical report LA-11560-MS*, Los Alamos National Laboratory, 1989.

Andreassi, L., Ubertini, S., and Allocca, L., "Experimental and numerical analysis of high pressure diesel spray–wall interaction", *International Journal of Multiphase Flow*, Vol. 33, No. 7, pp. 742-765, 2007.

Arcoumanis, C., and Chang, J.C., "Heat transfer between a heated plate and an impinging transient diesel spray", *Exp. Fluids*, Vol. 16, pp. 105–19, 1993.

Arcoumanis, C., and Cutter, P.A., "Flow and heat transfer characteristics of Impinging diesel sprays under cross-flow conditions", *SAE Tech. Paper 950448*, 1995.

Arcoumanis, C., Whitelaw, D.S., and Whitelaw, J.H., "Gasoline Injection against Surface and Films", *Atomization and Sprays*, Vol. 7, No.4, pp. 437-456, 1997.

Avedisian, C.T., and Koplik, J., "Leidenfrost boiling of methanol on hot porous/ceramic surfaces", *Int. J. Heat Mass Transfer, Vol.* 30, pp. 379–93, 1987.

Bai, C.X. and Gosman, A.D., "Development of a Methodology for Spray Impingement Simulation", *Society of Automotive Engineers*, SAE Paper 950283, 1995.

Bai, C.X., Rusche, H., and Gosman, A. D., "Modelling of Gasoline Spray Impingement", *Atomization and Sprays*, Vol. 12, No. 1-3, pp. 1-27, 2002.

Barata, J., Cometti, A., Mendes, A. and Silva, A., "Numerical Simulation of an Array of Droplets Through a Crossflow", *AIAA paper 2002-0872, 40th AIAA Aerospace Sciences Meeting and Exhibit*, Reno, Nevada, 14-17 January 2002.

Barata, J.M.M. and Silva, A.R.R., " On the Performance of Spray Impingement Models", *International Review of Mechanical Engineering (I.RE.M.E.)*, Vol. 4, n. 7, 2005.

Barata, J.M.M. and Silva, A.R.R., "The Impingement of a Deflected Spray", 8th International Conference on a Energy for a Clean Environment, Fundação Calouste Gulbenkian, Lisbon, Portugal, 2010.

Barata, J.M.M., Lopes, P.S.N.D. and Perestrelo, N.F.F., "*Numerical Simulation of Polydisperse Two-Phase Turbulent Jets*", AIAA, 1999.

Baumeister, K.J., and Simon, F.F., "Leidenfrost Temperature - Its Correlation for Liquid Metals, Cryogens, Hydrocarbons, and Water", *Journal of Heat Transfer*, pp. 166-173, 1973.

Bernardin, J.D., and Mudawar, I., "The Leidenfrost Point: Experimental Study and Assessment of Existing Models", *Journal of Heat Transfer*, Vol. 121, No. 4, pp. 894-903, 1999.

Bernardin, J.D., Stebbins, C.J., and Mudawar, I., "Effects of surface roughness on water droplet impact history and heat transfer regimes", *Int. J. Heat Mass Transfer*, Vol. 40, No. 1, pp. 73–8, 1997.

Bussman, M., Chandra, S., and Mostaghimi, J., "Modeling the splash of a droplet impacting a solid surface", *Phys. of Fluids, Vol.* 12, No. 12, pp. 3121–32, 2000.

Cartellieri, W.P., and Wachter, W.E., "Status Report on A Preliminary Survey of Strategies to Meet U.S.-1991 HD Diesel Emissions Standards without Exhaust Gas After-Treatment", *SAE Technical Paper Series* No. 870342, Feb. 1987.

Chandra, S., and Avedisian, C.T., "On the collision of a droplet with a solid surface", *Proc. R. Soc. Lond.*, Vol. 432, pp. 13–41, 1991.

Chen, X.Q., and Pereira, J.C.F., "Numerical Prediction of Non-evaporating and Evaporating Fuels Sprays Under Nonreactive Conditions", *Atomization and Sprays*, Vol.2, pp.427-443, 1992.

Coghe, A., Cossali, G.E., and Marengo, M., "Single Drop Impingement on Thin Liquid Film." *Proc. 2nd Int. Conf. Exp. Fluid Mech*, Turin, Italy, 4–8 July 1994, pp. 623.

Cossali, G.E., Coghe, A., and Marengo, M., "The Impact of a Single Drop on a Wetted Solid Surface", *Experiments in Fluids*, Vol. 22, No.6, pp. 463-472, 1997.

Crowe, C., Sommerfield, M. and Tsuji, Y., "Multiphase Flows with Droplets and Particles", *Boca Rathon, CRC,* 1998.

Emmerson, G.S., "The Effect of Pressure and Surface Material on the Leidenfrost Point of Discrete Drops of Water", *International Journal of Heat and Mass Transfer*, Vol. 18, No. 3, pp. 381-386, 1975.

Engel, O.G., "Water Collisions with Solid Surfaces", *J. Res. NBS,* Vol. 54, No. 5, pp. 281-298, 1955.

Faeth, G.M., Mixing, transport and combustion in sprays. *Prog. Ene. Combust. Sci.*, Vol. 13, No. 4, pp. 293-345, 1987.

Fedorchenko, A.I., and Wang, A.B., "The formation and dynamics of a blob on free and wall sheets induced by a drop impact on surfaces", *Phys. Fluids,* Vol. 16, pp. 3911–3920, 2004.

Fujimoto, H., Senda, J., Nagae, M., Hashimoto, A., Saito, M. and Katsur a , N., "Characteristics of a Diesel Spray Impinging on a Flat Wall", *COMODIA 90 Proceedings of International Symposium on Diagnostics and Modeling of Combustion in Internal Combustion Engines*, pp. 193-198, Kyoto, Japan, 1990.

Gavaises, M., Theodorakakos, A. and Bergeles, G., "Modeling wall impaction of diesel sprays", *Int. J. Heat Fluid Flow,* Vol. 17, No. 2, pp. 130–8, 1996.

Ghadiri, H., "Raindrop Impact, Soil Splashing and Catering", PhD Thesis, University of Reading, 1978.

Gosman, A.D., and Ioannides, E., "Aspects of computer simulation of liquid-fueled combustors", *Journal of Energy,* Vol. 7, No. 6, pp. 482–490, 1983.

Gottfried, B.S., Lee, C.J., and Bell, K.J., "The Leidenfrost phenomenon: film boiling of liquid droplets on a flat plate", *Int. J. Heat Mass Transfer*, Vol. 9, pp. 1167–87, 1966.

Grant, G., and Tabakoff, W., "Erosion Prediction in Turbomachinery Resulting from Environmental Solid Particles", *Journal of Aircraft*, Vol.12, No.5, pp.471-478, 1975.

Grover Jr., R.O., and Assanis, D.N., "A Spray Wall Impingement Model Based upon Conservation Principles", *The Fifth International Symposium on Diagnostics and Modeling of Combustion in Internal Combustion Engines - COMODIA 2001*, Nagoya, Japan, 1-4 July, pp. 551-558, 2001.

Habachi, C., Foucart, H., and Baritaud, T., "Influence of the Wall Temperature on the Mixture Preparation in DI Gasoline Engines", *Oil & Gas Science and Tecnology – Revue de L'Institut Francais du Petrole*, Vol. 54, No. 2, pp. 221-222, 1999.

Hardalupas, Y., Taylor, A.M.K.P. and Whitelaw, J.H., "Fringe count limitations on the accuracy of velocity and mass flux in two-phase flows", *Applications of laser techniques to fluid mechanics (Springer-Verlag, Berlin),pp. 183 – 203, 1991.*

Hobbs, P.V., and Osheroff, T., "Splashing of Drops on a Shallow Liquids", *Science*, Vol. 158, pp. 1184-1186, 1967.

Huang, Q. and Zhang, H., "A Study of Different Fluid Droplets Impacting on a Liquid Film", *Petroleum Science,* Vol. 5, No. 1, pp. 62-66, 2008.

Jayaratne, O.W., and Mason, B.J., "The Coalescence and Bouncing of Water Drops at an Air/Water Interface", *Proceedings of the Royal Society of London Series A-Mathematical and Physical*, Vol. 280, No. 138, pp. 545-565, 1964.

Kalantari, D., and Tropea, C., "Influence of Surface Roughness in Spray/Wall interaction phenomena," *ILASS- Europe, 23rd Annual Conference on Liquid Atomization and Spray Systems, Brno, Czech Republic, September*, 2010, pp. 1-6.

Kalantari, D., and Tropea, C., "Spray impact onto flat and rigid walls: empirical characterization and modeling", *Int. J. Multi Flow, Vol.* 33, pp. 525–44, 2007.

Katsura, N., Saito, M., Senda, J., Saito, M., and Fujimoto, H., "Characteristics of a diesel spray impinging on a flat wall", *SAE paper 89026*, 1989.

Launder, B.E., and Morse, A., "Numerical prediction of axisymmetric free shear flows with a Reynolds stress closure". *Durst F et al (eds) Turbulent shear flows I. Springer*, Berlin Heidelberg New York, pp. 279–294, 1979.

Launder, B.E., and Spalding, D.B., "The Numerical Computation of Turbulent Flows", *Computer Methods in Applied Mechanics and Engineering*, Vol.3, No.2, pp.269-289, 1974.

Lee, M.M., and Hanratty, T.J., "The Inhibition of Droplet Deposition by the Presence of a Liquid Wall Film", International Journal of Multiphase Flow, Vol. 14, No. 2, pp. 129-140, 1988.

Lee, S. H., "Development of a New Model and Heat Transfer Analysis of Impinging Diesel Sprays on a Wall", *PhD Thesis*, Department of Mechanical Engineering, Chung-Ang Univerisity, 1999.

Lee, S.H., and Ryou, H.S., "Development of new model and heat transfer analysis of impinging diesel sprays on a wall", *Atom. Sprays*, Vol. 1, No. 85, 2000.

Lee, S.Y., and Ryou, S.U., "Recent Progress of Spray-Wall Interaction Research", *Journal of Mechanical Science and Technology*, Vol. 20, No. 8, pp. 1101-1117, 2006.

Leidenfrost, J.G., "On the Fixation of Water in Diverse Fire", *International Journal of Heat and Mass Transfer*, Vol. 9, pp. 1153-1166, 1966.

Lemini, E., and Watkins, A.P., "Development of a Spray Wall Impaction Model without Discretisation into Droplet Size Classes", *ILASS-Europe 2002*, Zaragoza, Spain, 9-11 September.

Leonard, B.P., "A Stable and Accurate Convective Modelling Procedure Based on Quadratic Upstream Interpolation", *Computer Methods in Applied Mechanics and Engineering*, Vol.19, No.1, pp.59-98, 1979.

Levin, Z., and Hobbs, P.V., "Splashing of Water Drops on Solid and Wetted Surfaces - Hydrodynamics and Charge Separation", *Philosophical Transactions of the Royal Society of London Series A-Mathematical and Physical Sciences*, Vol. 269, No. 1200, pp. 555, 1971.

Marengo, M., and Tropea, C., "Aufprall von Tropfen auf Flüssigkeitsfilme", Tr 194/10 1, 2, Deutsche Forschungsgemeinschaft, 1999.

Marengo, M., Steigleder, T., and Tropea, C., "Aufprall Von Tropfen auf Flüssigkeitsfilmen", *2 Workshop über Sprays, Erfassung von Sprühvorgängen und Techniken der Fluidzerstäubung*, pp. A3-1 - A3-8, 1996.

Matsui, Y., Sugihara, K., "Sources of hydrocarbon emissions from a small direct injection Diesel engine", *JSAE Review*, Vol. 7, 1988.

Matsumoto, S., and Saito, S., "On the Mechanism of Suspension of Paticels in Horizontal Conveying: Monte Carlo Simulation Based on the Irregular Bouncing Model", *J. Chem. Engng. Japan*, Vol.3, pp. 83-92, 1970.

Meingast, U., Staudt, M., Reichelt, L., Renz, U., and Arnd Sommerhoff, P., "Analysis of spray/wall interaction under diesel engine conditions", *SAE Tech Paper,* 2000.

Moita, A.S., and Moreira, A.L.N., "Drop impacts onto cold and heated rigid surfaces: morphological comparisons, disintegration limits and secondary atomization", *Int. J. Heat Fluid Flow*, Vol. 28, No. 4, pp. 735–72, 2007.

Moreira, A.L.N., Moita, A.S. and Panão, M.R., "Advances and challenges in explaining fuel spray impingement: How much of single droplet impact research is useful", *Progress in Energy and Combustion Science*, Vol. 36, pp. 554-580, 2010.

Mostafa, A.A., and Mongia, H.C., "On the Modelling of Turbulent Evaporating Sprays: Eulerian versus Lagrangian Approach", *Int. J. Heat Mass Transfer*, Vol.30, No.12, pp.2593-2593, 1987.

Mundo, C., Sommerfeld, M., and Tropea, C., "Droplet-Wall Collisions: Experimental Studies of the Deformation and Breakup Process", *International Journal of Multiphase Flow*, Vol. 21, No.2, pp. 151-173, 1995.

Mundo, C., Sommerfeld, M., and Tropea, C., "Experimental Studies of the Deposition and Splashing of Small Liquid Droplets Impinging on a Flat Surface", *Proc. ICLASS 1994, Begell House*, New York, NY, pp. 1-18, 1994.

Mundo, C., Sommerfeld, M., and Tropea, C., "Numerical and Experimental Investigation of Spray Characteristics in the Vicinity of a Rigid Wall", *Experimental Thermal and Fluid Science*, Vol. 15, No. 3, pp. 228-237, 1997.

Mundo, C., Sommerfeld, M., and Tropea, C., "On the Modeling of Liquid Sprays Impinging on Surfaces", *Atomization and Sprays*, Vol. 8, No. 6, pp. 625-652, 1998.

Mutchler, C.K., "The Size, Travel and Composition of Droplets Formed by Waterdrop Splash in Thin Water Layers", Ph. D. Thesis, University of Minnesota, 1970.

Nabber, J.D. and Reitz, R.D., "Modelling Engine Spray/Wall Impingement", *SAE Paper 880107,* Society of Automotive Engineers, 1988.

Nabber, J.D., Farrel, P., "Hydrodynamics of droplet impingement on a heated surface", *SAE Tech. Paper*, 930919, 1993.

Nagaoka, M., Kawazoe, H. and Nomura, N., "Modelling Fuel Spray Impingement on a Hot Wall for Gasoline Engines", *SAE 940525*, 1994.

Nishio, S., and Hirata, M., "Direct contact phenomenon between a liquid droplet and high temperature solid surface", *6th Int. Heat Trans. Conf.*, Toronto, Canada, Hemisphere, New York; 1978; Vol. 1, pp. 245:50.

Nukiyama, S.J., "The Maximum and Minimum Values of the Heat Q Transmitted from Metal to Boiling Water under Atmospheric Pressure", *International Journal of Heat and Mass Transfer*, Vol. 9, pp. 1419-1433, 1966.

Oguz, H.N. and Prosperetti, A., "Bubble entrainment by the impact of drops on liquid surfaces," *J. Fluid Mech.* **219**, 143-179, 1990.

Okawa, T., Shiraishi, T. and Mori, T., "Effect of impingement angle on the outcome of single water drop impact onto a plane water surface", *Experiments in Fluids*, Vol. 44, No. 2, pp.331-339, 2008.

Okawa, T., Shiraishi, T. and Mori, T., "Production of secondary drops during the single water drop impact onto a plane water surface", *Experiments in Fluids*, Vol. 41, Oct. 2006, pp. 965-974.

Özdemir, I.B., and Whitelaw, J.H., "Impingement of an axisymmetric jet on unheated and heated flat plates", *J. Fluid Mech.,* Vol. 240, pp. 503–532, 1992.

Panão, M.R.O. and Moreira, A.L.N. "Thermo- and Fluid Dynamics characterization of spray cooling with pulsed sprays", *Experimental Thermal and Fluid Science*, Vol. 30, pp.79 – 96, 2005.

Park, S.W. and Lee, C.S., "Macroscopic and microscopic characteristics of a fuel spray impinged on the wall", *Exp. Fluids*, Vol. 37, pp. 745–62, 2004.

Park, K. and Watkins, A. P., "Comparison of Wall Spray Impaction Models with Experimental Data on Drop Velocities and Sizes", Int. Heat and Fluid Flow, Vol. 17, No. 4, pp. 424–438, 1996.

Pasandideh-Fard, M., Qiao, Y. M., Chandra, S. and Mostaghimi, J., "Capillary effects during droplet impact on a solid surface", *Phys. Fluids*, Vol. 8, No. 3, pp. 650–659, 1996.

Patankar, S.V.N., "Numerical Heat Transfer and Fluid Flow (Hemisphere Series on Computational Methods in Mechanics and Thermal Science)", *McGraw-Hill Education*, 1st Ed., 1980, ISBN-10: 0891165223.

Prosperetti, A., and Oguz, H.N., "The Impact of Drops on Liquid Surfaces and the Underwater Noise of Rain", *Ann. Rev. Fluid Mech.*, Vol. 25, pp. 577-602, 1993.

Randy, L., Vander Wal G., Berger, M., and Mozes, S.D., "Droplets splashing upon films of the same fluid of various depths", *Exp. Fluids*, Vol. 40, pp. 33–52, 2006a.

Randy, L., Vander Wal G., Berger, M., and Mozes, S.D., "The combined influence of a rough surface and thin fluid film upon the splashing threshold and splash dynamics of a droplet impacting onto them", *Exp. Fluids*, Vol. 40, pp. 23–52, 2006b.

Randy, L., Vander Wal G., Berger, M., and Mozes, S.D., "The splash/non-splash boundary upon a dry surface and thin fluid film", *Exp. Fluids*, Vol. 40, pp. 53–59, 2006c.

Ranz, W.E., and Marshall, W.R.J., "Evaporation from Drops. Part I", *Chemical Engineering Progress*, Vol.48, No.3, pp.173-180, 1952a.

Ranz, W.E., and Marshall, W.R.J., "Evaporation from Drops. Part II", *Chemical Engineering Progress*, Vol.48, No.3, pp.173-180, 1952b.

Rein, M., "Introduction Between Drops and Hot Surfaces." Drop-Surface Interactions, M. Rein, ed., Springer-Verlag Wien New York, Udine, pp. 185-217, 2002a.

Rein, M., "Introduction to Drop-Surface Interactions." Drop-Surface Interactions, M. Rein, ed., Springer-Verlag Wien New York, Udine, pp. 1-24, 2002b.

Rein, M., "Phenomena of Liquid Drop Impact on Solid and Liquid Surfaces", *Fluid Dynamics Research*, Vol. 12, No. 2, pp. 61-93, 1993.

Rioboo, R., Bauthier, C., Conti, J., Voue, M., and De Corninck, J., "Experimental investigation of splash and crown formation during single drop impact onto wetted surfaces", *Exp. Fluids*, Vol. 35, pp. 648–52, 2003.

Rioboo, R., Tropea, C., and Marengo, M., "Outcome from a drop impact on solid surfaces", *Atom. Sprays,* Vol. 11, pp. 155–65, 2001.

Rodriguez, F., Mesler, R., "Some drops don't splash", *Journal of colloid and interface science,* Vol. 106, No. 2, pp. 347–352, 1985.

Roisman, I.V., Berberović, E. and Tropea, C., "Inertia dominated drop collisions. I. On the universal flow in the lamella", *Physics of Fluids*, Vol. 21, No. 5, 2009.

Roisman, IV., Horvat, K., and Tropea, C., "Spray impact: rim transverse instability initiating fingering and splash: description of a secondary spray", *Phys. Fluids*, Vol. 18, 2006.

Senda, J., Kanda, T., Al-Roub, M., Farrel, P.V., Fukami, T., and Fujimoto, H., "Modelling Spray Impingement Considering Fuel Film Formation on the Wall", *SAE Paper 970047*, Society of Automotive Engineers, 1997.

Senda, J., Kobayashi, M., Iwashita, S. and Fujimoto, H., "Modeling of Diesel Spray Impinging on Flat Wall", *Proc. Int. Symposium COMODIA 94, pp. 411-416,* 1994a.

Shirolkar, J.S., Coimbra, C.F.M. and McQuay, M.Q., "Fundamental aspects of modeling turbulent particle dispersion in dilute flows", *Prog. Energy Combust. Sci.*, Vol. 22, pp. 363–399, 1996.

Shuen, J.S., Solomon, A.S.P., Zhang Q.F. and Faeth, G.M., "Structure of Particle-Laden Jets - Measurements and Predictions", *AIAA Journal*, Vol.23, No.3, pp.396-404, 1985.

Silva, A., "Experimental and Numerical Study of Physical Aspects of Fuel Processes", PhD Thesis, Universidade Beira Interior, Covilhã, Portugal, 2007.

Silva, A., Barata, J. and Rodrigues, C., "Influence of Spread/splash Transition Criteria on the Spray Impingement Modelling", *ILASS – Europe 2011, 24th European Conference on Liquid Atomization and Spray System*s, Estoril, Portugal, September 2011.

Silva, A.R.R., Mendes, A., Cometti, A. and Barata, J.M.M., "Estudos Numéricos de Escoamentos Bifásicos Tridimensionais", *V Congresso de Métodos Numéricos en Ingenéria*, Madrid, Spain, 3-6 June, 2002.

Sivakumar, D., and Tropea, C., "Splashing impact of a spray onto a liquid film", *Phys. Fluids*, Vol. 14, pp. L85–8, 2002.

Spalding, D.B., "A Novel Finite-Difference Formulation of Differential Expressions Involving both First and Second Derivatives", *lnternal Journal of Numerical Methods in Engineering*, Vol.4, No.4, pp.551-559, 1972.

Stanton, D., and Rutland, C., "Modeling Fuel film formation and wall interaction in diesel engines", *SAE Tech Paper 960628*, 1996.

Stow, C.D., and Hadfield, M.G., "An Experimental Investigation of Fluid-Flow Resulting from the Impact of a Water Drop with an Unyielding Dry Surface", Proceedings of the Royal Society of London Series a-Mathematical Physical and Engineering Sciences, Vol. 373, No. 1755, pp. 419-441, 1981.

Stow, C.D., and Stainer, R.D., "The Physical Product of a Splashing Water Drop", *J. Meteorol. Soc. Jpn.*, Vol. 55, No. 5, pp. 518-531, 1977.

Su, K., Yao, S.C., "Numerical studies of spray impacting normally on an infinite plate", *Atom. Sprays*, Vol. 9, pp. 431–44, 1999.

Thompson, J.J., and Newall, H.F., "On the Formation of Vortex Rings by Drops falling into Liquids", *Proc. R. Soc. Lond.*, Vol. 39, pp. 417, 1885.

Tomlinson, C., "On the Cohesion Figures of Liquids", *Phil. Mag. Ser.*, Vol. 4, No. 22, pp. 249-261, 1861.

Tomlinson, C., "On the Cohesion Figures of Liquids", *Phil. Mag. Ser.*, Vol. 4, No. 28, pp. 354-364, 1864.

Tropea, C., "Developments of specialized phase-Doppler techniques and refractive index measurements", *Lecture Series on Optical Diagnostics of Particles and Droplets*, von Karman Institute, Sint-Genesius-Rode, Belgium, 1999.

Tropea, C., and Marengo, M., "The impact of drops on walls and films", *Multi Sci. Tech., Vol.* 11, No. 1, pp. 19–36, 1999.

Wachters, L.H., and Westerling, N.H.J., "Heat Transfer from a Hot Wall to Impinging Water Drops in Spheroidal State", *Chemical Engineering Science*, Vol. 21, No. 11, pp. 1047-1056, 1966.

Wang, A.B., and Chen, C.C., "Splashing impact of a single drop onto very thin liquid films", *Phys. Fluids*, Vol. 12, No. 9, pp. 2155–8, 2000.

Wang, A.B., Lin, C.H., and Chen, C.C., "The critical temperature of dry impact for tiny droplet impinging onto a heated surface", *Phys. Fluids,* Vol. 12, pp.1622–5, 2000.

Wang, Y.P., Wilkinson, G.B., and Drallmeier, J.A., "Parametric study on the fuel film breakup of a cold start PFI engine", *Exp. Fluids*, Vol. 37, pp. 385-398, 2004.

Watkins, A.P. and Wang, D.M., "A New Model for Diesel Spray Impaction on Walls and Comparision with Experiments", *Proceedings of the Int. Symp. on Diagnostics and Modelling of Combustion in Internal Combustion Engines*, Kyoto, Japan, September, pp. 243-248, 1990.

Winterbone, D.E., Yates, D.A., Clough, E., Rao, K., Gomes, P.O. and Sun, J.H., "Combustion in high-speed direct-injection diesel engines—a comparative study". "*Proc. Instn Mech. Engrs",* Vol. 208, pp. 223–240, Part C, 1994.

Worthington, A.M., "On the Forms Assumed by Drops of Liquids Falling Vertically on a Horizontal Plate", *Proc. R. Soc. Lond.*, Vol. 25, pp. 261-271, 1876.

Worthington, A.M., "On the forms assumed by drops of liquid falling on a horizontal plate", *Proc. R. Soc. Lond."* Vol. 25, pp. 261–271, 1877.

Worthington, A.M., A Study of Splashes, Longmans, London, New York, Bombay, Calcutta: Longmans, Green, and Co., 1908.

Yao, S.C., and Cai, K.Y., "The dynamics and Leidenfrost temperature of drops impacting on a hot surface at small angles", *Exp. Therm. Fluid Sci.*, Vol. 1, pp. 363–71, 1988.

Yarin, A.L., "Drop Impact Dynamics: Splashing, Spreading, Receding, Bouncing", *Annual Review of Fluid Mechanics*, Vol. 38, pp. 159-192, 2006.

Yarin, A.L., and Weiss, D.A., "Impact of Drops on Solid-Surfaces-Self-Similar Capillary Waves, and Splashing as a New-Type of Kinematic Discontinuity", *Journal of Fluid Mechanics*, Vol. 283, pp. 141-173, 1995.

Yoshikawa, Y., Nakada, T., Itoh, T., and Takagi, T., "Numerical Simulation System for Analyzing Fuel Film Flow in Gasoline Engine", SAE 930326, 1993.

This page has been intentionally left blank for double-sided copying.

VI. Annexes

1. Annex 1

Table VI-1: Regime transition conditions for the impingement models.

Authors	Impingement regime and conditions					Notes
	Dry Wall		Wetted Wall			
	Regime	Condition	Regime	Condition		
Nabber and Reitz (1988)	Stick	Low We				Diesel Engine $T_w < T_B$
	Reflect	We = 40				
	Jet					
Watkins and Wang (1990)	Rebound	We = 80				$T_W > T_{Leid}$ Wachters and Westerling (1966)
	Breakup					
Nagaoka et al. (1994)	Stick	We = 80				Gasoline engine $T_w < T_B$
	Breakup					
Senda et al. (1994)	n/a		Spread	We = 80	$T_w < T_B$	Diesel engine We = We (v_b)
			Large Breakup			
			Large Breakup	We = 600		
			Small Breakup			
			Breakup	$T_w \geq T_B$		
Bai and Gosman (1995)	Stick/Spread	$We = A\ La^{-0.18}$	Stick	We = 1		Stow and Hadfield (1981) DI diesel engine A is function of the surface roughness R_a We = We (v_b)
			Rebound			
	Splash		Rebound	We = 5		
			Spread			
			Spread	$We = 1320\ La^{-0.18}$		
			Splash			

Authors	***Impingement regime and conditions***				***Notes***
	Dry Wall		***Wetted Wall***		
	Regime	***Condition***	***Regime***	***Condition***	
Gavaises et al. (1996)	Rebound	*We = 100*			Diesel spray engine *We = We (v_b)*
	Stick				
Stanton and Rutland (1996)	n/a		Stick	We = 5; $T_w < T_{PA}$	Jayaratne and Mason (1964) Stow and Hafield (1981) Rodriguez and Mesler (1985) Yarin and Weiss (1995) DI Diesel Engine We = We (v_b)
			Rebound		
			Rebound	We = 10	
			Spread		
			Spread	$We = 18_l^{2d}\sqrt{\frac{\rho}{\sigma}}^{4}\sqrt{\frac{\mu}{\rho}}f^{\frac{3}{4}}$	
			Splash		
Park and Watkins (1996)	Rebound	We = 80			Wachters and Westerling (1966) Diesel engine We = We (v_b)
	Breakup				
Cossali et al. (1997)	n/a		Coalescence	K_c=2100+5880$\delta^{1.44}$	For δ<0.1, the effect of R_a is negligible; Agree with data of Wang and Chen (2000) and Rioboo *et al.* (2003) for low-viscosity liquids.
			Splash		
Mundo et al. (1997) *Mundo et al. (1998)*	Deposition	K = 57.7	n/a		K = Oh.$Re^{1.25}$ Mundo *et al.* (1995) Mundo (1996)
	Splash				
TAR Model (Xu et al., 1998)	Rebound	$We = \frac{2.\sqrt{C_k}}{C_d\,.Oh}$			Diesel engine $\xi = \frac{C_d}{2.\sqrt{C_k}}.We.Oh$ Theoretical approach Tw > T_{Leid}
	Stick				
	Rebound	$We = 4C_k\,.\left(1-\xi^2\right).e^{\frac{\pi\xi}{\sqrt{1-\xi^2}}}$			
	Breakup				
Senda et al. (1997) *Senda et al. (1999)*	n/a		Deposition	$We = (2164 + 7560\,\delta_{non}^{1.78})\,La^{0.2}$	Port-injection gasoline engine Distinction between low We (We ≤ 300) and high We (We > 300).
			Splash		

Authors	Impingement regime and conditions				Notes
	Dry Wall		Wetted Wall		
	Regime	Condition	Regime	Condition	
Lee and Ryou (2000)	Rebound	We = 5			DI diesel engine Mundo *et al.* (1995) $K = Oh.Re^{1.25}$ $T_w < T_B$
	Deposition				
	Deposition	K = 57.7			
	Splash				
Grover and Assanis (2001)	Deposition	K = 57.7	Deposition	$K=Oh^{-0.4}$ $We=2100+5880\delta^{1.44}$	K = Oh.Re$^{1.25}$ Mundo *et al.* (1995) and Cossali *et al.* (1997) DISC engine
	Splash		Splash		
Bai et al. (2002)	Stick/Spread	$We = 2630.La^{-0.18}$	Stick	We = 2	Gasoline engine Lee and Hanratty (1988) Stow and Hadfield (1981) We = We (v_b)
			Rebound		
			Rebound	We = 20	
	Splash		Spread		
			Spread	$We = 1320.La^{-0.18}$	
			Splash		
Lemini and Watkins (2002)	Deposition	K = 15			K = Oh.Re$^{1.25}$ Mundo *et al.* (1995) Eulerian-Eulerian approach
	Rebound				
	Rebound	K = 57.7			
	Splash				
Randy et al. (2006)	Stick/Spread	$K_c=0.85$	Stick/Spread	$K_{c,wet}=63$	The correlation for dry surfaces fits well the experimental data for Re>7000, opposing to the results for Re<3000.
	Splash		Splash		
Huang and Zhang (2008)	n/a		Coalescence	$(We.Re)^{0.25} = 25 + 78^{1.44}$	Good results were found for thin oil and water film.
			Splash		

2. Annex 2

2.1. Nabber and Reizt (1988)

An early attempt to model spray impingement on walls was made by Nabber and Reitz (1988). In this model an impinging droplet is assumed to stick on the wall in a spherical form ("Stick" model), reflect elastically ("Reflect" model) or move tangentially along the surface like a jet ("Jet" model). In all three regimes the size of impinging drop was not changed by the wall interaction (see Table VI-2). There are three limitations of this model: (i) the conditions for the occurrence of each regime are not specified in relation to experimental data; (ii) the phenomenon of droplet shattering, which occurs at high collision energy is ignored, this effect is important in the wall spray dispersion and vaporization; and (iii) the energy and momentum losses of the impinging droplets are not accounted for. This model worked reasonably well in cases involving relative large injector-wall distances (> *60 mm*) it has proven less satisfactory when the wall is in closer proximity.

Table VI-2: The post impingement model proposed by Nabber and Reitz (1988).

	Velocity Components		Diameter	Number
	u_a	v_a	d_a	n_a
Stick	0	0	--	--
Reflect	u_b	$- v_b$	d_b	*1*
Jet	$\sqrt{u_b^2 + v_b^2}$	0	d_b	*1*
$\varphi_a = -\frac{\pi}{\beta} ln\left[1 - p\left(1 - e^{-\beta}\right)\right]$				

2.2. Watkins and Wang (1990)

Watkins and Wang (1990) later proposed a model, which differed from the one described above in two important ways. Firstly, an impinging droplet is assumed to suffer one of the two consequences, namely rebound or breakup, depending on the impact energy. The transition criterion between these two regimes is described by a critical Weber number (see Table VI-3), which was deduced by Wachters and Westerling (1966) from their experimental data on water drops impinging with a hot plate, whose temperature is above the Leidenfrost temperature.

Secondly, the modelling of post-impingement behaviour is different in the following ways. For the 'rebound' regime, the rebound angle is assumed to be equal to that of the incident angle but the magnitude of the rebound velocity is determined from an energy loss correlation proposed by Jayarantne and Mason (1964) for a water drop impinging on a 'deep' water layer, $\delta_{non} \gg 1$,

$$\frac{V_b^2 - V_a^2}{V_b^2} = 0.95 \sin^2(\theta_I) \qquad \text{(VI-1)}$$

For the 'breakup' regime, the ejected droplets are assumed to move tangentially to the wall at a velocity equal to the incident droplet tangential velocity. The sizes of the ejected droplets are assumed to be one-quarter of the incident ones.

The model Watkins and Wang (1990), was initially found to significantly under-predict wall spray dispersion (and hence wall spray volume as well) when compared with experimental data. In order to achieve better agreement, the authors modified the droplet binary collision model of O'Rouke and Bracco (1980) so that the colliding droplets were caused to move along the direction of maximum local void fraction gradient (Wang and Watkins, 1993). This gave a better prediction of the wall spray dispersion, but still the predicted wall spray volume was seen to be appreciably smaller than that of the experiment.

Table VI-3: The post impingement model proposed by Wang and Watkins (1990).

	Velocity components		Diameter	Number
	u_a	v_a	d_a	n_a
Rebound	$u_b \cdot \omega$	$- v_b \cdot \omega$	d_b	*1*
Breakup	u_b	0	$C_w \cdot d_b$	*64*

$$\omega = \sqrt{1 - 0.95\cos^2\varphi_b}\,;\; C_w = \frac{1}{4}$$

2.3. Nagaoka et al. (1994)

The model presented by Nagaoka *et al.* (1994) is derived from sprays impinging on hot walls in gasoline engines, where the wall temperature is below the fuel boiling point. In the model, a droplet parcel impinging on a wall with a Weber number higher than 80, is transformed into two secondary droplet parcels. Experimental data obtained by the authors were used to formulate equations for the droplet size and the Weber number for the secondary droplets. The droplet directions are specified stochastically.

The calculation results utilising this model agree very well with the experimental data and the model was also applied to the mixture formation process in lean-burn engine.

2.4. Senda et al. (1994)

The impinging spray model proposed by Senda *et al.* (1994) is based on experimental data obtained by the authors. In this model the authors divided the impact into two cases, with the surface temperature as the critical criterion. The critical temperature is the liquid boiling point, and depending on whether the surface temperature is above or below T_B, the interaction is treated differently. If $T_W < T_B$ an impinging droplet spreads over the surface and

create a liquid film. On the other hand, in case of $T_W \geq T_B$, part of the liquid vaporises immediately at the impact and the rest of the liquid forms a liquid film on the surface. As the surface temperature is above the boiling point, the liquid film will boil. This will cause vapour to blow upward and the liquid film will break up, owing to the boiling phenomena.

In the case when the T_W is below T_B the impingement has been divided into three groups, depending on the Weber number. The difference between these groups is whether there is or not a break-up. The break-up is also divided into a large and a small break-up, depending on the droplet size after the impingement (see Table VI-4).

Table VI-4: The post impingement model proposed by Senda et al. (1994).

	Velocity V_a	Diameter d_a	Number n_a
Spread	0	--	--
Large Breakup	$0.3 \, . \, V_b$	$0.5 \, . \, d_b$	n_b
Small Breakup	$0.5 \, . \, V_b$	$0.3 \, . \, d_b$	n_b
	$T < T_W$		

In the second case, $T_W \geq T_B$, the behaviour of the secondary droplets is described with functions based on the incoming Weber number. All Weber numbers are based on the velocity in the surface normal direction, thus taking the impingement angle into account.

The Weber number for the splashing droplets, We_a, is determined using the function

$$We_a = 0.678 \, We_b \, e^{[-4.415.10^{-2} We_b]} \qquad \textbf{(VI-2)}$$

The splashing velocity after reflection is expressed in terms of the outgoing Weber number, under the assumptions of conservation of mass and momentum of the droplet during impingement and reflection

$$\begin{cases} v_a = -\sqrt{\dfrac{We_a \sigma}{\rho d_b}} & if \; We_b > 80 \\ v_a = 0 & if \; We_b < 80 \end{cases} \qquad \textbf{(VI-3)}$$

The atomisation caused by the break-up of the droplet results in secondary droplets. The droplet size distribution can be estimated from:

$$\begin{cases} d_{32} = d_b & if \; We_b < 50 \\ d_{32} = (1.07 - 1.01 \times 10^{-2} We_b + 3.29 \times 10^{-5} We_b) d_b & if \; 50 \leq We < 140 \\ d_{32} = 0.416 \times 10^{(-1.02 \times 10^{-3} We_b)} . d_b & if \; 140 \leq We < 300 \\ d_{32} = 0.2 d_b & if \; We \geq 300 \end{cases} \qquad \textbf{(VI-4)}$$

The comparison of the experimental data with the calculated results from diesel spray impinging on a low temperature wall showed qualitative agreement. Nevertheless,

spray radius and height were underestimated. In the case of a high temperature wall the agreement was less satisfying.

2.5. Bai and Gosman (1995)

Bai and Gosman (1995) divided the post-impingement models into three groups based on the impingement regime from which the impact results. The groups are adhesion (i.e. consisting of both stick and spread regime), rebound and splash.

For the adhesion regime is assumed that arriving droplets coalesces to form a local film. For rebound regime, the droplet bounces off the wall and the problem is to determine velocity and direction. Jayarantne and Mason (1964) developed a relation that enabled the determination of the velocity rebound by the estimation of the kinetic energy loss, as described before in Watkins and Wang model (Watkins and Wang, 1990).

The correlation was derived from experiments with water droplets impinging on very deep water layers, $\delta_{non} \gg 1$, and therefore, it probably over-predicted the energy loss for a droplet bouncing from a very thin surface film, because a droplet would very frequently encounter a pre-existing cavity in the film surface. An alternative way of determining the velocity for a droplet is to use a correlation for a solid sphere that interacts with a solid wall proposed by Matsumoto and Saito (1970) (see Table VI-5). The quantity *e* is the "restitution coefficient" proposed by Grant and Tabakoff (1975) for rebound of the particles impacting on solid blades or channel wall.

Table VI-5: The post impingement model proposed by Bai and Gosman (1995).

	Velocity components		Diameter	Number
	u_a	v_a	d_{ia}	n_{ia}
Stick/Spread	--	--	--	--
Rebound	$5/7.u_b$	$-e \cdot v_b$	d_b	*1*
Splash	$u_{1a}+u_{2a}=\frac{2C_f}{rm}u_b$	$\sqrt{V_{ia}^2-u_{ia}}$	$\sqrt[3]{\frac{r_m}{2.n_i}}d_b$	n_{ia}
$N=\sum_{i=1}^{2} n_i = a_0\left(\frac{We_1}{We_{cr}}-1\right);$				

In case of splash regime is essential to determined quantities such as the total secondary to incident mass ratio, size, velocity and ejection angle of the secondary droplets. To do this, Bai and Gosman (1995) assumed that each droplet parcel produces two secondary parcels with equal mass and different sizes and velocities. Still it is assumed the secondary drops that are resultant of normal or oblique impact fall randomly within a cone. The ejection angle for a particular ejected can be sampled within the cone.

For determination of the mass ratio Bai and Gosman used experimental results of Stow and Stainer (1977) and Levin and Hobbs (1971) for a dry wall condition, whereas for a wetted wall used the study of Mutcher (1970).

The secondary droplet sizes were determined using mass conservation and a correlation for the number of secondary droplets per splash. The secondary droplet velocities were evaluated through the use of energy and tangential momentum conservation, see Table VI-5 and for details Bai and Gosman (1995).

2.6. Gavaises et al. (1996)

The Gavaises *et al.* (1996) presented a model for a diesel spray wall impact, which was based on the *We* number of normal component velocity. The regimes considered were the stick and rebound, with or without breakup. In order to determine the velocity after impact, the energy was examined. During collision the droplet loses kinetic energy. This loss is mainly due to energy transformed to the normal direction. One possible explanation pointed out by Gavaises *et al.* (1996) for this energy transformation was the surface roughness, which changes the real normal direction to the surface.

Table VI-6: The post impingement model proposed by Gavaises et al. (1996).

	Velocity components		Diameter	Number
	u_a	v_a	d_a	n_a
Rebound	$p\sqrt{v_b^2+u_b^2-v_a^2}$	$-v_b\sqrt{\frac{d_b We_a}{d_a We_b}}$	$f(d_{32})$	n_b
Stick	---	--	---	---

$$We_a = min\left[We_b, C_1 We_b e^{-C_2 We_b}\right]$$

p is a random number between *0* and *1*

The calculation of normal velocity component for the rebound velocity after impingement was based on the experimental results of Wachters and Westerling (1966). The experimental data showed that the droplets Weber number just before and just after the impingement were correlated (see Table VI-6). The effect of wall roughness was statistically taken into account on the prediction of the tangential velocity component of rebound droplet. To avoid any non-physical result, it was assumed that the droplet will stick to the surface if

$$\arctan\left(\frac{v_a}{u_a}\right) < 1^\circ \qquad \textbf{(VI-5)}$$

To be able to predict the behaviour of the break-up process, laws of energy and momentum were used. This results in the following formula for predicting the size of secondary droplets:

$$d_{32} = \frac{4\pi\sigma}{\frac{8\pi\sigma}{d_b} + \frac{\pi}{6}\rho d_b^2 \left(\frac{\partial y}{\partial t}\right)^2 + C_k \frac{8\sigma}{\rho d_b^3} y_l^2} \qquad \text{(VI-6)}$$

where *y* in this model is a non-dimensional measure of the droplet surface from its equilibrium position and C_k is an empirical constant. The non-dimensional parameter *y* also serves as a transition condition and if *y* > *1* the droplet will break up during impingement (Gavaises *et al.,* 1996).

During impact there is a possibility that the droplet will turn in the surface plane. This azimuthal angle can be determined by a probability distribution, derived from assumptions of mass and momentum conservation (Nabber and Reitz, 1988).

The comparison of the predictions with the experimental data from diesel spray wall impaction with and without cross-flow showed a distinct performance. In case of a presence of a cross-flow the spray radius and height result showed qualitative agreement. In absence of a cross-flow the predictions of spray radius was under-estimated, while the predictions of spray height was overestimated.

2.7. Stanton and Rutland (1996)

The model presented by Stanton and Rutland (1996) was validated for droplet impingement on a wetted wall with a temperature below the fuel boiling point. Stick, rebound, spread and splash are the different regimes included in the model. This model has many similarities with the Bai and Gosman (1995) model.

For rebound regime, Stanton and Rutland (1996) use the correlation proposed by Matsumoto and Saito (1970) to determine the droplet velocity, as described before by Bai and Gosman model. The azimuthal angle, ϕ_{az} , in the circumferential direction within the plane tangential to the wall is randomly sampled in a range $[\pi/2\,;3\pi/2\,]$ with an equal probability. This variation in ϕ_a was observed experimentally by Levin and Hobbs (1971) and Stow and Stainer (1977) on rough surfaces. These investigators reported little difference between drop impact with liquid film and that of a rough surface.

In order to determine how the secondary droplets behave Stanton and Rutland (1996) assumed that each incident droplet parcel can produce three secondary parcels, *p*. Each parcel contains a calculated number of droplets, n_{ia}, with the same kinematic and thermodynamic properties. The number of parcels chosen by Stanton and Rutland (1996) was a compromise between the number of sampling points minimal to provide adequate sampling of the secondary droplet distribution curves and the computational effort and memory requirements to run the code. The droplet size distribution was determined with a Weibull

distribution that followed the experimental work of Mundo *et al.* (1995) for multi-drop impingement on rough surfaces (see Table VI-7).

Table VI-7: The post impingement model proposed by Stanton and Rutland (1996).

	Velocity components		Diameter	Number
	u_{ia}	v_{ia}	d_{ia}	n_{ia}
Stick/Spread	--	--	--	--
Rebound	$\frac{5}{7}u_b$	$-e \cdot v_b$	d_b	*1*
Splash	$\sqrt{k}\frac{v_{ia}}{tan\theta_S}$	$\sqrt{k}v'_{ia}$	$pdf\left(\frac{d_{ia}}{d_b}\right)$	$N.pdf\left(\frac{d_{ia}}{d_b}\right)_i$

$$pdf\left(\frac{d_{ia}}{d_b}\right)=\frac{c}{\theta_w}\left(\frac{1}{\theta_w}.\frac{d_{ia}}{d_b}\right)^{c-1}.e^{-\left(\frac{1}{\theta_w}.\frac{d_{ia}}{d_b}\right)^c};\ pdf\left(\frac{v'_{ia}}{v_b}\right)=\frac{b_v}{\theta_v}\left(\frac{1}{\theta_v}.\frac{v'_{ia}}{v_b}\right)^{b_v-1}.e^{-\left(\frac{1}{\theta_v}.\frac{v'_{ia}}{v_b}\right)^{b_v}}$$

$$\frac{\pi}{6}N\sum_{i=1}^{p}\left[pdf\left(\frac{d_{ia}}{d_b}\right)_i.d_{ia}^3\right]=r_m m_I;$$

The total number of secondary droplets, *N*, and number of droplets each parcel, n_{ia}, was calculated by requiring mass conservation once the mass ratio, r_m, was determined. Stanton and Rutland (1996) used a curve-fit to data from the experimental work of Yarin and Weiss (1995) to determine mass ratio,

$$r_m = -27.2 + 3.15u - 0.116u^2 + 1.4\times10^{-3}u^3 \qquad \textbf{(VI-7)}$$

where *u* is a non-dimensional velocity, and according to Yarin and Weiss (1995) the splashing threshold occurs at a non-dimensional velocity equal to *18*.

Finally, the remaining quantity to be calculated is the velocity of secondary droplets. The normal component velocity of each parcel uses a Weibull distribution (see Table VI-7), similar to the droplet size distribution. This droplet velocity distribution and the ejection angle are estimated from the experimental observations of Mundo *et al.* (1995). Once the normal velocity component and the ejection angle are known, the tangential velocity component can be estimated.

Stanton and Rutland (1996) proposed a correction factor, *k*, derived from energy balance and used it to compensate the small number of sampling points used to calculate the normal velocity of the secondary droplets. The correction factor was applied to both the normal and the tangential velocity components of each parcel.

A fuel film model was developed by Stanton and Rutland (1996) to help account for fuel distribution during combustion in diesel spray (see Figure VI-1). According to Nabber *et al.* (1988), spray impingement models should include the possibility of the formation of a

liquid film on the combustion chamber surfaces to accurately model spray-wall phenomena. The model simulates this film flow on solid surfaces of arbitrary configuration. The continuity and momentum equations were applied to each film cell. By integrating across the film thickness and using "thin film" assumptions, the equations were reduced to a two-dimensional film flowing across a three-dimensional surface. The major physical effects considered in the model include mass and momentum contributions to the film due to spray drop impingement, splashing effects, various shear forces, piston acceleration, dynamics pressure effects and gravity driven flows (for details see Stanton and Rutland, 1996). Later, Stanton and Rutland (1997, 1998) added the thermal and evaporative processes to the fuel film model.

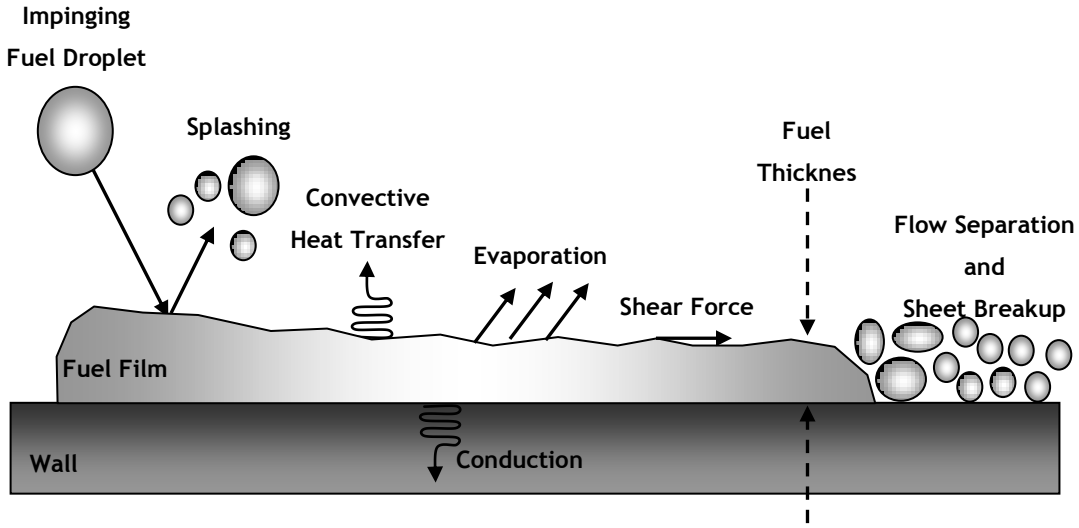

Figure VI-1: The major physical phenomena governing film flow (Stanton and Rutland, 1996).

In Stanton *et al*. (1998) the equation for the droplet size distribution in Stanton and Rutland (1996) was changed. Instead of a Weibull distribution a four-parameter log hyperbolic distribution was used. The equation used is the following

$$f(x,\alpha,\beta,\delta,\mu) = \frac{\sqrt{\alpha^2-\beta^2}}{2\alpha\delta K_1\left(\delta\sqrt{\alpha^2-\beta^2}\right)} \cdot e^{-\alpha\sqrt{\delta^2+(x-\mu)^2}+\beta(x-\mu)} \qquad \text{(VI-8)}$$

where δ and μ are the scale and location parameters, α and β determine the form and shape of the density function, and K_1 is the modified Bessel function of third kind and first order. According to Stanton *et al*. (1998) this was the distribution that fit different measurements best.

2.8. Park and Watkins (1996)

The Park and Watkins (1996) presented a model for a diesel spray wall impact, where the rebound and breakup regimes were modelled. The rebound model of Park and Watkins (1996) was very similar to that of Watkins and Wang (1990) and Wang and Wackins (1993), except that the data of Wachters and Westerling (1966) was properly taken into account. For

each impacting drop, the Weber number before impact was calculated and the Weber number after impact was obtained from the experimental data (Wachters and Westerling, 1966). As Weber number was based on the normal velocity component to the surface as well as the droplet size didn't change during the rebound regime, then velocity normal to the surface after rebounding could be calculated (see Table 1.9). According to Wachters and Westerling (1966), the tangential velocity component was unaffected by impaction.

The break-up model of Park and Watkins (1996) was assumed that the entire incident droplet originate new droplet, i.e., no liquid was left on the surface. Park and Watkins (1996) analysed the data of Nabber and Farrel (1993) to obtain drop sizes after break-up. Nabber and Farrel (1993) showed that, over the range of We_b examined, up to *120*, the number of droplets resulting from the break-up of a single drop impacting on a hot surface was a linear function of the Weber number before impact (see Table VI-8). Afterwards the number of secondary droplets was calculated from mass conservation, and then the size of the secondary droplet could be estimated.

Table VI-8: The post impingement model proposed by Park and Watkins (1996).

	Velocity components		Diameter	Number
	u_a	v_a	d_a	n_a
Rebound	u_b	$-\sqrt{\frac{We_a}{We_b}}.v_b$	d_b	n_b
Breakup	$u_b \pm p.\ u_f$	$-\sqrt{\frac{\sigma We_a}{\rho d_a}}$	$\frac{d_b}{\sqrt[3]{n_a}}$	$0.187We_b - 14.0$
$u_f = 0.835(3.096 - 2\xi)u_b;\ \xi \in [1.0, 1.548]$				
p is a random number between *0* and *1*				

The velocity components of the droplets after break-up were estimated from experimental data of Wang and Watkins (1993). The normal velocity component was obtained from the experimental Weber number after impaction, as described for the rebound regime.

In this model, in agreement with the data of Mundo *et al*. (1995), the incident drop was assumed on average to retain its original tangential velocity component after impaction. But also the droplets after break-up had an additional component due to the spread of the liquid film. The edge of the film propagated radially outwards from the impaction site with a velocity u_f, see Table VI-8. Droplets which result from the break-up would have a range of this additional velocity from zero, at the centre of impinging site, to u_f, at the film edge. The azimuthal angle, ϕ_{az}, of new droplets were determined by selecting an angle randomly in a range [0, 2π].

The model Park and Watkins (1996) model was based on experimental data obtained from drops impacting on a hot surface (Wachters and Westerling, 1966), above the

Leidenfrost point of the liquid, but was tested for impaction on a cool surface. As a consequence, the model could not perform very well. The larger difficulty of the model was in the prescription of the normal velocity components of droplets after impaction. For cool wall situations, the model could therefore be substantially improved by adopting the data of Mundo *et al.* (1995) to select normal velocities after impaction.

2.9. Mundo et al. (1997, 1998)

Mundo *et al.* (1997, 1998) proposed a model using experimental results obtained from Mundo (1996; 1995). All correlations, which are needed in modelling the impingement process, namely number, size and velocity components of secondary droplets, were given in the form of exponential or polynomial functions. In the experiments underlying this model, influences of wall roughness on the impingement process were also included. These experiments showed that roughness influenced the outcome of splashing, while the transition condition for deposit/splash regime remained unchanged with increasing wall roughness (Mundo *et al.,* 1994, Mundo *et al.,* 1955). The measurements were done by directing mono-dispersed droplets with known viscosity and surface tension, produced by a vibrating orifice generator, towards a rotating disc.

From experiments Mundo *et al.* (1994, 1995) established a three-parameter log-hyperbolic distribution to determine the size distribution of the secondary droplets, where the coefficients lineally from the *K* parameter and the surface roughness. The velocity distribution and the ejection angle of splash droplets were strongly dependent on the incident angle of the primary droplet. These experiments also indicated that the surface roughness influenced the tangential velocity component.

The weakness of these measurements lies in the effect of the boundary layer on the approaching droplets as stated by Rusche (1997). Nevertheless, excellent agreement is obtained for the test cases presented by Mundo (1996).

The experiments done in Mundo *et al.* (1994, 1995) also form the base for other correlations, made by the same authors. In Mundo *et al.* (1997, 1998) post-impingement model, for a smooth surface, was presented only considering two of the seven impingement regimes proposed by Bai and Gosman (1995), *stick* and *splash*. Splashing was divided into two parts, which also include partial deposition on the wall. In the case of complete deposit, the impinging droplets coalesced and formed a surface film.

The diameter and the number of the secondary droplets were given as function of the *K* parameter (see Table 1.10). Therefore, the mass contained in the secondary droplets did not necessarily equal that of the incident droplets, a film could build up on the surface (Mundo *et al.,* 1994, Mundo *et al.,* 1995). The mean velocity components normal and tangential to the wall depend on the impingement velocity components.

In the case of disintegration into more than one secondary droplet, the additional droplets were calculated as additional parcel, injected at the point of impingement. To limit

the computational effort, a maximum five new parcels were calculated and if this value was exceeded, the additional droplets were added to the number of droplets per parcel.

Table VI-9: The post impingement model proposed by Mundo et al. (1997, 1998).

	Velocity components		Diameter	Number
	u_a	v_a	d_a	n_a
Deposition	--	--	--	--
Splash	$sign\left[\left\|\overline{u_a}+u_a'\right\|,\frac{\pi-2\theta_I}{\pi}-p(1)\right]$	$\overline{v_a}+v_a'$	$min\left[8.72e^{-0.028K},1.0\right]d_b$	$\left(1.676\cdot10^{-5}K^{2.539}\right)n_b$

$$\overline{u_a}=\left[1.337-1.318\frac{d_a}{d_b}+2.339\left(\frac{d_a}{d_b}\right)^2\right]\cdot u_b;\sqrt{\sigma_{u_a}^2}=\left[0.229\frac{d_a}{d_b}+1.428\left(\frac{d_a}{d_b}\right)^2\right]\cdot u_b;\ u_a'=f\left(p,\sigma_{u_a}\right)$$

$$\overline{v_b}=\left[-0.249-2.959\frac{d_a}{d_b}+7.794\left(\frac{d_a}{d_b}\right)^2\right]\cdot v_b;\sqrt{\sigma_{v_a}^2}=\left[0.130+1.941\frac{d_a}{d_b}+6.539\left(\frac{d_a}{d_b}\right)^2\right]\cdot v_b;\ v_a'=f\left(p,\sigma_{v_a}\right)$$

$$r_m=\frac{n_R}{n_I}\left(\frac{d_R}{d_I}\right)^3;\ p \text{ is a random number between } 0 \text{ and } 1$$

The parameters u_a' and v_a' are the fluctuation in velocity for each individual parcel calculated in a random manner assuming a Gaussian distribution with the variance σ_{u_a} and σ_{v_a}.

2.10. Xu et al. (1998)

A complete theoretical approach for modelling an impinging droplet was presented by Xu *et al.* (1998). The dynamic behaviour of a droplet impinging on a surface was assumed to be similar to the motion of a spring-mass system. The seven-impingement regimes proposed by Bai and Gosman (1995) were divided into three types: *rebound*, *break-up* and *stick* (see Figure VI-2).

The numerical model was derived from the equation of a damped spring-mass system:

$$m\ddot{x}+c\dot{x}+kx=F \qquad \textbf{(VI-9)}$$

where *x* is the displacement of the top point of a droplet from its equilibrium position.

The authors only presented results for cases at surface temperature above the Leidenfrost temperature. At such high temperature, as demonstrated by several authors (Anders *et al.*, 1993; Chandra and Avedisian, 1991; Habachi *et al.*, 1999), the Leidenfrost phenomena occurred and the liquid evaporated so fast that the vapour generated between

the impinging droplet and the hot wall could prevent droplet wall contact. Therefore, the gravity and wetting forces were negligible for this condition.

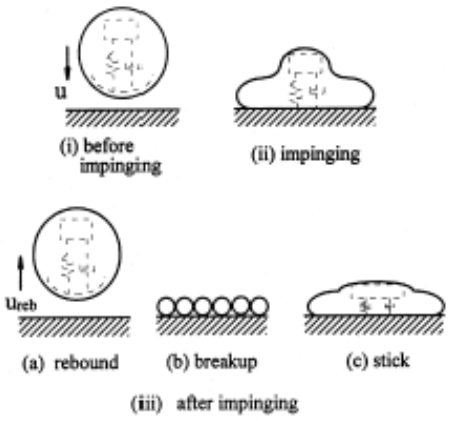

Figure VI-2: The process of droplet-wall impingement is analogous to the motion of a spring-mass system impinging on the wall (Xu et al., 1998).

The TAR model considered the effects of liquid viscosity. Although, experiments have shown these effects are negligible for large droplets, while for small droplets the liquid viscosity has influenced significantly the deformation. The equation of a damped spring-mass system can be rewritten (further detail see Xu *et al.*, 1998),

$$\ddot{y} + C_d \frac{\mu We_l}{\rho r^2}\dot{y} + C_k \frac{\sigma}{\rho r^3} y = 0 \qquad \textbf{(VI-10)}$$

where $y = x / 2r$. For a certain impinging velocity, the initial conditions of previous equation are

$$\begin{aligned} y(0) &= 0 \\ \dot{y}(0) &= V_l/2r \end{aligned} \qquad \textbf{(VI-11)}$$

The solution of the equation above is written in the following form:

$$y(t) = \frac{V_l}{2\omega r}.e^{-\frac{t}{t_d}}\sin(\omega t) \qquad \textbf{(VI-12)}$$

where

$$\frac{1}{t_d} = \frac{C_d}{2}.\frac{\mu We_l}{\rho r^2} \qquad \textbf{(VI-13)}$$

$$\omega^2 = \frac{C_{k\sigma}}{\rho r^3} - \frac{1}{t_d^2} \qquad \textbf{(VI-14)}$$

2.11. Senda et al. (1999)

In the model of Senda *et al.* (1999) the spray impingement process on a surface was divided into two cases. The Weber number was used here to separate the droplets into high or low energy impact cases.

In the case for $We \leq 300$ with the droplet impinging on a dry surface, a liquid film is formed on the surface. However, when the succeeding droplets impinge on that adhered film, the breakup small droplets are formed from the film due to the interaction process between the droplets and the film in relation to the surface wave mode. The break-up probability is estimated with a formula based on the non-dimensional film thickness.

$$\psi = 0.423 - 0.096\delta_{non} + 1.610\delta_{non}^2 + 1.470\delta_{non}^3 + 0.367\delta_{non}^4 \quad \textbf{(VI-15)}$$

In Senda *et al*. (1999) model, this break-up probability was assumed to be equal to the mass fraction of the break-up of small droplets from the film at one parcel impingement.

Adhering droplets on the surface were assumed to spread into the liquid film with the diameter χd_b where χ is determined from

$$\chi = \sqrt{\frac{We_b}{6} + 2} \quad \textbf{(VI-16)}$$

As mentioned above, the non-dimensional film thickness influenced the droplet diameter ratio in the case of break-up (Al-Roub and Farrel, 1996, and Al-Roub and Farrel, 1997). Therefore, correlations for secondary droplets were derived based on the non-dimensional film thickness

$$\frac{\overline{d_a}}{d_b} = 0.06478 - 0.5480\delta_{non} + 1.9825\delta_{non}^2 - 2.1082\delta_{non}^3 + 0.6894\delta_{non}^4 \quad \textbf{(VI-17)}$$

where $\overline{d_a}$ represents the mean diameter of secondary droplets. The amount of liquid mass that is splashed is estimated with

$$m_s = \rho \frac{\pi}{6} d_a^3 n_a \quad \textbf{(VI-18)}$$

where n_a is the number of secondary droplets. The number of secondary droplets depends on what type of break-up the impact results in Senda *et al*. (1999). Thus, the break-up form was classified into three types of *rim*, *cluster* and *column* type along with the non-dimensional film thickness. Briefly, these break-up modes for impingement onto a liquid film included break-up or droplet ejection of one or a few droplets at the outer edge of the film (*rim type*), break-up into clusters of many small droplets (*cluster*), and break-up into one or a few droplets from a column of fluid at the centre of the spreading droplet resulting from the surface waves reflecting back to their source. And the number of splashing droplets n_a was *1*, *4* and *1*, respectively in these break-up types.

The velocity components of the secondary droplets are estimated using the Weber numbers in the normal and tangential direction

$$We_{u_a} = 0.3818 - 0.00537\delta_{non} - 0.8937\delta_{non}^2 + 0.8644\delta_{non}^3 - 0.2301\delta_{non}^4 \quad \textbf{(VI-19)}$$

$$We_{v_a} = -2.1518 + 1.1493\delta_{non} + 26.238\delta_{non}^2 - 24.480\delta_{non}^3 - 5.5650\delta_{non}^4 \quad \textbf{(VI-20)}$$

An increase in the kinetic energy of an incoming droplet also means an increase in the incoming Weber number. If the Weber number increases to a value above *300* one important feature is that the high-energy droplet which collides with the surface disperses the liquid film, due to the splashing process. In Senda *et al*. (1999) model, a dry surface was assumed to be the smooth surface, while a wetted surface is treated as rough surface.

The distribution in this case is predicted with an expression based on *K* parameter from Mundo *et al*. (1995). The secondary droplet diameter is given as follows:

$$\frac{d_a}{d_b} = 3.392 \times 10^2 K^{-1.416} \quad for\ a\ rough\ surface \qquad \textbf{(VI-21)}$$

$$\frac{d_a}{d_b} = 3.903 \times 10^{10} K^{-5.116} \quad for\ a\ smooth\ surface \qquad \textbf{(VI-22)}$$

The number of broken-up droplets is obtained from the mass conservation

$$n_b = r_m \frac{d_b^3}{d_a^3} \qquad \textbf{(VI-23)}$$

For this model, and according with experiments performed by Yarin and Weiss (1995), the value assumed for mass ratio was *80* %.

The droplets splashing velocity is assessed from the energy conservation relation between incoming droplet on the wall and the splashing droplets from the wall,

$$E_{KI} + E_{I\sigma} = 1/2\, m_s V_a^2 + E_D + E_{S\sigma} \qquad \textbf{(VI-24)}$$

The secondary droplets injection angle is correlated with the incident angle of the impinging droplet, as demonstrated by the experimental data of Mundo *et al*. (1995).

Senda *et al*. (1999) added to the previous model a film movement sub-model. The movement model was based on a balance of the forces applied to the film in horizontal direction that is parallel to the wall (Figure VI-3):

1. Momentum of impinging droplets and ejected droplets – the difference in the momentum of impinging droplets on the film and ejected splashing droplets from the film is given by the following equation:

$$\sum (m_I . V_b) - \sum (m_S . V_a)$$

2. Shearing force exerted by the ambient gas – the shearing force between the film upper surface and the entrainment of ambient gas can be obtained as follows:

$$\sum \tau_{air} . A_c . dt$$

where τ_{air} is the shearing force between the film and the gas by unit surface area, A_c is the film upper surface area and *dt* is the time step. This shearing force should act on the film spreading.

3. Shearing force exerted by the wall – the shearing force between the film lower surface and the wall surface at the liquid-solid interface should be given as follows:

$$\sum \tau_w . A_c . dt$$

where the shearing stress τ_w is determined by $\tau_w = 2\mu V_f / \delta_0$. The mean film movement velocity, V_f, was defined as the horizontal velocity at the centre of the liquid film thickness. This shearing force should be operating on the film to be shrunk.

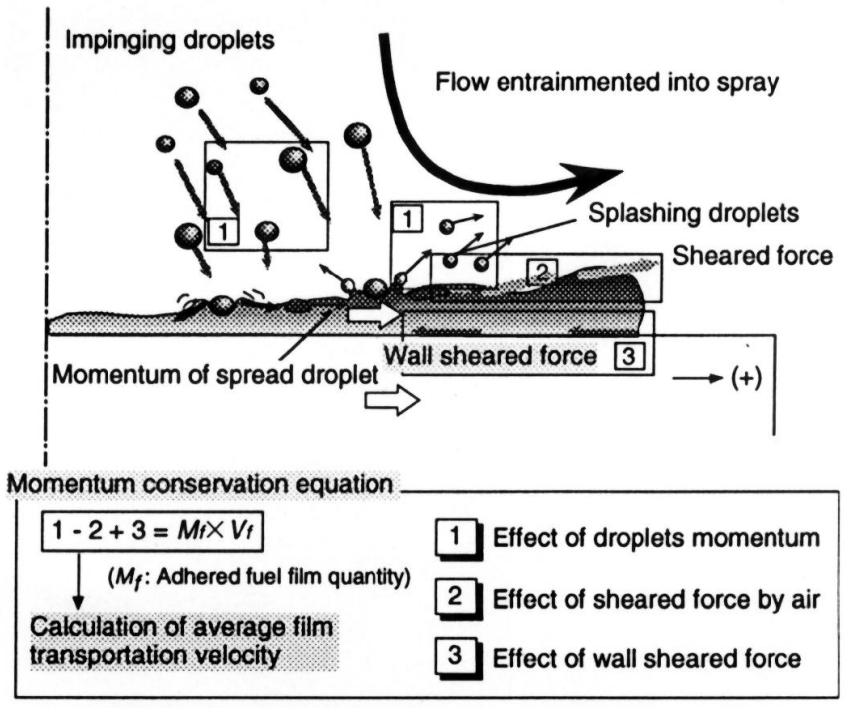

Figure VI-3: Phenomenological model for fuel film movement (Senda et al., 1999).

From the equations derived above, the following equation for the momentum conservation should be obtained to estimate the film spreading velocity V_f on the wall:

$$\sum (m_I . V_b) - \sum (m_S . V_a) - \sum (\tau_{air} . A_c dt) + \sum (\tau_w . A_c . dt) = M_f . V_f$$

where, M_f is the mass of the film adhered on the wall. The fuel film spreading process along the wall was modelled with the movement of the discrete film elements. The film transportation model showed good agreement in the case of small injection quantity, due to little influence of the inside flow (Senda *et al.*, 1999).

2.12. Lee and Ryou (2000)

Lee and Ryou (2000) proposed to study three regimes such as *rebound*, *deposition* and *splash* in which the wall temperature was below fuel boiling point. The post-impingement models for *rebound* and *deposition* regimes used by Lee and Ryou were the same adopted by Bai and Gosman model (Bai and Gosman, 1995).

In this model (Lee and Ryou, 2000) only one secondary parcel was produced and the first step was to determine the mass of these splashed droplets. For a wetted surface, the ratio of the splashed mass to the incident droplet was determined by using the work of Mutcher (1970) as described by Bai and Gosman (1995).

In the splash regime, the secondary droplet size and the number of ejected droplets were determined from the mass conservation law. The number of ejected droplet in a parcel was given from the experimental data of Nabber and Farrel (1993) (see Table VI-10).

Table VI-10: The post impingement model proposed by Lee and Ryou (2000).

	Velocity components		Diameter	Number
	u_a	v_a	d_a	n_a
Stick/Spread	--	--	--	--
Rebound	$\frac{5}{7}u_b$	$-e \cdot v_b$	d_b	1
Splash	$\frac{0.452K_f \cdot Re_{v_b}^{1/8} \cdot v_b}{\sqrt{\Psi}}$	$-\sqrt{V_a^2 - u_a^2}$	$C_w d_b$	$0.187We - 4.45$

$$C_w = (r_m / N_S)^{1/3}; We_a^T = \frac{C_w We_b^T}{r_m} - \left(\frac{K_V C_w We_{v_b} \gamma_{max}^4}{r_m Re_{v_b}} - \frac{12 C_w}{r_m} \right) - 12$$

The secondary velocity component of splashed droplet was determined from the energy conservation. From the observation of Yarin and Weiss (1995) was considered that the *splash* regime occurs at the moment of crow emergence and assumed that the tangential component of the droplet velocity after impingement can be approximated by the tangential velocity of the crown, a liquid sheet virtually normal to the wall.

In this model, the azimuthal angle was chosen stochastically by using the correlation proposed by Nabber and Reitz (1988).

2.13. Grover and Assanis (2001)

Grover and Assanis (2001) proposed a model focused on spray impact on dry wall and wet surface below the fuel's Leidenfrost temperature, a scenario encountered under typical engine operating conditions (Han *et al.*, 2000). This model conserved the mass, tangential momentum, and energy of an impinging droplet, while using splash criterion to account for

dry and wet wall collisions. Furthermore, the model incorporated a viscous dissipation model that performed adequately when compared against single droplet CFD. In addition, the model distinguished between the energy lost to viscous dissipation and wall film formation.

In the Grover and Assanis model (Grover and Assanis, 2001) three splashing parcels and one wall film parcel were formed in the splashing event. The total mass of the secondary droplets m_s was estimated by using an empirical correlation consistent with the results of Senda *et al*. (1994) and Yarin and Weiss (1995).

The secondary droplets sizes resulting from splashing were determined by probability density function, *pdf*, pointed out in Han *et al*. (2000).

The total number of droplets in each of the splashing parcels was computed by using the weighting factor and the weighting factors were computed from ratios of the *pdf* values of splashing parcels. The total number of droplets in the first splashing parcel was computed by requiring mass conservation (see Table VI-11) and the number of droplets in the wall film parcel was assumed to be equal to the number of droplets in the incident parcel.

Table VI-11: The post impingement model proposed by Grover and Assanis (2001).

	Velocity components		Diameter	Number
	u_{ia}	v_{ia}	d_{ia}	n_{ia}
Stick/Spread	--	--	--	--
Splash	$\left\|\vec{V}_{S,i}\right\| \cos\theta_s$	$u_{ia}\tan\theta_S$	*pdf(d)*	$n_{ia} = \dfrac{f(d_{ia})}{f(d_{1a})} n_{1a}$

$$n_{1a} = \frac{6m_s}{\rho\pi\left(d_{1a}^3 + \dfrac{f(r_{2a})}{f(r_{1a})}d_{2a}^3 + \dfrac{f(r_{3a})}{f(r_{1a})}d_{3a}^3\right)}; \quad f(d) = \frac{3}{2}\frac{d^2}{d_m^3}.e^{-\left(\frac{d}{d_m}\right)^{3/2}}$$

As in the previous models, the secondary velocity component of splashed droplet, which is determined from the mechanical energy conservation equation, links the total energy of impinging parcel before the impact to the splashing parcel. The kinetic and surface energy is equated to the sum of the energy of the droplet dissipated during impact, kinetic energy of the wall film parcel, and the kinetic and surface energies of the three secondary parcels via the following relationship:

$$E_{KI} + E_{I\sigma} = E_{KS} \times E_{K\,wall\,film} + E_D + E_{S\sigma} \qquad \textbf{(VI-25)}$$

The viscous dissipation model was formulated by Mao *et al*. (1997) and incorporated a viscous dissipation of an impinging droplet of Pasandideh-Fard *et al*. (1996) (Vignes-Adler, 2002). In addition, the model could distinguish between the energy lost to viscous dissipation and wall film formation.

For this model, in the case of splashing, the tangential momentum of the impinging parcel should be divided amongst three splashing parcels and one wall film parcel (see Figure VI-4) and according to the assumption of Bai and Gosman (1995) approximately 70% of the incoming tangential momentum was divided per splashing parcels. The remaining part contributes to the motion of the wall film parcel.

The secondary droplets injection angle was correlated with the incident angle of the impinging droplet, as demonstrated by the experimental data of Mundo *et al.* (1995) and the azimuthal angle was randomly sampled with an equal probability in the circumferential direction within the plane tangential to the wall (Grover and Assanis, 2001).

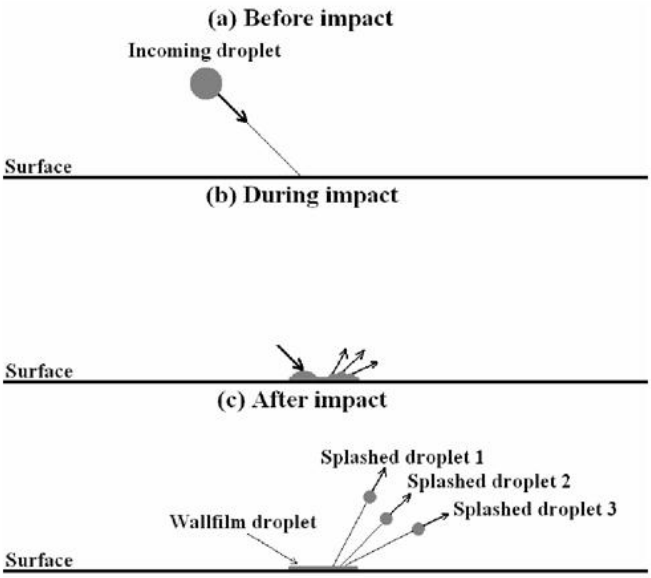

Figure VI-4: Overview splash model: (a) before impact one droplet approaches the surface, (b) during impact the incoming droplet is transformed into 1 wall film droplet and 3 splashed droplet, (c) after impact 1 wall film droplet sticks to the surface and 3 splashed droplets rebound into the gas phase.

2.14. Bai et al. (2002)

This new model (Bai *et al.* 2002) is a refinement of the proposed by Bai and Gosman in 1995. Oversee the adjustment of the transition criteria used by Bai and Gosman (1995) as mentioned before, another aspect of the new model like post-impingement characteristics for each regime undergo modification.

For the *stick/spread* and *rebound* regimes, the approach adopted in Bai and Gosman (1995) is carried over unchanged. However, modifications were made for the *splash* regime. In the Bai and Gosman model (Bai *et al.,* 2002) it is assumed that each incident droplet parcel can produce up to *6* secondary parcels, *p*. Each of these parcels contains an equal proportion of mass. The sizes of the secondary droplets are evaluated from a *pdf* (see Table 1.13) fit to existent experimental data (Stow and Stainer, 1977, Levin and Hobbs, 1971, Yarin and Weiss, 1995, and Mundo *et al.* 1995), instead of the uniform probability previously assumed. The *pdf* can now be integrated to obtain a cumulative probability function, which is then used to determine the sizes of *p* secondary droplets, d_i ($i = 1, \ldots, p$) by taking *p* random samples, each with a probability γ_i ($0 < \gamma_i < 1$).

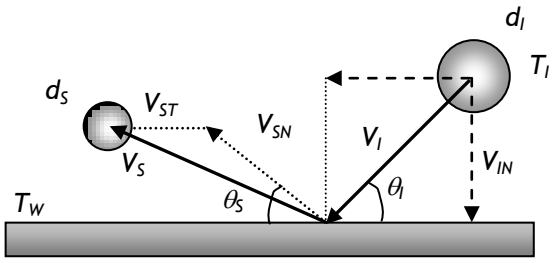

Figure VI-5: Diagram illustrating droplet impingement on to a wall.

Information on the velocities of secondary droplets resulting from impingement is very scarce, especially for oblique impingement angles. In the Bai and Gosman model the secondary droplet velocities resulting from oblique impingement can be analysed as a superposition of those arising from normal impingement and wall-tangential component. The splash velocity vector, $\vec{V_S}$, of a secondary droplet is calculated from

$$\vec{V_S} = \vec{V}_{ST} + \vec{V}_{SN} \qquad \textbf{(VI-26)}$$

where, as shown in Figure VI-5, $\vec{V}_{ST}$ and $\vec{V}_{SN}$ are due to the tangential and normal components of the incident velocity, respectively. (Note that $\vec{V}_{SN}$ is not, in general, normal to the surface). Bai *et al.* (2002) consider from the point of view that the impact energy imparted to the disintegration process of a splashing event is mainly due to normal incident velocity, $\vec{V}_{IN}$, while the effect of incident tangential velocity, $\vec{V}_{IT}$, is simply to transfer a portion of its tangential momentum to each secondary droplet, with friction loss included. In this way, evolution of $\vec{V}_{SN}$ can be by considering a normal impingement case with incident velocity V_{IN}.

Table VI-12: The post impingement model proposed by Bai et al. (2002).

	Velocity components		Diameter	Number
	u_a	v_a	d_{ia}	n_{ia}
Stick/Spread	--	--	--	--
Rebound	$\frac{5}{7}u_b$	$-e \cdot v_b$	d_b	*1*
Splash	$C_f V_{IT} + \left\|\vec{V_{SN}}\right\|.\cos\theta_{S,i}$	$-\left\|\vec{V_{SN}}\right\|.sen\,\theta_{S,i}$	*pdf(d)*	$\frac{r_m}{p}.\left(\frac{d_b}{d_{ia}}\right)^3$

$$N = \sum_{i=1}^{2} n_i = a_0\left(\frac{We_I}{We_{cr}} - 1\right); E_{KI} + E_{I\sigma} = \frac{1}{2}\frac{m_s}{p}\left[\left(V_{SN,1}\right)^2 + \ldots + \left(V_{SN,p}\right)^2\right] + E_D + E_{S\sigma};$$

$$pdf(d) = \frac{1}{\bar{d}}.e^{-\frac{d}{\bar{d}}}$$

The velocity magnitude $\vec{V}_{SN,\ i}$ of droplet i is estimated by considering energy conservation law (see Table VI-12).

The ejection angle, θ_S, is estimated from Mutchler (1970) and Ghadiri (1978) experimental observations and finally, the azimuthal angle ϕ_{az} is predicted by the same way that in Grover and Assanis model (Bai *et al.*, 2002).

2.15. Lemini and Watkins (2002)

In 2002, Lemini and Watkins (2002) proposed and presented some preliminary results of a spray impingement on a surface using an Eulerian-Eulerian approach (Beck, 2000). The presented impact model used the droplet number size distribution proposed by Beck and Watkins (2002; 2003a; 2003b; 2003c; 2004) to predict the amount of liquid within a computational cell that lies in each impingement regimes,

$$n(r) = \frac{16r}{r_{32}^2} e^{-\frac{4r}{r_{32}}} \qquad \textbf{(VI-27)}$$

where r_{32} is the local Sauter Mean Radius (SMR) of the spray.

In the model presented in Lemini and Watkins (2002) the transition criteria used to predict the splash limit, the dimensionless parameter *K*, developed by Mundo *et al*. (1994, 1995), also provided some information about the outgoing droplet size distribution, by the '*K density distribution*', *g(K)*,

$$g(K) = AK^{5/3} e^{-BK^{4/3}} \qquad \textbf{(VI-28)}$$

where

$$A = \frac{16}{3r_{32}^2\rho^2}\left(\frac{\sigma^{2\mu}}{u^5}\right)^{\frac{2}{3}} \qquad \textbf{(VI-29)}$$

and

$$B = \frac{2}{r_{32}\rho}\left(\frac{\sigma^2\mu}{u^5}\right)^{\frac{1}{3}} \qquad \textbf{(VI-30)}$$

With this distribution the fraction of droplets, wf_j, that are included in each of the impinging regimes can be calculated as follows:

$$wf_D = \int_0^{K_D} g(K)dK \qquad (deposition\ regime) \qquad \textbf{(VI-31)}$$

$$wf_R = \int_{K_D}^{K_S} g(K)dK \qquad (rebound\ regime) \qquad \textbf{(VI-32)}$$

$$wf_S = 1 - wf_D - wf_R \qquad (splash\ regime) \qquad \textbf{(VI-33)}$$

The integration limits K_D and K_S refer to the liquid characteristic transition numbers of deposition and splash, respectively.

The approach proposed by Beck and Watkins (2002; 2003a; 2003b; 2003c; 2004) solved both the liquid and the gaseous phases in an Eulerian manner. In this way, the liquid phase is considered as a coherent whole and its properties are written in terms of the first four moments of its number size distribution function.

The amount of liquid that spread on a surface is represented in the moment equations by the sink terms, SQ_{iD}:

$$SQ_{iD} = wf_D . Q_i \qquad \textbf{(VI-34)}$$

where the Q_i are the number size distribution moments,

$$Q_i = \int_0^\infty n(r) . r_i dr \qquad \textbf{(VI-35)}$$

and the subscript *i* indicates the moment number (*i = 0, 1, 2, 3*).

For the rebound fraction all moments of the spray remain constant, since there are no changes to the drop sizes and only the velocity component of the liquid normal to the wall in the cell changes. This velocity component is determined with the correlations for solid spheres that interact with a solid wall proposed by Matsumoto and Saito (1970) and reported in Bai and Gosman (1995). The liquid velocity components parallel to the wall are calculated by the liquid phase continuity equations with appropriated wall boundary conditions.

The splashing regime is modelled through source terms for each moment Q_i. In fact, only the source terms for Q_0, Q_1 and Q_2 have to be calculated since the volume of liquid, represented by Q_3, is already known through eq. 1.45 after the splash.

In order to calculate the remaining source terms a droplet size distribution of the outgoing droplets is necessary. Lemini and Watckins (2002) use a set of data reported by Mundo *et al.* (1995), for a dimensionless droplet size distribution of secondary droplets for a smooth surface and different *K* numbers, to generate a droplet size density distribution, $m(K, r_{out}/r_{in})$. This density distribution is function of *K* and ratio of radius between the splash droplet and the incident droplet. Lemini and Watkink (2002) deduced the number distribution, (K, v), of the secondary droplets based on the fact that volume of splashing liquid is equal to the volume of liquid after the splashing takes place. This expression is a function of *K* and the relative velocity of the liquid phase in the computational cell and the wall. This way the general form to calculate the source term for the i^{th} moment of the secondary droplets is:

$$SQ_{iS} = r_{in}^{i-1} \int_{K_S}^{\infty} \int_0^1 d(K, v) . g(K) . m\left(K, \frac{r_{out}}{r_{in}}\right) . \left(\frac{r_{out}}{r_{in}}\right)^i d\left(\frac{r_{out}}{r_{in}}\right) dK \qquad \textbf{(VI-36)}$$

The mean velocity of secondary droplets is assumed one quarter of incident of the incident velocity, according to the experimental data of Mundo *et al*. (1995),

$$u_{35} = u_{2S} = -\frac{u_3}{4} \qquad \textbf{(VI-37)}$$

The final moment-averaged velocities of the droplets within a computational cell are calculated as a weighted average velocity between the rebound and the splashing velocities.

$$u_2 = u_3 = Cu_n + (1 - C).u_{35} \qquad \textbf{(VI-38)}$$

where

$$C = \frac{wf_R}{wf_R + wf_S} \qquad \textbf{(VI-39)}$$

This post-impingement model proposed by Lemini and Watkins (2002) shows incapacity to predict adequately the SMD and the velocity component normal to wall in regions closer to the surface. Besides is computationally expensive, the droplet size density distribution is a Poisson distribution of variable exponent the integration has to be made numerically.

References

Al-Roub, M., and Farrell, P.V., "Atomization of Thin Liquid Films by Droplet Impact", *Atomization and Sprays*, Vol. 7, No. 5, pp. 531-547, 1997.

Bai, C.X. and Gosman, A.D., "Development of a Methodology for Spray Impingement Simulation", *Society of Automotive Engineers*, SAE Paper 950283, 1995.

Bai, C.X., Rusche, H., and Gosman, A. D., "Modelling of Gasoline Spray Impingement", *Atomization and Sprays*, Vol. 12, No. 1-3, pp. 1-27, 2002.

Chandra, S., and Avedisian, C.T., "On the collision of a droplet with a solid surface", *Proc. R. Soc. Lond.*, Vol. 432, pp. 13–41, 1991.

Gavaises, M., Theodorakakos, A. and Bergeles, G., "Modeling wall impaction of diesel sprays", *Int. J. Heat Fluid Flow,* Vol. 17, No. 2, pp. 130–8, 1996.

Grant, G., and Tabakoff, W., "Erosion Prediction in Turbomachinery Resulting from Environmental Solid Particles", *Journal of Aircraft*, Vol.12, No.5, pp.471-478, 1975.

Grover Jr., R.O., and Assanis, D.N., "A Spray Wall Impingement Model Based upon Conservation Principles", *The Fifth International Symposium on Diagnostics and Modeling of Combustion in Internal Combustion Engines - COMODIA 2001*, Nagoya, Japan, 1-4 July, pp. 551-558, 2001.

Habachi, C., Foucart, H., and Baritaud, T., "Influence of the Wall Temperature on the Mixture Preparation in DI Gasoline Engines", *Oil & Gas Science and Tecnology – Revue de L'Institut Francais du Petrole*, Vol. 54, No. 2, pp. 221-222, 1999.

Jayaratne, O.W., and Mason, B.J., "The Coalescence and Bouncing of Water Drops at an Air/Water Interface", *Proceedings of the Royal Society of London Series A-Mathematical and Physical*, Vol. 280, No. 138, pp. 545-565, 1964.

Lee, S.H., and Ryou, H.S., "Development of new model and heat transfer analysis of impinging diesel sprays on a wall", *Atom. Sprays*, Vol. 1, No. 85, 2000.

Lemini, E., and Watkins, A.P., "Development of a Spray Wall Impaction Model without Discretisation into Droplet Size Classes", *ILASS-Europe 2002*, Zaragoza, Spain, 9-11 September.

Levin, Z., and Hobbs, P.V., "Splashing of Water Drops on Solid and Wetted Surfaces - Hydrodynamics and Charge Separation", *Philosophical Transactions of the Royal Society of London Series A-Mathematical and Physical Sciences*, Vol. 269, No. 1200, pp. 555, 1971.

Matsumoto, S., and Saito, S., "On the Mechanism of Suspension of Paticels in Horizontal Conveying: Monte Carlo Simulation Based on the Irregular Bouncing Model", *J. Chem. Engng. Japan*, Vol.3, pp. 83-92, 1970.

Mundo, C., Sommerfeld, M., and Tropea, C., "Droplet-Wall Collisions: Experimental Studies of the Deformation and Breakup Process", *International Journal of Multiphase Flow*, Vol. 21, No.2, pp. 151-173, 1995.

Mundo, C., Sommerfeld, M., and Tropea, C., "Experimental Studies of the Deposition and Splashing of Small Liquid Droplets Impinging on a Flat Surface", *Proc. ICLASS 1994, Begell House*, New York, NY, pp. 1-18, 1994.

Mundo, C., Sommerfeld, M., and Tropea, C., "Numerical and Experimental Investigation of Spray Characteristics in the Vicinity of a Rigid Wall", *Experimental Thermal and Fluid Science*, Vol. 15, No. 3, pp. 228-237, 1997.

Mundo, C., Sommerfeld, M., and Tropea, C., "On the Modeling of Liquid Sprays Impinging on Surfaces", *Atomization and Sprays*, Vol. 8, No. 6, pp. 625-652, 1998.

Mutchler, C.K., "The Size, Travel and Composition of Droplets Formed by Waterdrop Splash in Thin Water Layers", Ph. D. Thesis, University of Minnesota, 1970.

Nabber, J.D. and Reitz, R.D., "Modelling Engine Spray/Wall Impingement", *SAE Paper 880107*, Society of Automotive Engineers, 1988.

Nagaoka, M., Kawazoe, H. and Nomura, N., "Modelling Fuel Spray Impingement on a Hot Wall for Gasoline Engines", *SAE 940525*, 1994.

O'Rourke, P.J., Bracco, F.V., "Modeling of droplet interactions in thick sprays and a comparison with experiments", *Startified Charge Auto. Eng. Conf.*, 101–115 Inst. Mech. Eng. Pub. ISMB 0-85298-4693,1980.

Park, K. and Watkins, A. P., "Comparison of Wall Spray Impaction Models with Experimental Data on Drop Velocities and Sizes", Int. Heat and Fluid Flow, Vol. 17, No. 4, pp. 424–438, 1996.

Pasandideh-Fard, M., Qiao, Y. M., Chandra, S. and Mostaghimi, J., "Capillary effects during droplet impact on a solid surface", *Phys. Fluids*, Vol. 8, No. 3, pp. 650–659, 1996.

Rusche, H., PhD Thesis, 1997.

Senda, J., Kanda, T., Al-Roub, M., Farrel, P.V., Fukami, T., and Fujimoto, H., "Modelling Spray Impingement Considering Fuel Film Formation on the Wall", *SAE Paper 970047*, Society of Automotive Engineers, 1997.

Senda, J., Kobayashi, M., Iwashita, S. and Fujimoto, H., "Modeling of Diesel Spray Impinging on Flat Wall", *Proc. Int. Symposium COMODIA 94, pp. 411-416,* 1994.

Stanton, D. W. and Rutland, C. J., "Multi-dimensional Modelling of Thin Liquid Films and Spray Wall Interactions Resulting from Impinging Sprays,"Int. J. Heat and Mass Transfer, Vol. 41, pp. 3037–3054, 1998.

Stanton, D., and Rutland, C., "Modeling Fuel film formation and wall interaction in diesel engines", *SAE Tech Paper 960628*, 1996.

Stow, C.D., and Hadfield, M.G., "An Experimental Investigation of Fluid-Flow Resulting from the Impact of a Water Drop with an Unyielding Dry Surface", Proceedings of the Royal Society of London Series a-Mathematical Physical and Engineering Sciences, Vol. 373, No. 1755, pp. 419-441, 1981.

Stow, C.D., and Stainer, R.D., "The Physical Product of a Splashing Water Drop", *J. Meteorol. Soc. Jpn.*, Vol. 55, No. 5, pp. 518-531, 1977.

Wachters, L.H., and Westerling, N.H.J., "Heat Transfer from a Hot Wall to Impinging Water Drops in Spheroidal State", *Chemical Engineering Science*, Vol. 21, No. 11, pp. 1047-1056, 1966.

Wang, D.M. and Watkins, A.P., "Numerical modeling of diesel spray wall impaction phenomena", *Int. J. Heat Fluid Flow*, Vol. 14, 1993.

Watkins, A.P. and Wang, D.M., "A New Model for Diesel Spray Impaction on Walls and Comparision with Experiments", *Proceedings of the Int. Symp. on Diagnostics and Modelling of Combustion in Internal Combustion Engines*, Kyoto, Japan, September, pp. 243-248, 1990.

Yarin, A.L., and Weiss, D.A., "Impact of Drops on Solid-Surfaces-Self-Similar Capillary Waves, and Splashing as a New-Type of Kinematic Discontinuity", *Journal of Fluid Mechanics*, Vol. 283, pp. 141-173, 1995.

3. Annex 3

Table VI-13: Characteristics and conditions under which the transitions criteria between the regimes "deposition" and "splash" used in this study have been proposed.

Characteristics and Conditions of the Studies						
	Bai *et al.* (2002)	Mundo *et al.* (1995)	Cossali *et al.* (1997)	Senda *et al.* (1999)	Huang and Zhang (2008)	Okawa *et al.* (2008)
Description	Development of sub-model based on experimental data	Experimental study and proposition of empirical correlation for splashing/deposition limit	Experimental study and proposition of empirical correlation for splashing/deposition limit	Development of sub-model based on experimental data	Experimental study and proposition of empirical correlation for splashing/deposition limit	Experimental study and proposition of empirical correlations
Splash Transition Criteria	$We_c = 1320.La^{-0.18}$	$K_c = (Oh.Re\text{^}1.25) = 57.7$	$K_c = (Oh^{-0.4}.We)_c = 2100 + 5880.\delta^{1.44}$	$We_c = (2164 + 7560.\delta^{1.78}).La^{0.2}$	$K_c = (We.Re)^{0.25} = 25 + 7.\delta^{1.44}$	$K_c = (Oh^{-0.4}.We)_c \approx 2100$
Criteria in terms of We	$We_c = 1320.La^{-0.18}$	$We_c = \frac{57.7^2}{Re^{0.5}}$	$We_c = \frac{2100+5880.\delta^{1.44}}{Oh^{-0.4}}$	$We_c = (2164 + 7560.\delta^{1.78}).La^{0.2}$	$We_c = \frac{(25+7.\delta^{1.44})^4}{Re}$	$We_c \approx \frac{2100}{Oh^{-0.4}}$
Secondary Droplet Size	$f(d) = 1/\bar{d}\exp\left(-\frac{d}{\bar{d}}\right)$ $\bar{d} = 1/6^{\frac{1}{3}}\left(\frac{r_m}{N_s}\right)^{\frac{1}{3}} d_I$	PDF – Probability Density Function of own data $\frac{d_s}{d_I} = f(Oh, Re)$ for smooth and rough surface.		PDF – Probability Density Function $\frac{d_s}{d_I} = f(Oh, Re)$ for smooth and rough surface.		
Number of Secondary Droplets	$N = 5(We/We_c - 1)$ $N_i d_i^3 = \frac{r_m d_I^3}{p}$			For $We \leq 300$: $0.6 < \delta < 1.35 - N_s = 4$; $Otherwise - N_s = 1$ For $We > 300$: $N_s = 0.8\frac{d_i^3}{d_s^3}$		$N_s = \max(4.97 \times 10^{-6}; 7.84 \times 10^{-6}(\delta)^{-0.3})\mathrm{K_c}^{1.8}$
Observations	The effects of the liquid film is accounted in the fitting constant A, by comparing the presence of the film to a rough surface	Monodisperse droplets generated with specific frequency.	For non-dimensional film thickness less than unity ($\delta < 1$)	The droplet-wall interaction is classified in two case: lower Weber number ($We \leq 300$) and higher Weber number ($We > 300$)	Good results were found for thin oil and water liquid film on thin liquid film	It is used the absolute value – and not the normal component – of the primary drop velocity vector to calculate the impact dimensional numbers.

Generated Droplets						
	Bai *et al.* (2002)	Mundo *et al.* (1995)	Cossali *et al.* (1997)	Senda *et al.* (1999)	Huang and Zhang (2008)	Okawa *et al.* (2008)
Fluid	Gasoline (Trimethylpentane)	Water-ethanol-sucrose	Water-glycerine	Isooctane (Gasoline)	Water/Oil	Water
Viscosity $[mPa.s]$	0.466	$1-2.9$	$1-60$	0.466	$1/22.5$	1
Surface Tension $[mN/m]$	18.2	$22-72$	$65-73$	18.2	$72/29$	72
Density $[Kg/m^3]$	692	$789-998$	$997.1-1208.1$	692	$998/854$	998
Diameter $[\mu m]$	$90-160$	$60-150$	$3.1\times10^3-3.5\times10^3$		$1.8\times10^3-4\times10^3$	$0.15\times10^3-1.21\times10^3$
$V_{0,n}$ $[m/s]$	~20	$12-18$	<6.5	22.84		$0.368-9.46$
We	$800-9000$	$94-2204$	$200-1600$			$5.7-573$
Oh		$6.3\times10^{-3}-5.4\times10^{-2}$	$2.2\times10^{-3}-0.141$			
Frequency $[kHz]$	10×10^{-3}	$27.2-64.3$	Single drop			Single Drop
Test rig						
Surface Material		Stainless Steel	Aluminum	Glass		Aluminium with black alumite coating
Dry/Wetted	Both	Dry	Wetted	Wetted	Wetted	Wetted
Injection Angle	20	$4.1-65.4$	0	0	0	$11-75$
Wall Temperature $[K]$	298	298	$<< T_{leid}$	293	298.15	308
Wall Roughness $[\mu m]$	A	$2.8/78$	0.14			
Impingement Distance $[mm]$	32		$50-2000$	30		$200-440$

Note that in the case of the Bai et al. (2002) and Senda et al. (1999), the characteristics presented in the table refer to the conditions used in their simulation and not experimental conditions. The blank cells are parameters not found.

This page has been intentionally left blank for double-sided copying.